Weddell Sea Polynya Sea Ice Thickness Analysis

MASTER'S THESIS

SUBMITTED IN PARTIAL FULFILMENT OF THE REQUIREMENTS FOR THE DEGREE OF MASTER OF SCIENCE IN ENVIRONMENTAL PHYSICS

Supervised by Prof. Dr. Justus Notholt and Dr. Christian Melsheimer of the Institute of Environmental Physics Remote Sensing Group

Alexander Mchedlishvili

October 19, 2020

Matriculation No.: 3180761

Abstract

The Weddell Sea Polynya is an irregular opening in thick pack ice near Maud Rise, an oceanic plateau within the Weddell Sea of the Southern Ocean near the Antarctic coast. Due to its rare occurrence, it is still shrouded in mystery and is thus far not characterized by a regularity of any sort. This study seeks to contribute in the understanding of this event by studying the previously unexplored sea ice-thickness over Maud Rise in polynya and polynya-free years. The sea ice thickness retrieval uses the brightness temperature data from ESA's Soil Moisture and Ocean Salinity (SMOS) satellite as well as NASA's Soil Moisture Active Passive (SMAP). Using the derived sea ice thickness data, in conjunction with atmospheric reanalysis ERA5 data, local mooring data and ASI sea ice concentration data: sea ice anomalies were studied in detail and the polynya as well as said anomalies were proven to be highly susceptible to atmospheric forcing as well as oceanic influence going against the notion that the Weddell Sea Polynya is purely an open-ocean polynya. Most importantly, it was shown that sea ice cover above Maud Rise is constantly subject to polynya-inducing effects such that even when the polynya does not occur there is plenty of evidence, as captured by the sea ice thickness retrieval, that suggests the area is acting anomalously. Namely, in the austral winter of 2018, when the Weddell Sea Polynya was expected to reoccur but surprisingly did not, there was an ice-thinning above Maud Rise with ice thickness reaching as low as 20 cm over an expanse comparable to the polynya opening of 2017 ($50 \cdot 10^3$ km^2). There are multiple effects that determine whether or not the polynya occurs such as the overlying wind stress curl, both magnitude and direction of wind velocities, upwelling of warm deep water, underlying bathymetry and how the oceanic plateau interacts with the overlying water, and while this research has effectively proven that Weddell Sea Polynya is no simple open-ocean polynya but rather a complicated natural phenomenon subject to several sources of forcing it has also shown that these effects do not stay dormant for years as was thought previously but rather are all present with their own regularity and only when they interfere constructively does the polynya occur.

Contents

List of Figures

Chapter 1

Introduction

1.1 General Introduction and Motivation

From 1974 to 1976, for three consecutive winters, the post-1972 satellite microwave radiometer record shows a persistent opening of a polynya in the Weddell Sea region near the Maud Rise seamount. After that, the polynya disappears and is not to return until August 2016 and once again become sizeable in September of the following year. These occurrences have been documented and many have hypothesized as to why they happen. Some statistically significant multidecadal trend in polynya-favorable conditions have been identified to be strengthening of the Southern Annular Mode, Weddell low (mean sea-level pressure over the Riiser-Larsen Sea), cyclonic wind stress curl and winter storm activity which reflect the continued poleward shifts in Southern Hemisphere westerly winds and storm tracks due to anthropogenic forcing (Campbell et al. 2019). In other words, there exists a link between climate change and Weddel Polynya favorable conditions which bring enhanced upwelling and more frequently disturbed sea ice cover to the Weddell Sea region. This implies a greater future role for the Weddell Sea Polynya in opening a window to the abyssal ocean which is another reason for studying and carefully analysing its occurrence.

Moreover, it becomes interesting to investigate these polynya-favorable conditions near the Maud Rise seamount in polynya-free years as well as prominent 1970s and 2010s occurrences. For this purpose, this study proposes the use of derived sea ice thickness data via the empirical retrieval algorithm (Huntemann et al. 2014). Unlike the Antarctic satellite sea-ice extent 1972-present record, the SMOS thin ice thickness maps offer unique data that can be used to identify the regional anomalies in all years. Most importantly, we see the Weddell Sea Polynya more frequently, albeit not as an open-water surrounded by sea ice as per its definition but a clearly-distinguished thin-ice feature.

1.2 Sensible-Heat (Open-Ocean) Polynyas

Polynyas are large, persistent regions of open water at locations where climatologically, thick sea ice would be expected (Martin 2001). This sea ice is in the form of pack ice: a sea ice type that drifts with winds and currents but still maintains a complete cover across the ocean. Polynyas tend to have irregular shapes but can often be likened to that of an oval with length scales of an order of 100 km. They occur as intermittent openings and closings at relatively the same location for up to several months and recur over many years. Importantly, their recurrence is not purely seasonal, in that it does not occur consistently on certain days of the year, but is rather initiated by a combination of climatological and/or oceanic processes. Polynyas should not be confused with shore leads which are another type of open water feature. Shore leads are characterized as long, linear transient features associated with the pack ice deformation, are not restricted to any particular location and tend to have a much smaller areal coverage than polynyas (Martin 2001). Polynyas occur in both winter and summer (Martin 2001), the focus of this paper is their physical behaviour in wintertime, specifically the behaviour of the Weddell Sea Polynya during austral winters.

The Weddell Sea Polynya is an open-ocean or 'sensible heat' polynya (Campbell et al. 2019). Sensible-heat transfer occurs between two bodies at different temperatures when in contact with one another. The higher temperature body transports what is known as sensible heat to the lower temperature body, unlike latent heat which is absorbed or emitted based on the change of state that is taking place. In basic terms, a 'sensible heat' polynya forms when water above freezing temperature upwells or rises, the water then imparts heat on the sea ice layer above and melts it. These polynyas get their name from the fact that the resultant atmospheric heat loss from their opening goes into cooling of the water column. It is also known as a 'open-ocean' polynya as these types of polynya tend to form far from continental coastlines. Polynyas forming along the continental coast are known as coastal 'latent heat' polynyas often maintained by winter winds pushing the adjacent pack ice in a particular direction and not giving time for the ice-free region to freeze up. The heat loss from 'latent heat' polynyas goes into ice growth, hence their name.

The polynya is an ice feature present in both Arctic and Antarctic. Present in the Northern Hemisphere are mostly coastal polynyas with Kashevarov Bank Polynya in the Okhotsk Sea being the only purely open-ocean polynya (Martin 2001). The Kashevarov Polynya occurs over the 200 meter deep Kashevarov Bank, where the turbulence associated with a strong tidal resonance generates a heat flux to the surface that creates a region of reduced ice cover with a characteristic diameter of about 100 km (Martin 2001). In the Southern Hemisphere, there are also more coastal than open-ocean polynyas. Specifically, there is the Cosmonaut Polynya occurring in the 1980s in the Cosmonaut Sea, and the Weddell and Maud Rise polynyas. The distinction between the Weddell Polynya (also referred to as the Weddell Sea Polynya) and the Maud Rise polynya is their respective location of occurrence. It is often the case (the 1973 occurence of the Maud Rise polynya

followed by three consecutive Weddell Polynya years) that the Maud Rise polynya transforms into or subdivides itself thus creating the much larger Weddell Polynya. For the purposes of this paper, the name Weddell Sea Polynya will encompass both the Maud Rise Polynya and Weddell Polynya as they are sufficiently interconnected.

Although polynyas, both open-ocean and coastal, occupy only a small area fraction of the areal winter pack ice extent, because the polar pack ice is a good insulator, very large atmospheric heat losses occur from both polynya types often leading to a freeze-up of the top layer when no maintaining mechanism in place (Martin 2001). While in the case of coastal polynyas this maintaining mechanism is predominantly winds that push away the newly formed sea ice, open-ocean polynyas in the Southern Hemisphere are generally maintained by the upwelling of warm water which overtime cools and modifies the underlying Antarctic Bottom Water.

1.2.1 Formation and Natural Maintenance

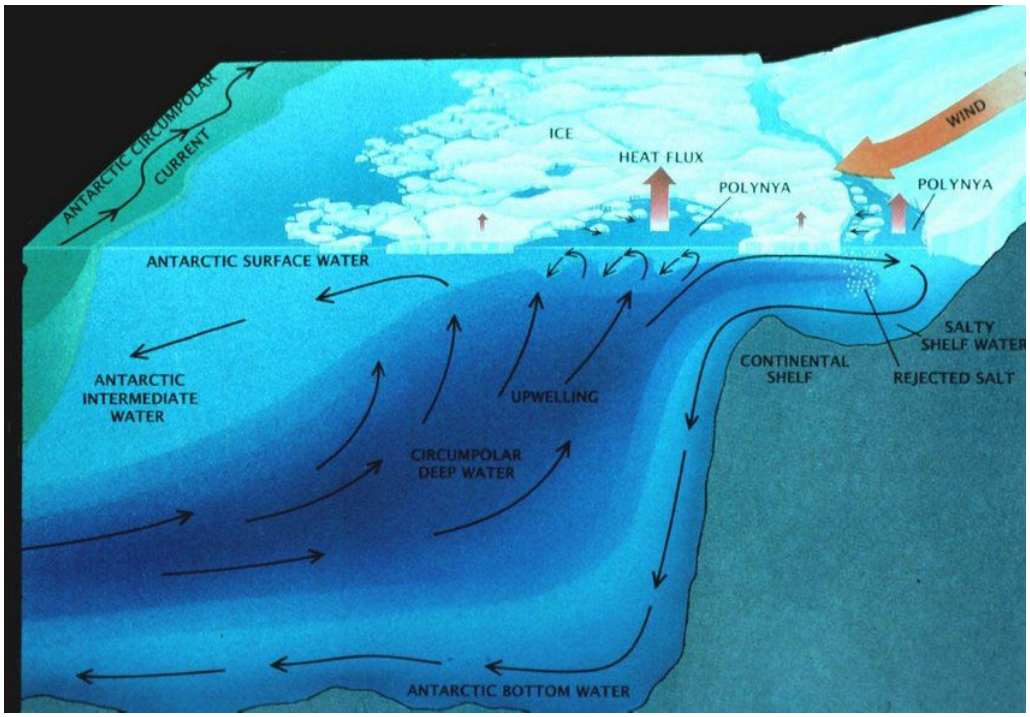

Figure 1.1: Diagram of two polynya-types and their impact on surrounding water, ice and atmosphere [Source: Comiso 1986].

In general, because of the relative accessibility to coastal polynyas, their dynamics are better understood than that of the open-ocean polynyas. (Fig. 1.1), a schematic drawing of the Antarctic coast, depicts a polynya near the continental coastline. As the winds advect the pack ice away from the coast, open water is exposed to the cold winds generating a wind-wave field on the open water surface, where the wave amplitudes and wavelengths increase away from the coast (Martin 2001). Coastal polynya formation results in a lot of ice generation as the top layers of the water

begin to freeze. As the water freezes up, salt is rejected in mass to the underlying water column, leading to an oceanic brine flux.

Open-ocean polynya formation is driven by the upwelling of saline warm sea water as depicted in Figure 1.1. They occur in oceanic regions with large reservoirs of relatively warm water just beneath a weak pycnocline. This contrast, in turn, drives the upwelling which brings the warm water to the surface. These polynyas maintain themselves through the heat flux from the ocean to the atmosphere; the flux then cools the surface water. The surface water then becomes denser and sinks, generating a turbulent convection which brings warm deep water to the surface (Martin 2001). As is often the case, due to the larger size of the warm water reservoir below and a steady temperature gradient with water depth, open-ocean polynyas have a stronger and more consistent heat-flux to the atmosphere as compared with the coastal ones. This convection that maintains Arctic and Antarctic open-ocean polynyas generally ceases in spring and austral spring, respectively. This is because the melting of neighbouring sea ice introduces a fresh water low-salinity cap on the convection cell. The freshwater can be produced locally by melting of the rim of the polynya or it can be advected into the region by ocean dynamics. Regardless of the method of how this fresh water was introduced to the system, the salty warm ocean water can no longer reach the surface effectively putting a stop to the ocean dynamics that kept the polynya open.

1.2.2 Recurrence and Frequency

It is assumed that the first to lay eyes upon a polynya were the Native American whalers and hunters of the pre-Columbian era (Martin 2001). Ever since, humanity's knowledge of the phenomenon, although staggered, increased over time. Since the 2nd half of the 20th century, satellite observations have allowed us to obtain a detailed daily coverage of polynya regions. In the 1970s and 80s, the instrumentation was still new and provided 1 km resolution visible and thermal imagery of polynyas, but only under cloud-free conditions (Martin 2001). It was not until passive microwave instruments such as Electrically Scanning Microwave Radiometer (ESMR)(Operating between 1972 and 1976) succeeded by the Scanning Multichannel Microwave Imager (SMMR)(operating between 1978 and 1987), and finally the Special Sensor Microwave/Imager (SSM/I)(operating between 1989 and the present), that cloud-independent low-resolution (25 km spatial sampling - down to 12.5 for 85.5 GHz frequency for the SSM/I) imagery of the entire polar pack was possible. This observation led to the discovery of all of the open-ocean polynyas, and many of the coastal polynyas (Martin 2001). The next innovative step in terms of polynya remote sensing was the deployment of Advanced Microwave Scanning Radiometer - Earth Observing System (EOS)(AMSR-E)(operating between 2002 and 2011) that greatly improved resolution. AMSR-E was later replaced by another Advanced Microwave Scanning Radiometer (AMSR2)(operating since 2012 until present). Using the various satellite instruments since the 1970s, there is a time series for all polynya openings in the last half-century. A more detailed look at the satellites and instruments used, specifically for

the data presented in this paper, can be found in chapter 2.

1.2.3 Implications

Polynyas are persistent openings in the ice cover that occur during the Arctic and Antarctic winters respectively. They facilitate heat exchange between the warm ocean and the cold atmosphere. While much is known about coastal polynyas that are often seasonal in terms of occurrence, open-ocean polynyas are more elusive and although their fundamental dynamics are understood, it is often the case that several preconditions must first be met for it to appear in the ice cover. In the Southern Hemisphere, open-ocean polynyas lead to a cooling of the upwelled ocean water and its modification into Antarctic bottom water thereby impacting the global ocean circulation (Martin 2001). The Antarctic Bottom Water that fills the global abyss today originates from the Antarctic continental margin (Campbell et al. 2019). It is speculated that in past glacial climates this deep water formation mechanism was impeded or completely halted by grounded ice sheets. But given that the global ocean circulation could not simply stop, open-ocean polynyas may have offered an ideal pathway for deep water to form thanks to the generation of the convection cell due to atmospheric cooling. The offshore deep water formation pathway is prevalent in many present-generation climate models (Campbell et al. 2019), and introduces biases into the present and future Southern Ocean properties, circulation and sea ice area. Considering the Antarctic open-ocean polynyas as a means of vertical transport in the meridional overturning circulation has one flaw in that they are intermittently occurring, which based on climate models might not have been the case in glacial times. Lastly, like their coastal counterparts, open-ocean polynyas tend to absorb more solar radiation than the surrounding ice at the start of the melt-season. As a result, the polynya regions tend to have a much greater primary productivity than regions with heavy winter pack ice at the turn of the season. The photosynthesis carried about by the ice algae then kick-starts the food chain in the region which allows marine mammals and birds to flock to the area (Stirling 1997).

1.3 The Weddell Sea Polynya

The Weddell Sea Polynya is perhaps the most famous, intriguing and mysterious of the ocean polynyas. It reached sizes comparable to the isle of Great Britain in the 1970s, laid dormant for almost half-century, and briefly re-appeared, albeit smaller than before, in 2016 and 2017.

1.3.1 1974 to 1976 Large-Scale Openings

As early as 1974, two years after the first satellite observation of the austral winter sea ice cover was available, a persistent larger scale open-ocean polynya was observed (Cheon and Gordon 2019). This was the Weddell Sea Polynya which then maintained itself throughout three consecutive austral winters (1974-1976). The average size of the polynya back then was about $250 \cdot 10^3$ km^2 (Fig. 1.2: (a–c)). Throughout the period, via measurements done by CTDs (Conductivity-Temperature-Depth recorders) it is known that the Weddell Deep Water (WDW) was signifcantly cooled and freshened to nearly 2700-m depth by open-ocean deep convection (Cheon and Gordon 2019). During three years of the Weddell Sea Polynya, the total heat loss of the WDW was estimated to be $12.6 \cdot 10^{20}$ Joules (Cheon and Gordon 2019).

It is important to mention that although satellite observations of the 1970s Weddell Sea Polynya occurence exist and many studies regarding this event have been done, they were based only on numerical models derived from simple to fully coupled climate models and very limited, short-term observation data measured in the Weddell Sea, in which the models did not include a data assimilation process (Cheon and Gordon 2019). The cross-examination study done in detail by Cheon and Gordon 2019 where they aim to compare the 1970s occurrences to the more recent 2016 and 2017 occurrences, concluded that due to the deep extent of the open-ocean convection near Maud Rise, the locally measured water column shows a very unique deep water formation that can be likened to a chimney (Cheon and Gordon 2019). This 'chimney formation' is what was described in chapter 1.2 as the convection that maintains the open-ocean polynya. In the case of the 1970s Weddell Sea Polynya occurrence, it was a water column that was homogeneous from the surface to the base of the convection layer (Cheon and Gordon 2019). In the Weddell Sea Polynya simulated in sea-ice - ocean coupled general circulation model (Rayner et al. 2003), this phenomenon took only one year to transport surface water masses to the sea floor suggesting a constant but slow convection cell was what in part maintained the polynya in those years (Cheon and Gordon 2019).

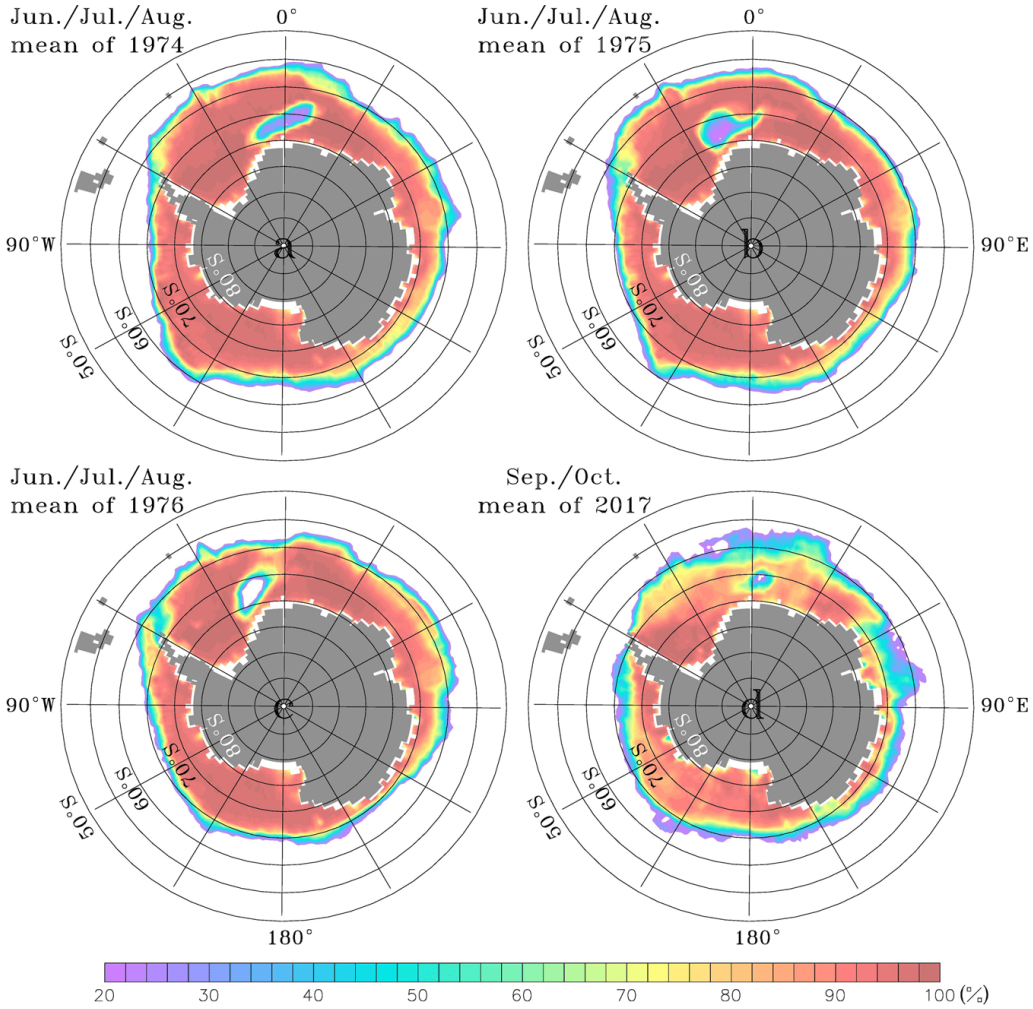

Figure 1.2: (a–c) June/July/August mean sea-ice concentrations of 1974/1975/1976 and (d) September/October mean sea-ice concentration of 2017 derived from the HadISST data (a blend of historical SST and modern SST observations from ships, buoys, drifters and sea ice observations, partly from historical ship- and air-borne measurements and partly from satellite data). Areas of low sea ice concentration (blue/ purple/white colors) enclosed within areas of high sea ice concentration (orange/red colors) between 30°W and 10°E indicate the Weddell Polynya occurring at 1970s and the Maud Rise Polynya occurring at 2017, respectively [Source: Cheon and Gordon 2019].

1.3.2 2016-2017 Recurrence

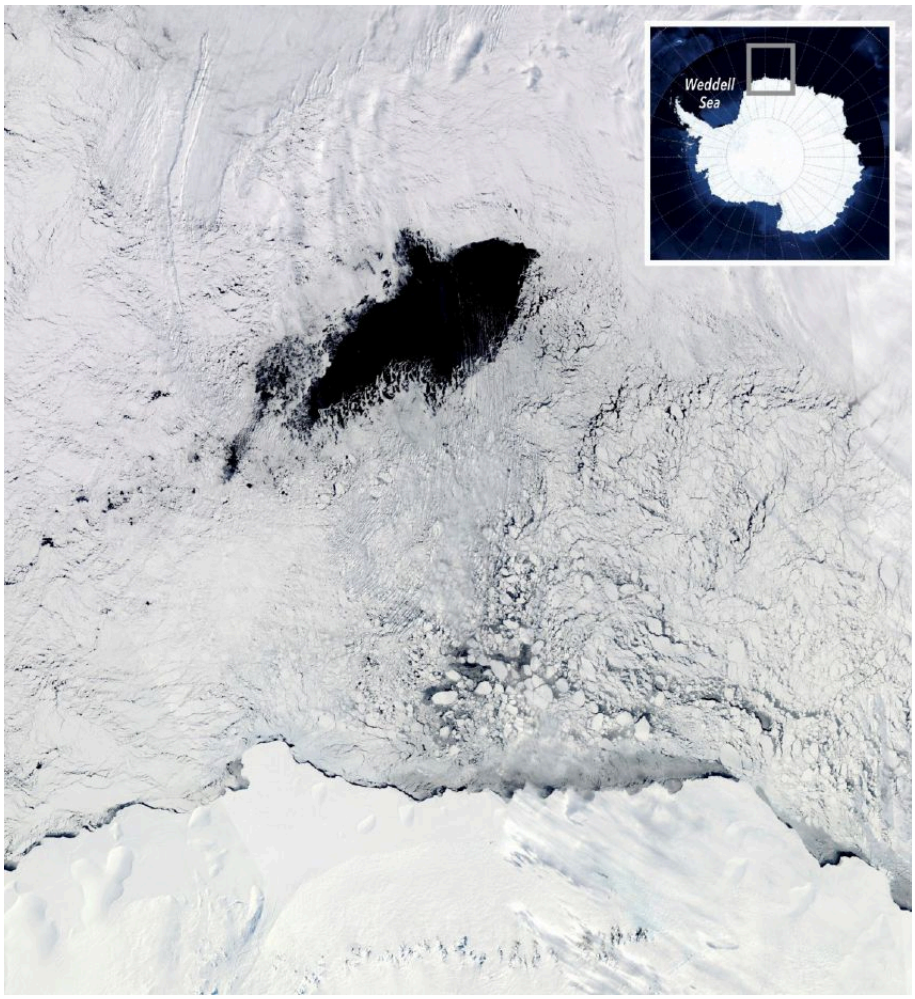

Figure 1.3: The Weddell Sea Polynya as seen by a NASA satellite in the visible channel on September 25, 2017 [Source: NASA Worldview/NASA Blue Marble].

The most recent and well documented re-occurrence of the Weddell Sea Polynya, although exclusively near the Maud Rise area, was in 2016 and 2017. Following the brief week-long august 2016 occurrence, a longer-lived, larger open-ocean polynya was observed from September to November of 2017 (Cheon and Gordon 2019). Notably, the 2016-2017 polynyas accompanied a reversal of the positive trend in Antarctic sea ice extent of 2014 (Campbell et al. 2019), suggesting that the Maud Rise events may reflect a larger climate signal. The 2017 opening reached size of up to $50 \cdot 10^3$ km^2 (Cheon and Gordon 2019). Contrary to the behaviour of the Weddell Sea Polynya in the 70s, it did not begin as the smaller Maud Rise Polynya to then shift westward in the following austral winter to become the much larger Weddell Polynya as was generally expected by the scientific community.

1.3.3 The Low Sea Ice Concentration Halo

Although not well documented, the ice cover above Maud Rise is prone to anomalous behaviour even in years where no polynya occurs. The 23–year mean ice concentration for the months of July through November (1979–2001) show a distinctive nearly-circular halo of low ice concentration with a diameter of about 300 km (Lindsay, Holland, and Woodgate 2004). Shaped much like the seamount below, the halo is located around the flanks of Maud Rise. Notably, the shape, location and the intensity of this effect is highly variable and rather than being a circular halo, more often than not, it is asymmetric in its configuration. The emergence of the halo feature in the time-averaged satellite record then, rather than suggesting a permanent circular thin lead around Maud Rise, can be interpreted as sporadically occurring individual small polynya around the seamount (Lindsay, Holland, and Woodgate 2004).

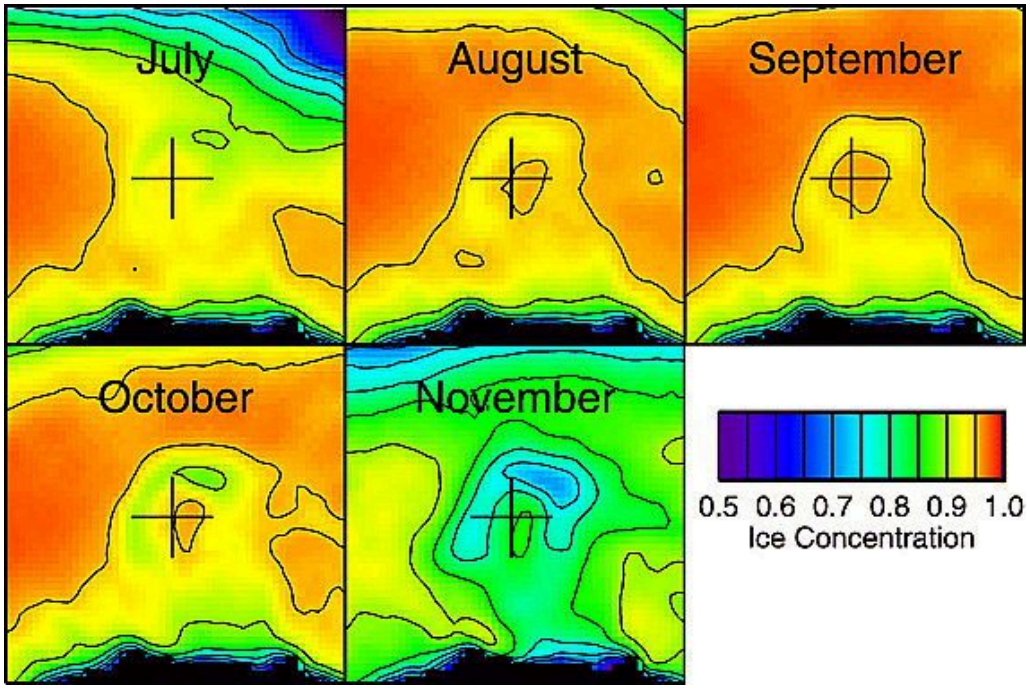

Figure 1.4: Monthly-mean ice concentration around Maud Rise from 23 years of observations (1979–2001) from the satellite-based passive microwave sensors SMMR and SSMI where the 300–km cross marks the location of Maud Rise and the black shading at the figure bottom indicates the Antarctic continent [Source: Lindsay, Holland, and Woodgate 2004].

Notably, the anomalous halo is proof of underlying processes being active even in years when the polynya does not occur going against the false notion that the Maud Rise region is susceptible to anomalous behaviour only during polynya years.

1.4 Weddell Sea Polynya Favorable Conditions

In order to understand the formation mechanism of the Weddell Sea Polynya, theoretical and modelling studies have linked its occurrence to static stability and open-ocean convection (Jena, Ravichandran, and Turner 2019). The poles are characterized by deep convection which often reaches from the seascape to the surface due to the lack of stratification in the cold waters. This deep convection leads to upwelling of warm circumpolar deep-water from the Weddell Gyre favoring the formation of a polynya. In addition, the oceanic diffusion and entrainment heat fluxes maintain its stability. A overlying negative wind stress curl over the Weddell Sea intensifies the cyclonic Weddell Gyre and causes the upwelling of warm-saline deep water to the surface (Cheon and Gordon 2019). The oceanographic and atmospheric effects that give rise to the Weddell Sea Polynya shall be discussed in the subsequent sections (1.4.1 and 1.4.2).

1.4.1 Maud Rise Seamount and Deep Mixing

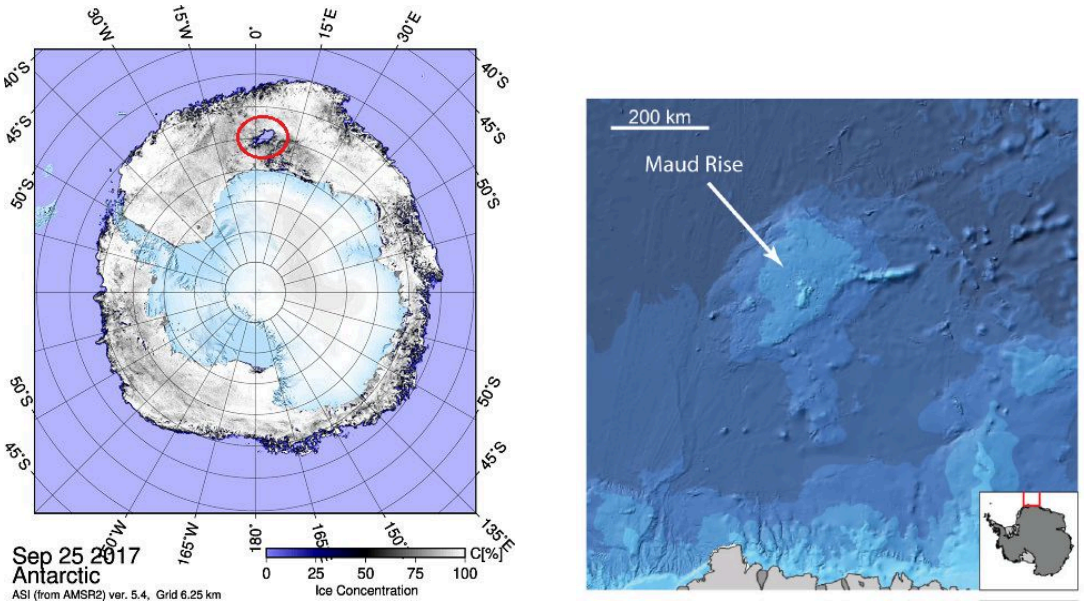

(a) (b)

Figure 1.5: The figure on the left shows the location of the Weddell Sea Polynya on September 25, 2017 in relation to the Antarctic continent [Source: University of Bremen Sea Ice Portal] and the figure on the right shows the shape and bathymetry of Maud Rise as well as its relative location.

The Maud Rise seamount is an oceanic plateau located in the eastern Weddell Sea rising from the abyssal plain at 5000 m to within 1700 m of the surface (Lindsay, Holland, and Woodgate 2004). The tendency of polynyas to emerge near the seamount is not a coincidence (Campbell et al. 2019). The interaction between water flow and topography enhance upward heat fluxes and generate eddies that transmit divergent strain to the ice cover. The more vigorous the Weddell Gyre, the higher the likelihood to activate cyclonic eddies that shed from the flank of Maud Rise

which are the principal cause of the stress from below (Cheon and Gordon 2019). The 2015 measured depth of the 0 °C isotherm in the Maud Rise region reveals shallowing (approaching the surface) of warm deep water in the southwestern flank of Maud Rise, indicative of a cyclonic eddy. The same measurements (covered in further detail in Cheon and Gordon 2019) reveal a deepening of the 1 °C isotherm indicating that the warm deep water layer is substantially thickened in the region. This homogeneous water layer is indicative of the previously-explained convection cell that maintains open-ocean polynyas. The large reservoir of steadily upwelling warm water maintains the ice-free conditions of the polynya, and the atmosphere then cools the entire water column creating a sensible heat gradient that drives the convection cell.

Similarly, vertical profiles of the temperature and salinity in the region further support the existence of a precondition for the Weddell Sea Polynya. The Maud Rise cyclonic eddy generated in the austral winter of 2015 weakened the water column stratification, generating the precondition for the small-scale Weddell Sea Polynya of 2016 and 2017 (Cheon and Gordon 2019). However, the preconditioning cannot be attributed to the topography alone which is unchanging and by that logic, the polynya would be a constant feature of the Antarctic sea ice cover. The cyclonic eddy activated in 2015 happened as a result of a more vigorous Weddell Gyre present in the region far exceeding the vicinity of Maud Rise. This macro-scale effect can be attributed to Climate variability.

1.4.2 Role of Climate Variability

Parts of the Weddell Sea including the vicinity of Maud Rise is under the influence of the Antarctic Subpolar current (the counter-current to the Antarctic Circumpolar current). The interaction between the ocean and the atmosphere is triggered by the intensifying Southern Hemisphere westerly winds due to a positive Antarctic oscillation (AAO or Southern Annular Mode SAM) the westerly wind belt that drives the Antarctic Circumpolar Current intensifies and contracts towards Antarctica. This process enhances the negative (cyclonic) wind stress curl over the Weddell Sea and, in effect, the Weddell Gyre (Cheon and Gordon 2019). The intensified Weddell Gyre plays a crucial role in the upward doming of the pycnocline (layer where the density gradient is greatest) which separates the previously mentioned warm deep water from the colder surface layer right below the ice. In the data presented by Cheon and Gordon 2019, the wind stress curl anomaly does not vary much from 1995 to mid-2014 and then strengthens which is indicative of enhanced cyclonic circulation in 2015 (Cheon and Gordon 2019). This is followed by the intensification of the Weddell Gyre in the same year, consistent with the overlying negative wind stress curl. Thus the intensified Weddell Gyre and the weakly stratified waters near Maud Rise (as shown through available potential energy anomaly calculations in Cheon and Gordon 2019) give rise to the initial preconditions of the Weddell Sea Polynya.

In addition to indirect atmospheric effects, Campbell et al. 2019 attribute the 2016 polynya

occurence in part to winter storm activity. There is a correspondence (r = 0.81) between the evolution of the extent of the polynya in 2016 and the cumulative wind-speed anomaly from a baseline value (10 m/s), which indicates that the polynya grew with strong winds from storms and shrank during quiescent periods (Campbell et al. 2019). Similar to the driving mechanisms of the coastal polynya, wind-driven ice advection is a dominant factor in the Weddell Sea Polynya's maintenance. Campbell et al. 2019 postulate that along the ice-covered perimeter of the polynya, high winds may have triggered ice loss and destabilization through turbulent mixing. Within its interior, heat extraction and salty turbulent entrainment from high winds would have driven convection, preventing ice from reforming (Campbell et al. 2019). Similarly, in 2017, a storm between 13th and 18th of September is what is attributed to be one of the driving forces behind the prolonged 2017 opening. Unlike 2016 however, quiescent periods of no storm did not result in the closing of the polynya and instead the Weddell Sea Polynya remained open until the austral summer of that year.

1.4.3 Weddell Sea Polynya Life Cycle

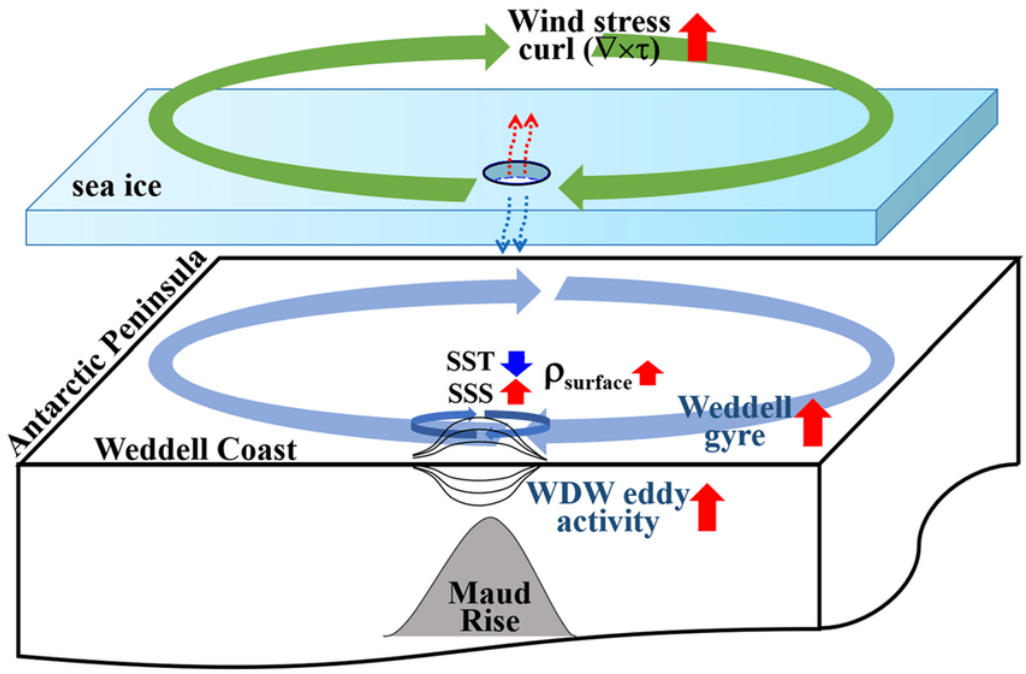

Figure 1.6: A simple schematic diagram to illustrate how an open-ocean polynya is triggered by both hydrological and dynamic processes where the red arrows for the wind stress curl and Weddell gyre indicate intensification as opposed to an increase in value i.e. the wind stress curl gets more negative and sea surface height still decreases in the cyclonic gyre [Source: Cheon and Gordon 2019].

In conclusion, the preconditioning as well as the eventual occurrence of the polynya can be summarized in the following steps (all of which are nicely depicted in Figure 1.6):

1. The upper ocean stratification weakens.
2. The water column becomes sufficiently destabilized which triggers small-scale convection in the upper ocean, causing the relatively warm deep water below the pycnocline depth to rise to the surface.
3. The upwelled warm deep water melts the overlaying sea ice and through convection maintains ice-free conditions.
4. Once the Weddell Sea Polynya occurs, the relatively warm surface water is exposed to the cold winter atmosphere, cooling the water column.
5. At this point two mechanisms can lead to the closing of the polynya:
   (a) Local or advected freshwater introduced by regional sea ice melting can effectively cap the the convection cell, limiting warm deep water transfer to the surface.
   (b) The ocean-to-atmosphere heat loss cools the water column consuming the ocean heat content and cooling the regional warm deep water reservoir.
6. Finally, the polynya disappears due to the above-mentioned processes and so does the open-ocean deep convection. The impact of convection persists until the warm deep water heat is restored by advection from the Antarctic Circumpolar current.

1.4.4 Role of Topography

Although the dynamics and interplay between ocean and atmospheric effects are well formulated and ultimately necessary for the occurrence of the polynya, it is also worth discussing how important the underlying bathymetry is. Findings presented in Jiang et al. 2020 suggest that the location and slope of the steep part of the local terrain greatly affected the formation and location of the polynyas. By analysing local wind patterns, Jiang et al. 2020 revealed that at locations where the terrain changes abruptly wind tends to first decrease and then increase in magnitude. This holds true for most Antarctic coastal polynyas, which is in fact the focus of (Jiang et al. 2020), but there is also a detailed analysis of the Weddell Sea Polynya in the paper and how Maud Rise acts as the abrupt terrain change. Parallels between the coastal topographic deepening and the slopes surrounding Maud Rise suggest that the the Weddell Sea Polynya mirrors the curvature of the outer contour of the Maud Rise on the seabed (much like the halo described in Lindsay, Holland, and Woodgate 2004). That would suggest that not only does the seamount force warmer water upwards as discussed previously but it also has some effect on the wind patterns in the area, further aiding the opening of the polynya. The specific example of the sea ice concentration analysis that took place in Jiang et al. 2020 is from October 2018, suggesting ice concentration anomalies to exhibit this shape similarity much like the polynya itself. Thus, although the preconditioning and driving mechanics of the polynya can be attributed to external forcing as discussed in (Cheon and

Gordon 2019), it is also apparent that the topography introduced by Maud Rise is a determining factor in its occurrence.

Another interesting, but perhaps not apparent, contribution from Maud Rise is the possibility of a Taylor cap atop Maud Rise. A Taylor cap is the region of fluid trapped inside a Taylor column; a Coriolis-induced column above a solid body submerged in a rotating fluid that is parallel to the axis of rotation. On a much larger, oceanic scale, a Taylor column can be described as a fluid column being compressed vertically on the upstream side of a topographic feature and stretched on the downstream side. The Taylor column would only appear in the event of a steady current impinging on said topographic feature and would result in anticyclonic and cyclonic vortices that corotate about the feature (Muench et al. 2001). In the case of Maud Rise, most of the necessary conditions for the formation of the Taylor column are met. The incident mean current strength is expressed in terms of the Rossby number R_0:

$$R_0 = \frac{U}{fL} \tag{1.1}$$

where U is the incident current speed, f is the Coriolis parameter and L is the horizontal length scale of Maud Rise (estimated to be 100 km). From the observations presented in Muench et al. 2001 the incident current speed U is estimated to be 1-2 cm/s, resulting in a R_0 of order 10^{-3} which is sufficient for there to be a Taylor column atop Maud Rise. The column would be further facilitated by the lack of stratification above Maud Rise as highly stratified water would decouple upper layer flow from the deeper circulation. The resulting Taylor cap dynamics force the ocean flow to intensify around the flanks of the seamount while the quasi-trapped anticyclonic circulation present in the middle helps with the upward doming of the pycnocline (Lindsay, Holland, and Woodgate 2004). This further consolidates the idea that all aspects of polynya preconditioning are deeply interconnected and highly dependent on each other.

1.5 Weddell Sea Polynya Sea Ice Thickness Analyses

To justify the use of further analyses of the Weddell Sea Polynya event there must first be a need to do so. This section aims to first and foremost show the ambiguity that still remains with regards to this irregular occurrence and then how the relatively new method of sea ice thickness analysis can contribute to the field. While the basics are well understood, papers on the subject have no definite forecast on how the Maud Rise region will behave in coming years. This is in part due to the lack of a satellite record before the 1970s, and yet there are no definite proxy data that can be used to study polynya events of the past. Perhaps the most important question that the scientific community currently tackles is whether there will be more or fewer polynya events in the Weddell Sea region in the years to come.

While the Weddell Sea Polynya life cycle is, as shown in the previous section, relatively well-

understood, there is still some ambiguity as to how many different factors contribute to its occurrence. The kick-starter of this life-cycle, which as previously described is the positive Antarctic Oscillation (AAO) also known as Southern Annular Mode (SAM) is a 'double-edged sword' in terms of opening the polynya. While the Antarctic Oscillation in its positive state does intensify the westerly winds over Maud Rise which leads to polynya-favorable conditions, if it persists too long it can obstruct it. The surface salinity of the Weddell Sea correlates inversely with the SAM index (Cheon and Gordon 2019). A prolonged positive SAM induces humid conditions as the intensified westerly winds sweep across the pack ice and bring with them moisture from the surrounding ocean. As a result, the sea surface salinity remains relatively fresh in the area hindering the maintenance of the polynya. The fresh water acts as a cap to the convection cell below and warm water no longer reaches the surface, allowing the area to freeze over. The Weddell Sea Polynya of the 1970s followed a prolonged negative SAM, which conversely induces a drier-than-normal atmosphere over the Weddell Sea, increasing the salinity of the cold surface layer, weakening the pycnocline and separating it from the warmer deep water (Cheon and Gordon 2019). In the 1970s, when the SAM was predominantly negative, the weakened pycnocline acted to increase transfer of the ocean heat to the sea surface. Currently, the SAM has long been in positive mode since the mid-1990s, suggesting the presence of more freshwater in the area.

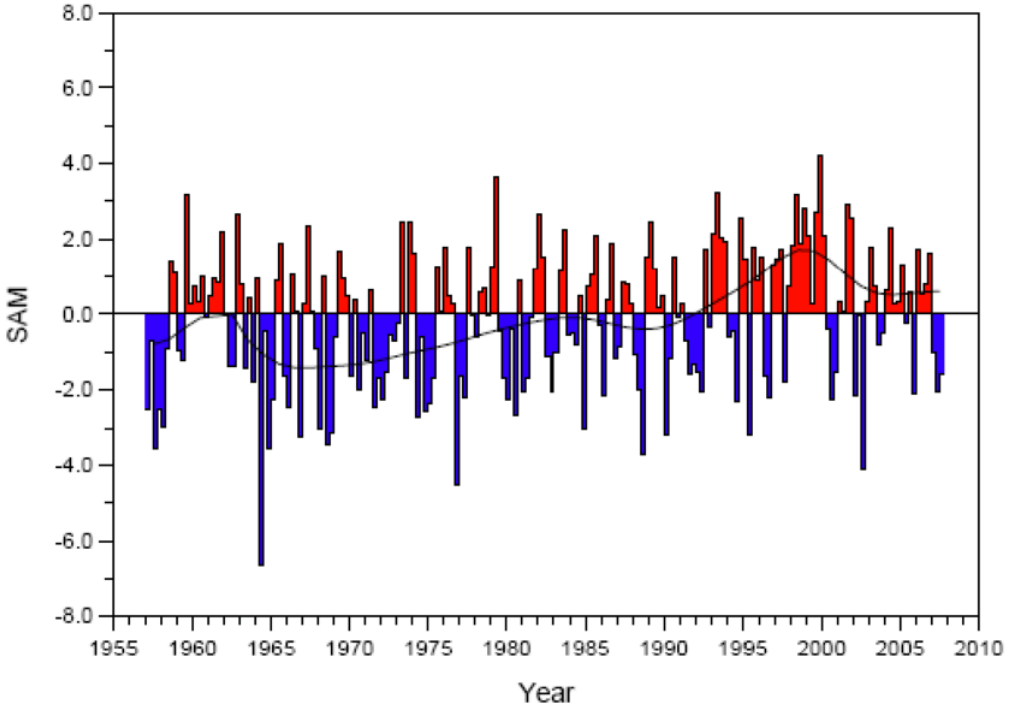

Figure 1.7: 2 Seasonal values of the SAM index calculated from station data (Marshall 2003). The smooth black curve shows decadal variations i.e. the average SAM for every decade calculated at each point along the line [Source: Figure 3.32, IPCC (2007)].

As discussed in Cheon and Gordon 2019 this effect could be one reason why a larger Weddell

Sea Polynya did not follow the smaller-scale events near Maud Rise (as it did in the 1970s). Other causes, all of which hinder the standard life-cycle of the polynya, are the weakening of the negative wind stress curl in 2017, and the loss of heat in the vicinity of Maud Rise suggesting that that the deep water temperature in the austral winter of 2018 might not have been warm enough to melt the overlaying ice.

While some climate models predict a prohibition on the formation of Southern open-ocean polynyas due to a freshening trend of about 0.01 psu per decade (associated with anthropogenic climate change), Campbell et al. 2019 proposes that the strengthening of SAM, cyclonic wind stress curl and winter storm activity reflects a poleward shift in Southern Hemisphere westerly winds and storm tracks which will inevitably enhance upwelling thereby leading to a more frequently disturbed sea ice cover over the Weddell Sea region (Campbell et al. 2019).

Sea ice thickness analyses offers a different view of the situation, namely, while polynya events are defined as exposed water surrounded by thick pack ice, in the case of open-ocean polynyas a particularly thin ice layer near Maud Rise, a negative ice thickness anomaly, should retain some of the properties of the Weddell Sea Polynya. Specifically, it should retain signs of warm deep water upwelling which is a fundamental condition that must be met for the opening of the polynya. It would also be of value to compare the obtained results with storm data and see if thin ice events are characterized by relatively calm weather which would explain as to why we do not see a polynya then. The debate as to which mechanism is the dominating factor in polynya-formation as well as what each can individually achieve is another important point of interest. These thin-ice events, along with the major Weddell Sea Polynya events are discussed in this Master's Thesis, to hopefully further the understanding of the mechanisms at play in the Maud Rise region.

1.5.1 Polynya-Free Years and their Implication

All published material on the subject focuses on the recent and 1970s Weddell Sea Polynya occurrences. The time-span for these events is researched and cross-referenced with various data sets as in Campbell et al. 2019. One aspect that is neglected for the sake of focusing on what is important is the years when the Weddell Sea Polynya has not occurred. Using the sea ice thickness analysis methods (which will be presented in detail in the following chapter), this paper aims to view the ice sheet above Maud Rise in all years. Due to the peculiarity of the region and several essential preconditioning events taking place on a regular basis, the hypothesis presented here suggest that there should be points in time when although the polynya could not open, the ice in the region became increasingly thin.

Antarctic open-ocean polynya study has advanced significantly since the 2016 and 2017 occurrences, but as of yet there is no fully understood method of forecasting the event. This is in part due to the fact that there is no identifiable cycle that the Maud Rise region undergoes, there seems

to be certain preconditions that must be met and only then the polynya appears. An example of this uncertainty is the general consensus that the 1970s Weddell Sea Polynya behaviour (the small open-ocean polynya over Maud Rise forming into the much larger polynya spanning a sizeable part of the Eastern Weddell Sea) was expected to occur again in 2018. This specific matter, as discussed briefly previously, is explained in more detail in Cheon and Gordon 2019. Although the scientific community has formed several hypotheses as to why 2018 was a polynya-free year, it is aim of this study to identify any existing signs of an 'incomplete' polynya in 2018 which, if found, should dispel some ambiguity towards the unforeseen change of behaviour.

Moreover, the direct data on this subject, which is the ice extent maps of the Antarctic, is quite small. This data set begins in the 1970s giving the scientific community very little to work with, especially in view of the handful major polynya events that have occurred since the first satellite that looked at the Antarctic went into orbit. The aim of this study is to increase the data that is available on the subject by adding all the hypothesized 'incomplete' (thin-ice) polynya events to the record of the Weddell Sea Polynya occurrences in hopes of reaching a better understanding as to why, when and how the event takes place. Furthermore, a bigger data-set should give a better idea as to how this event will re-occur in the future and what will be its impact.

1.5.2 Finding a Tipping Point

Lastly, it is important to discuss how sea ice thickness analysis can further contribute to the carefully studied polynya events like those in 2016 and 2017, respectively. The opening of the polynya is a gradual process, during which time, it can be hypothesized that the ice begins thinning some time before the polynya opens. Using the methods described in this paper, it is possible to distinguish ice up to 50 cm in thickness and while thick pack ice in the region should be 1 to 2 meters, it should be easy to tell apart any major thinning that occurs. In other words, if the above-stated is indeed true, a measure of processes leading to the eventual occurrence of the polynya should be possible. Different ice types classified purely by thickness can be plotted along with time to reveal how fast we arrive from thick pack ice to open water during a polynya event. With this data, it should be possible to identify some type of 'tipping point' which should consolidate the prediction of open-ocean polynya events. Cross-referencing this with all the times the polynya was unable to form despite local thinning and the SIC maps readily available exposing the polynya during the exact days when it was open should further the understanding of the thus-far ambiguous topic.

Chapter 2

Materials and Methods

2.1 Sea Ice Thickness Retrieval from SMOS Observations

Sea ice thickness information is important for sea ice modelling, sea ice monitoring and as a forecast for ship operations (Huntemann et al. 2014). The space-borne passive microwave sensor Soil Moisture Ocean Salinity (SMOS) provides brightness temperature data at L band (1.4 GHz), a frequency so low such that the atmosphere, when viewed through SMOS, is close to transparent. This method, when applied to polar regions, can be used to derive the thickness of thin sea ice.

SMOS has been developed for retrieving soil moisture and ocean salinity by inferring the surface emissivity which is correlated with the moisture content and surface salinity for land and sea, respectively. The measured brightness temperatures are linked with the sea salinity through the dielectric constant of the water in the first few centimeters (Patilea et al. 2019). Modeling and observations showed that at this frequency, the radiation is sensitive to ice thickness up to 50 cm (Kaleschke et al. 2010). The atmosphere, as mentioned before, has negligible influence in the retrieval at such a low frequency as both absorption and scattering components are small. The correlation of ice thickness with emitted radiation and the ability to ignore atmospheric influence makes SMOS an able candidate for thickness retrieval of thin sea ice (Patilea et al. 2019).

2.1.1 SMOS Data Retrieval

SMOS carries the first ever, polar-orbiting, space-borne, 2-D interferometric radiometer measuring at L-Band: the MIRAS (Microwave Imaging Radiometer using Aperture Synthesis) instrument. MIRAS has been providing data since 2010, months after the launch date of SMOS on the 2nd of November 2009. MIRAS has 69 receivers, which are equally distributed along three arms and the central structure (Huntemann et al. 2014). The receivers measure radiance values from which

brightness temperatures are determined (Huntemann et al. 2014). One aperture synthesis step produces one unit of data called a snapshot, a set of about 100 × 100 brightness temperature pixels is generated from the initial observations by correlating the signals from the 69 receivers amongst each other and applying a Fourier-like back transform (Huntemann et al. 2014).

Along with the ability to provide brightness temperature data one unique capability that sets SMOS apart from other similar satellites is that it operates in full polarisation mode since May 2010 (Huntemann et al. 2014). In other words, in addition to the usually observed vertically and horizontally polarized brightness temperatures T_v and T_h, the third and fourth components of the Stokes vector, called U and V are measured as well. Huntemann et al. 2014 discusses further as to how the data sets with respect to the instrument reference plane (X,Y) are converted to the Earth's surface plane (V,H) by a given transformation (Huntemann et al. 2014). The SMOS sea ice thickness data retrieval was trained by the Cumulative Freezing Degree days CFDD model (Bilello 1960) in the Kara and Barents seas during the freeze-up period. It uses the average of horizontally and vertically polarized brightness temperatures as well as the polarisation difference (i.e. the difference between horizontally polarized and vertically polarized brightness temperature) at incidence angles between 40 and 50°. Because of the high penetration depth at L band and the high brightness temperature contrast of over 100K between ice and open water, sea ice thickness is reflected in the L-band emission (Huntemann et al. 2014).

The SMOS sea ice thickness range retrieval is only found during the freezing season (Huntemann et al. 2014). For the Antarctic, that means the duration of the austral winter: from March to October. During the austral summer, the 'melt season', sea ice cover decreases. Wet sea ice, melt ponds and increasing amount of open water makes the retrieval process impossible

Another restriction that needs to be taken into account for the purposes of this study is the assumptions the data-processing algorithm takes. Namely, since observing the polynya inevitably involves the observation of ice-water boundaries and regions with variable ice concentration it must be noted that the algorithm assumes 100 % sea ice concentration to retrieve sea ice thickness (Huntemann et al. 2014). Restricting the retrieval to near 100 % sea ice cover could improve accuracy of the retrieval (Huntemann et al. 2014). This can be done via cross-referencing the sea ice thickness maps produced with the SIC maps produced via the ARTIST Sea Ice (ASI) algorithm (Spreen, Kaleschke, and Heygster 2008). By doing so, the respective sea ice concentration can act as maps depicting where uncertainty is highest in the sea ice thickness maps, and offer a better picture of which data is to be trusted.

2.2 Combined SMAP–SMOS thin SIT retrieval

In 2015 the Soil Moisture Active Passive (SMAP) satellite was launched by NASA (Paţilea et al. 2019). Like SMOS, SMAP was developed to retrieve soil moisture with its own L-band radiometer and a radar which is no longer functional (Paţilea et al. 2019). SMAP is different to SMOS in the following ways: firstly, unlike the synthetic aperture observations of SMOS, SMAP carries out *real aperture antenna* observations which cover an area of 35 km × 47 km at a fixed incidence angle of 40° resulting in a swath with an approximate width of 1000 km. Secondly, SMAP includes on-board detection and filtering of radio frequency interference (RFI).

The combined SMAP-SMOS thin ice sea ice thickness retrieval improves the SMOS retrieval by adapting it to SMAP by modifying it to use 40° incidence angle instead of average in the range 40 to 50° and establishes a linear regression between the SMOS and SMAP brightness temperatures at a 40° incidence angle. SMAP top-of-the-atmosphere data and SMOS data are fitted via an analytical function to the same incidence angle which yields a small brightness temperature root mean square difference (RMSD) between the two datasets at both polarizations (T_h and T_v) of 2.7 and 2.81 K, respectively.

For the purpose of this research, in addition to the SMOS thin sea ice thickness retrieval the combined SMAP-SMOS thin sea ice thickness retrieval will be used. In fact, as discussed in Paţilea et al. 2019, the combined method should provide better retrievals less influenced by RFI (due to the new filtering routine used that exploits the dependence of the brightness temperatures on the incidence angle) and be more representative for daily mean (due to the 12 hour difference in the Equator crossing time between SMAP and SMOS). Most importantly for this study, brightness temperatures retrieved via SMOS have small variability at lower thicknesses due to the iterative observations' removal operation (Paţilea et al. 2019), which is the necessary step taken to remove RFI-influenced data. Variability in the SMAP-SMOS sea ice thickness retrieval is higher which allows for better and more accurate monitoring of ice of different thicknesses above Maud Rise.

Like SMOS, the combined SMAP-SMOS sea ice thickness retrieval assumes 100 % ice concentration. What this essentially means is that the retrieved sea ice thickness decreases if the sea ice concentration is below 100 % (Paţilea et al. 2019). The impact of sea ice concentration is studied in detail in (Paţilea et al. 2019), the findings from the paper show that retrieved sea ice thickness varies relative to the actual ice thickness which in turn depends on sea ice concentration. The paper (Paţilea et al. 2019) also mentions specific examples and ratios like sea ice concentration of 90% at 10 cm ice thickness for which the retrieved sea ice thickness is 8.5 cm. Meanwhile 50 cm ice thickness at 90% sea ice concentration is just 28 cm. Conclusively, all sea ice concentration algorithms show less than 100% SIC for thicknesses below 30 cm (Paţilea et al. 2019). The reason as to why there is no SIC-based correction to the sea ice thickness retrieval is that the the uncertainty of SIC algorithms at high concentration and their covariation at thin thicknesses will cause

high errors. As a result full ice cover is assumed for the SIT retrieval.

2.3 SIC Retrieval Using the ARTIST Sea Ice Algorithm

For the purposes of producing local Maud Rise sea ice concentration maps the ARTIST Sea Ice (ASI) algorithm will be used. Originally adapted for the Advanced Microwave Scanning Radiometer - Earth Observing System (AMSR-E) sensor on NASA's Aqua satellite (Spreen, Kaleschke, and Heygster 2008), it now takes input brightness temperature data from the successor AMSR2 since AMSR-E ceased operations on 04 October 2011. The ASI algorithm has been developed and validated with AMSR-E brightness temperatures and since the successor instrument AMR2 has similar but not identical channels to channel characteristics, coefficients for converting AMSR2 brightness temperatures into equivalent AMSR-E brightness temperatures are used.

The ASI algorithm retrieves SIC from the difference between brightness temperatures at 89 GHz at vertical and horizontal polarizations. This polarization difference is then converted into SIC using pre-determined fixed values for 0% and 100% SIC polarization differences known as tie points. It is known from surface measurements that the polarization difference of the emissivity near 90 GHz is similar for all ice types and much smaller than for open water (Spreen, Kaleschke, and Heygster 2008). At such high frequency (89 GHz for both AMSR-E and AMSR2) atmospheric influence is high also. This effect is dealt with in a bulk correction for atmospheric opacity and by implemented weather filters. Because the Bootstrap (BBA) (Comiso 1986) algorithm uses the 18 and 37 GHz channels which are less sensitive to atmospheric phenomena, it is also used to essentially filter the produced ASI SIC concentration by setting SIC to zero where the Bootstrap algorithm retrieves less than 5% SIC.

Since the sea ice thickness retrieval methods mentioned assume 100% ice concentration, it is of paramount importance to isolate all cases where the ASI algorithm shows below 100% SIC and compare it with the sea ice thickness maps produced. Naturally, as the topic of this paper is polynya study, less-than-100% SIC concentrations are to be expected and although it is not worth completely dismissing sea ice thickness values collected there, it is nevertheless necessary to point out that they may not be accurate and, if possible, access the level of accuracy.

2.4 ERA5 Meteorological Reanalysis Data

ECMWF Reanalysis 5th Generation (ERA5) is a dataset made available by the European Centre for Medium-Range Weather Forecasts (ECMWF) which provides hourly estimates of a large number of atmospheric, land and oceanic climate variables. It was produced using 4D-Var data assimilation in CY41R2 of ECMWF's Integrated Forecast System (IFS), with 137 hybrid sigma/pressure (model)

levels in the vertical, with the top level at 0.01 hPa (Hennermann 2020). Along with covering all these levels, the dataset contains hourly realizations referred to as "reanalysis".

By 'reanalysing' archived observations of the climate, ECMWF creates global data sets describing the recent history of the atmosphere, land surface and oceans via forecast models and data assimilation. ERA5 is the latest climate reanalysis succeeding the previous ERA-Interim (ERA-I). Meteorological reanalysis can be summarised as the combination of models and observations that gives a numerical description of the recent climate.

Campbell et al. 2019 report that there exist a high degree of similarity between six-hourly mean sea level pressure (MSLP) from SANAE-AWS weather station, south of Maud Rise, and the nearest ERA-I grid cell from 1997 to 2019 (r = 0.93; mean absolute deviation = 2.2 hPa; mean bias = 0.8 hPa). On these grounds, ERA-I was deemed accurate for gathering signs of storm activity as it skillfully represented MSLP variability near Maud Rise. Assuming central pressure values below 950 hPa to be indicative of storm activity, it was found that 5.3% of ERA-I sic-hourly MSLP fields feature one or more grid cells below this pressure threshold (Campbell et al. 2019). From the ERA-I reanalysis, it was discovered that anomalous wind speeds coincide with the openings of both 2016 and 2017 Weddell Sea Polynya events (Campbell et al. 2019).

ERA5 is a reanalysis with a much higher temporal resolution than ERA-I. It improves upon its predecessor in terms of information on variation in quality over space and time as well as an improved troposphere modelling. In effect, it should offer a better, or at least identical, assessment of the wind speeds near Maud Rise that are going to be compared with the presented sea ice thickness retrievals.

2.5 Physical Oceanography Data from Mooring

A mooring is a collection of devices mounted on a wire anchored on the sea floor. A mooring implemented by the Alfred Wegener Insititute near Maud Rise (AWI229-13 at 64° S, 0° W Rohardt and Boebel 2019) was deemed as the most relevant and most recent ocean data to which the SIT of early austral spring periods of 2017 and 2018 can be compared to. Having instruments vertically along the water column allows accurate monitoring of water properties like salinity and temperature in reference to any sea ice anomaly nearby. AWI229-13 is predominantly mounted with Sea-Bird Electronic 37 (SBE37) devices able to measure temperature and conductivity (from which salinity can be derived). These devices are externally powered, therefore they can be used for moored applications requiring fast sampling. As a result. the data has a high temporal frequency of a measurement every two hours. In addition to SBE37 every 100 meters starting at 410 m depth, the mooring is also mounted with recording current meters at 310 and 810 m depth respectively. These units, although primarily implemented for current measurements, also have the capability

of measuring temperature and conductivity (Rohardt and Boebel 2019).

Chapter 3

Results

3.1 2017 and 2018 SMOS Sea Ice Thickness Retrievals

After collecting sufficient data on sea ice thickness above Maud Rise, retrievals from September 2018 and September 2017 were chosen as the most compelling example of a recurring sea ice anomaly and the Weddell Sea Polynya, respectively. This section present findings that suggest a previously unrecognized similarity between the two September anomalies.

Fig. 3.1 shows the segment of area directly above Maud Rise (66°S 3°E) chosen for the regional analysis of sea ice thickness. Figure 3.2 shows the SMOS sea ice thickness retrieval in the given segment between 13 and 18 September, 2017. Image `SMOS SIT (20170918)` in figure 3.2 is the section surrounded by the black outline in figure 3.1. The frame of each image, which is a small section of the full standardized SSM/I Polar Spatial Coverage Map extent for which the data is processed, is identical for all images in figure 3.2 and the subsequent figure 3.3. Figure 3.3 shows the sea ice thickness within the segment between 6 September and 4 October 2018. The above maps were generated via SMOS sea ice thickness retrieval as developed by Huntemann et al. 2014.

Notably, in figure 3.3, sea ice as thin as 20 cm can be seen restricted to the region above Maud Rise on multiple days of the same month which, just the year before, featured the biggest Weddell Sea Polynya opening since the 1970s. In 2017, as can be seen in figure 3.2, an identical section of the map is open water surrounded by varying levels of ice thickness. Interestingly, even the shape of the ice thickness anomaly in 2018 is somewhat similar to the shape of the polynya of 2017.

The full satellite image where the SMOS sea ice thickness retrieval algorithm is used has the nominal gridded resolution of 12.5 km with total of 664 rows and 632 columns. The segments shown in Figure 3.3 and 3.2 are rows 100 through 160 and columns 300 through 360 which are ideal for observing any effects on sea ice that the region above Maud Rise might have.

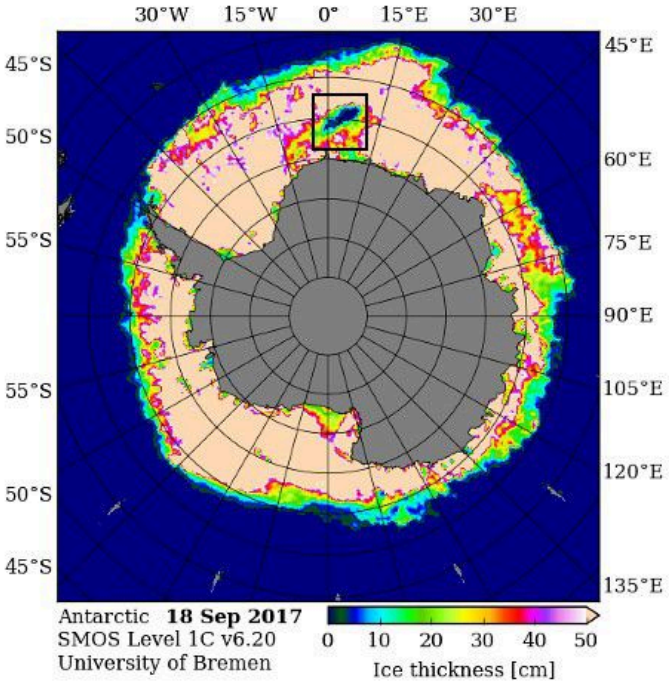

Figure 3.1: SMOS sea ice thickness map retrieved over the entire Antarctic continent on 18 September 2017, the segment in black indicates the area chosen for regional analysis in figure 3.3 [Source: University of Bremen Sea Ice Portal]

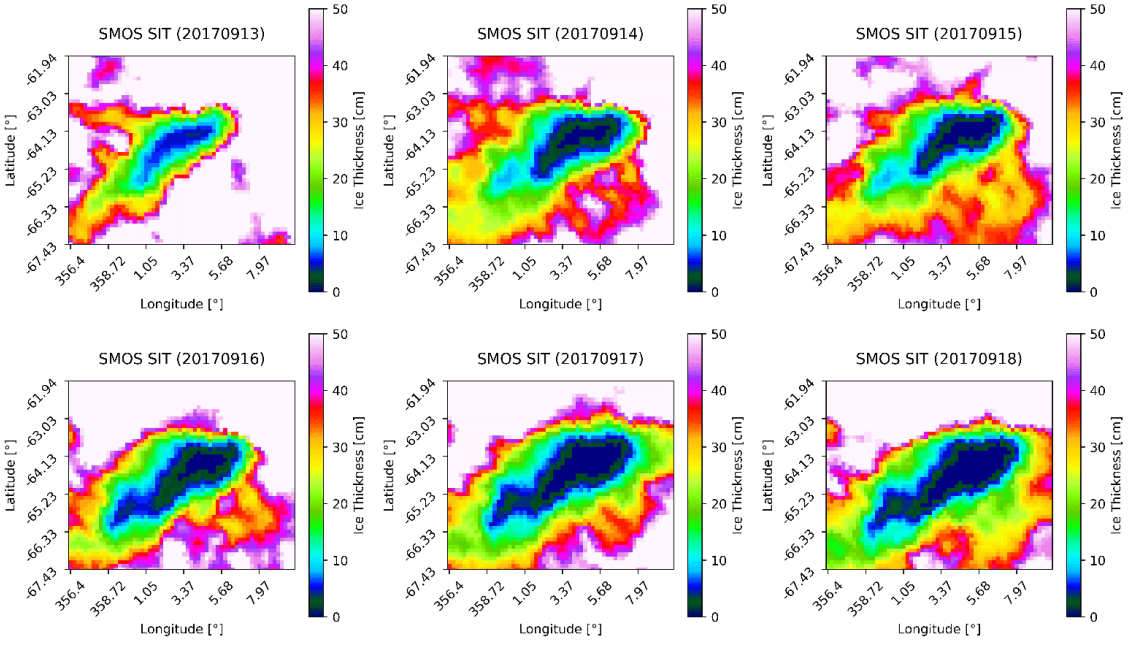

Figure 3.2: SMOS sea ice thickness retrieval above Maud Rise between 13 and 18 September 2017.

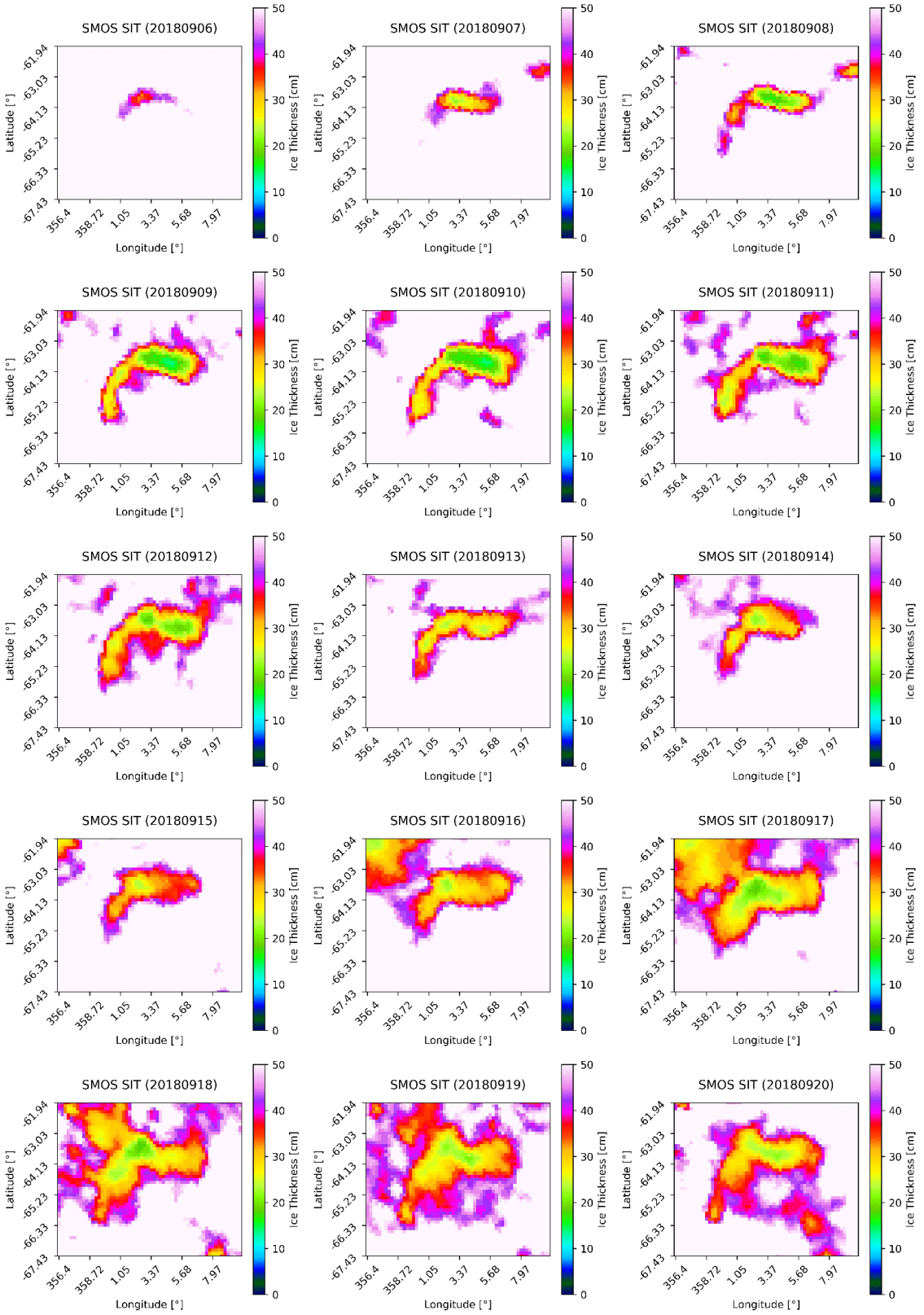

Figure 3.3: SMOS sea ice thickness retrieval above Maud Rise between 6 and 20 September 2018.

3.2 SMOS and combined SMAP-SMOS Retrieval Comparison

Fig. 3.4 shows some of the 2017 SMOS sea ice thickness retrievals accompanied by the combined SMAP-SMOS thickness retrievals as well as ASI sea ice concentration maps from the same dates. Notably, little difference can be observed between the two sea ice thickness retrievals and with reference to the Materials and Methods section, a lot of the segment is filled with sub-100% sea ice concentration as can be seen in the sea ice concentration maps. Worth mentioning is that the ASI algorithm here is used on the nominal gridded resolution of 6.25 km instead of 12.5 km, meaning that the chosen segment (Fig 3.1) although identical in coverage, is twice as many pixels as the sea ice thickness retrievals.

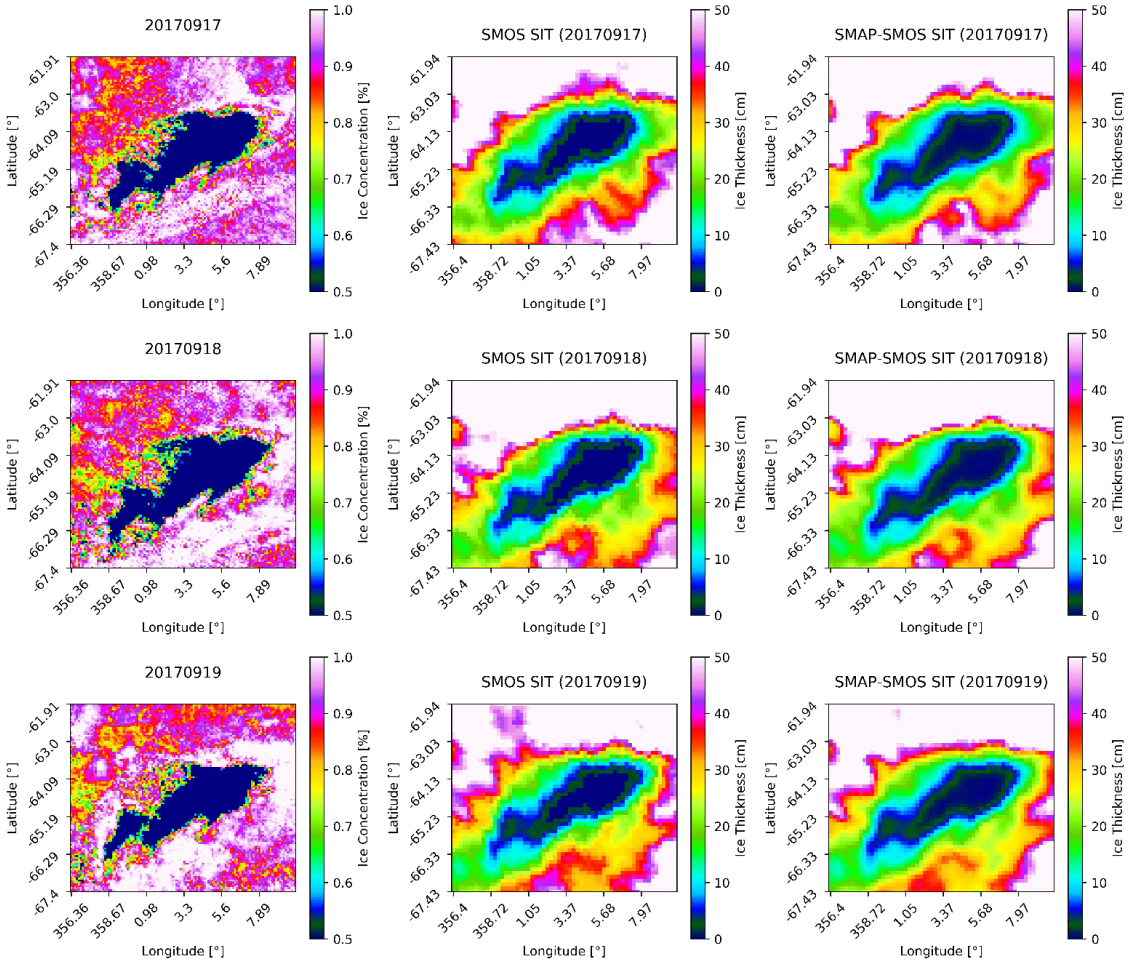

Figure 3.4: 17 September to 19 September, 2017, as seen via the AMSR2 data processed by ASI, SMOS sea ice thickness retrieval and the combined SMAP-SMOS sea ice thickness retrieval, respectively.

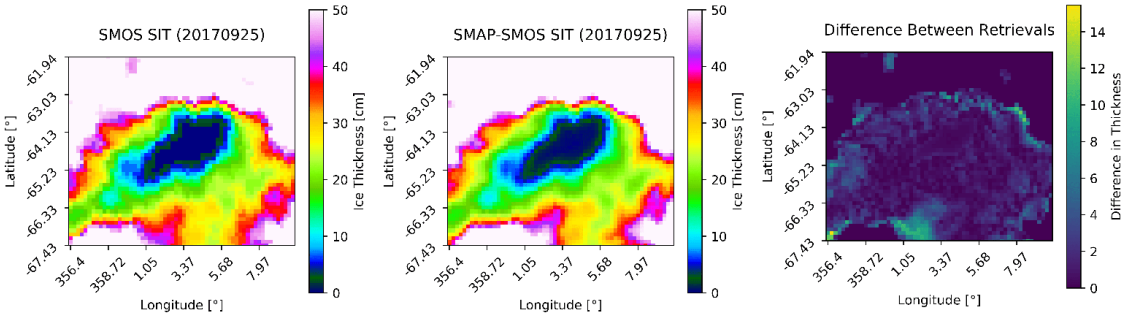

Figure 3.5: 25 September 2017 as seen via the SMOS sea ice thickness retrieval and the combined SMAP-SMOS sea ice thickness retrieval. The rightmost image is the absolute difference per pixel between the two maps to the left.

Figure 3.5 is two different retrievals on 25 September 2017 (date chosen so that the maps shown are comparable to the real-color Blue Marble image shown in figure 1.3), as well as the map showing the absolute difference in thickness between the two (the relevance of the third map will be discussed in the Chapter 4). Figures 3.6 and 3.7 are of the same type but with retrievals taken on 14 September 2017 and 18 September 2018, respectively.

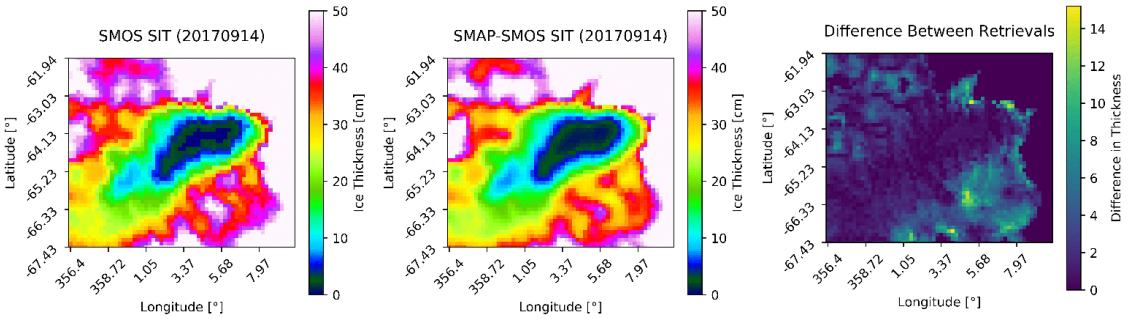

Figure 3.6: 14 September 2017 as seen via the SMOS sea ice thickness retrieval and the combined SMAP-SMOS sea ice thickness retrieval. The rightmost image is the absolute difference per pixel between the two maps on the left.

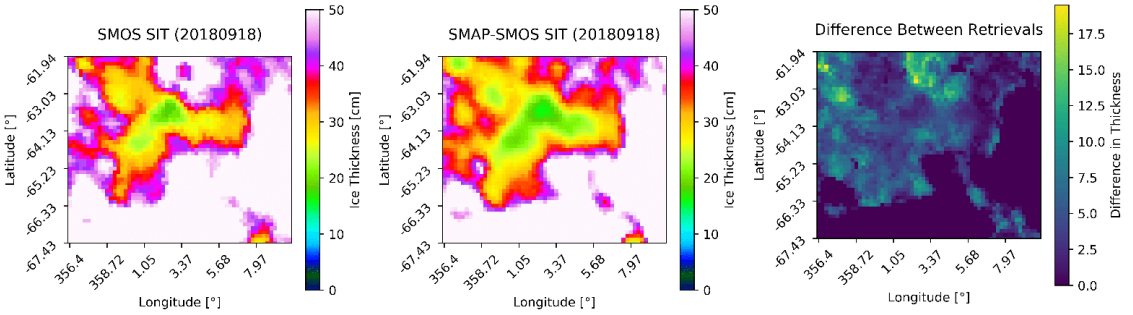

Figure 3.7: 18 September 2018 as seen via the SMOS sea ice thickness retrieval and the combined SMAP-SMOS sea ice thickness retrieval. The rightmost image is the absolute difference per pixel between the two maps on the left.

3.3 Sea Ice Thickness and Concentration Time Series

Below are shown the sea ice thickness and sea ice concentration time series over the dates of interest. Figure 3.8 depicts sea ice concentration derived from AMSR2 data via the ASI algorithm as well as SMOS and SMAP-SMOS sea ice thickness retrieval for August and September, 2018 , respectively. Each different line represents the amount of pixels below a certain threshold thickness (or sea ice concentration) indicated in the respective legend. Figure 3.11, like figure 3.8, is the same type of plot covering the months August and September of 2017.

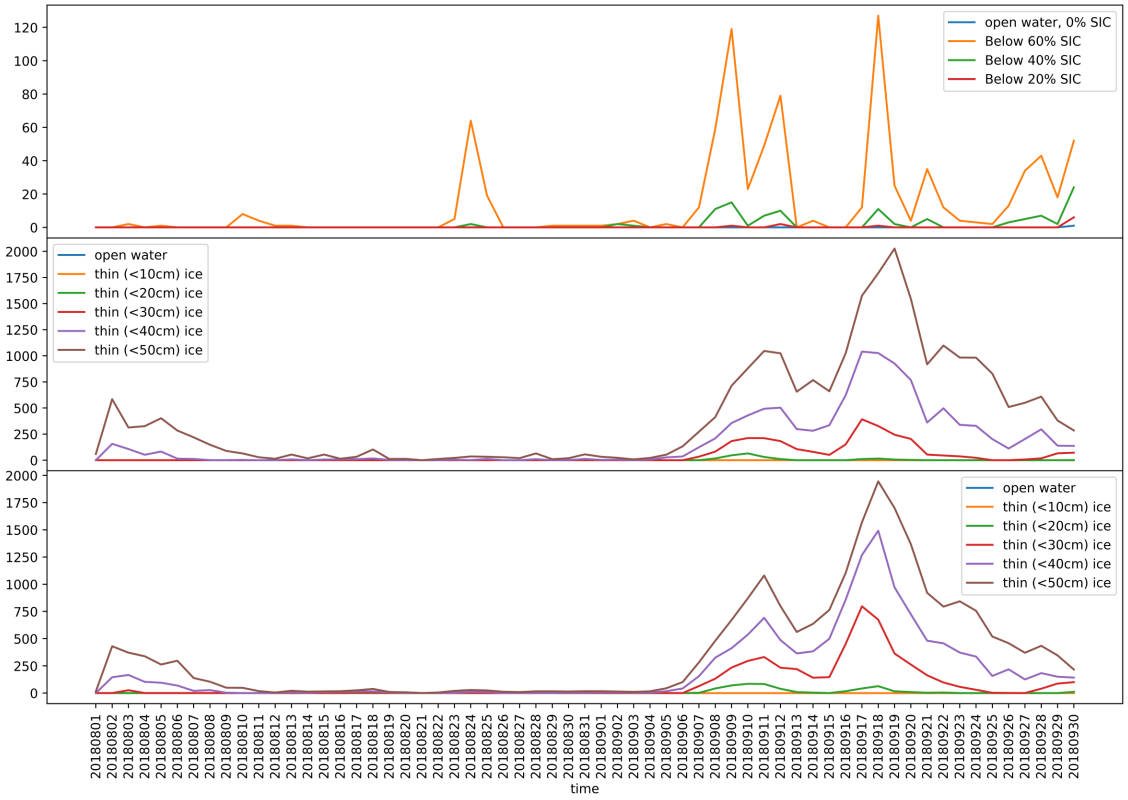

Figure 3.8: From top to bottom: ASI sea ice concentration, SMOS sea ice thickness retrieval and SMAP-SMOS sea ice thickness retrieval, respectively. All data covers the time range 1 August to 30 September 2018.

The sea ice anomaly, partially observed in sea ice thickness maps in figure 3.3, can be clearly seen forming, reaching a peak, and dissipating during September 2018 in the sea of thickness plots from figure 3.8. Corresponding peaks, albeit of a much smaller magnitude, can be observed also in sea ice concentration maps. Analysing the main peak of the anomaly with all three of the aforementioned retrievals, figure 3.9 is obtained.

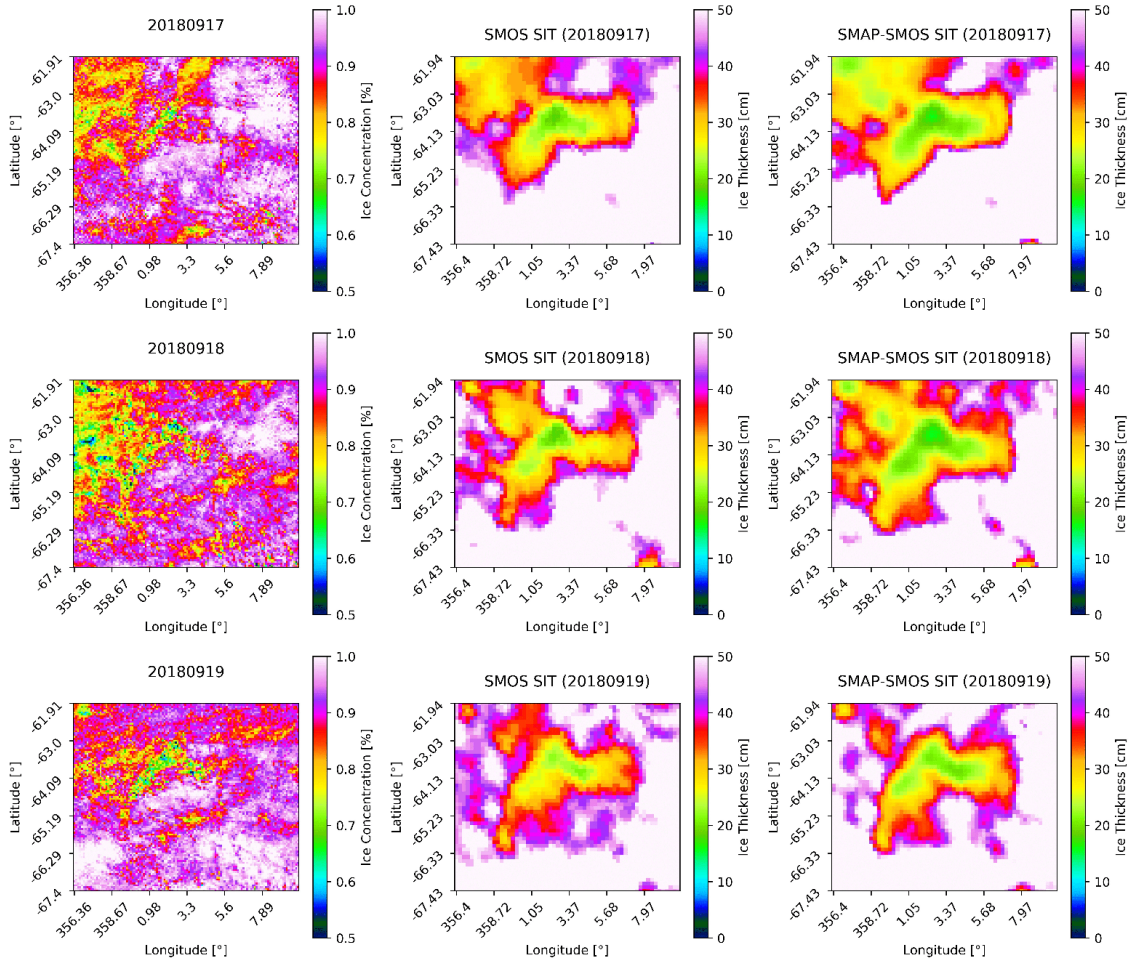

Figure 3.9: 17 September to 19 September, 2018, as seen via the AMSR2 data processed by ASI, SMOS sea ice thickness retrieval and the combined SMAP-SMOS sea ice thickness retrieval, respectively.

Sea ice concentration maps depict a low sea ice concentration area northwest of the region while sea ice thickness maps are predominantly showing low sea ice thicknesses directly north of Maud Rise, much like the polynya from 2017. The sea ice concentration anomaly eventually culminates into the halo (ring-shaped feature) of low sea ice concentration described in (Lindsay, Holland, and Woodgate 2004). The halo, as can be seen in figure 3.10, is smaller than the standard Maud Rise Polynya and exhibits some characteristics of a lead.

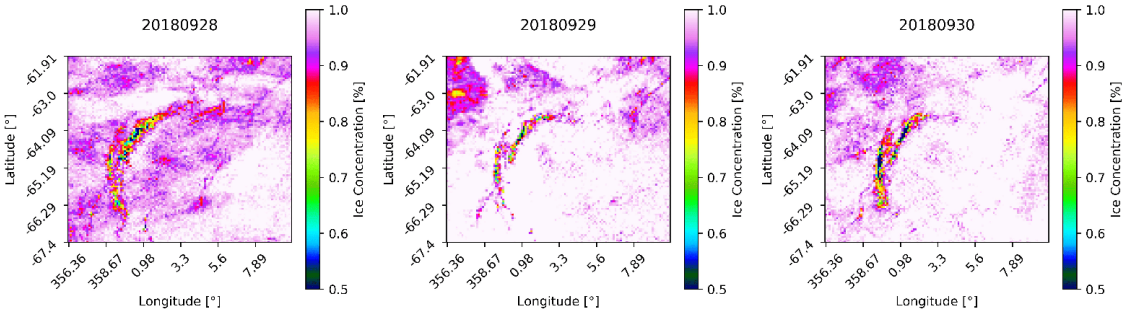

Figure 3.10: The low sea ice concentration halo observed 28 September to 30 September, 2018, as seen via the AMSR2 data processed by ASI.

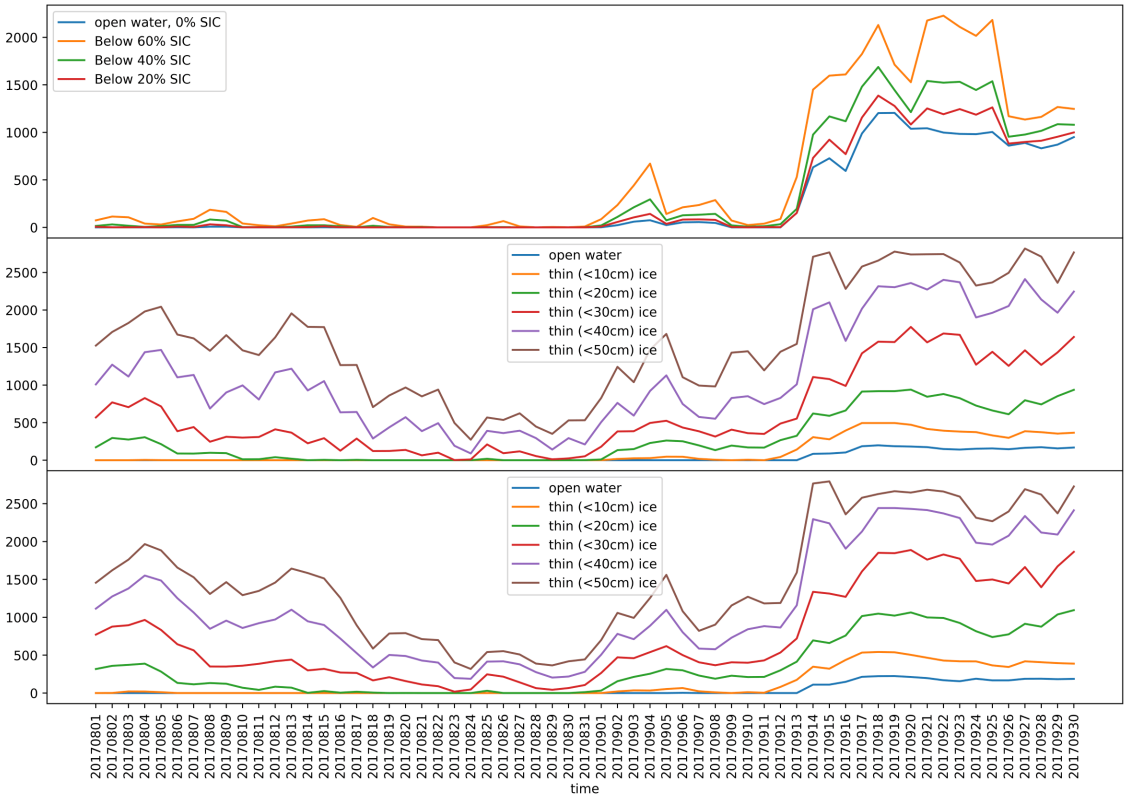

Figure 3.11: From top to bottom: ASI sea ice concentration, SMOS sea ice thickness retrieval and SMAP-SMOS sea ice thickness retrieval, respectively. All data covers the time range 1 August to 30 September 2017.

3.4 Storm Data Comparison

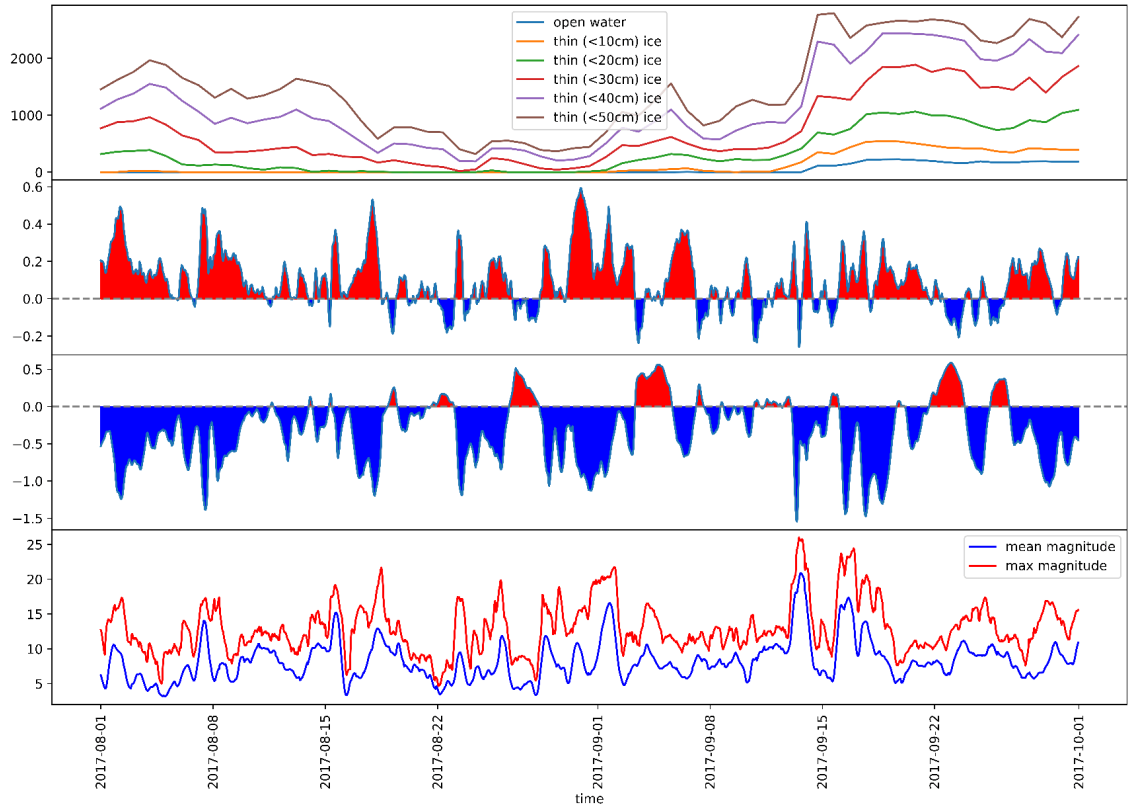

Figure 3.12: From top to bottom: SMAP-SMOS sea ice thickness retrieval as well as wind curl [m/s^2], divergence [m/s^2], mean and maximum magnitude [m/s] during the months August and September 2017 derived from ERA5 data at 1000 hPa. Plots derived from ERA5 data are compared with the SMAP-SMOS SIT retrieval from the same time range.

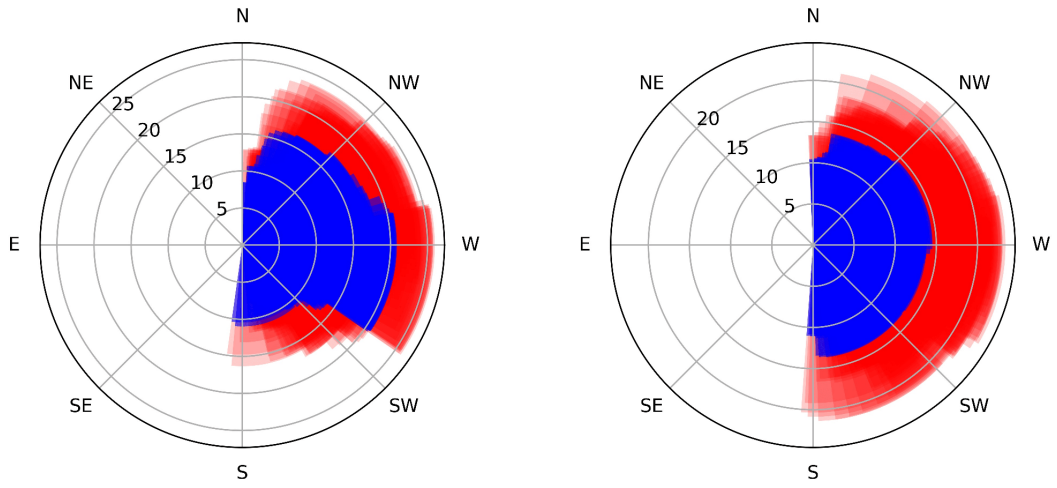

Figure 3.13: Wind direction and magnitude throughout August and September 2017 (left) and 2018 (right), respectively, where red indicates the maximum wind speed and blue the mean.

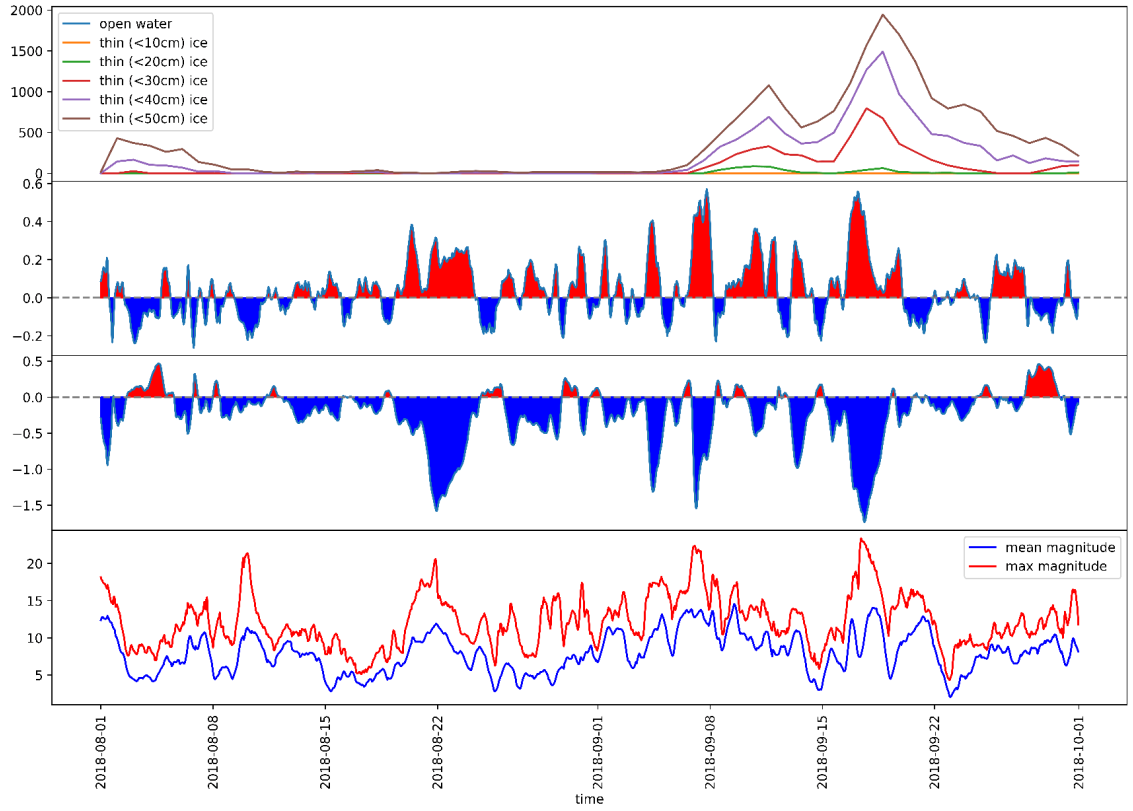

Figure 3.14: From top to bottom: SMAP-SMOS sea ice thickness retrieval as well as wind curl [m/s^2], divergence [m/s^2], mean and maximum magnitude [m/s] during the months August and September 2018 derived from ERA5 data at 1000 hPa. Plots derived from ERA5 data are compared with the SMAP-SMOS SIT retrieval from the same time range.

Wind reanalysis data from August and September 2017 (Fig. 3.12) shows a particularly stormy month with wind speeds of above 20 m/s specifically around the time when the 2017 Weddell Sea Polynya opens. A positive mean curl can be noted to be leading up to the event and an overall negative mean divergence in the wind vector field. The SMAP-SMOS sea ice thickness retrieval plot is the same as the third plot in figure 3.11. Figure 3.13 shows both the wind direction and magnitude throughout the period of interest from both 2017 (left) and 2018 (right). Notably all winds above 25 m/s are blowing from the west in 2017. The 2018 wind direction and magnitude plot shows a more broad distribution of 20 m/s winds blowing from the North, West and South. The plot for 2018 (Fig. 3.14) shows calmer months with wind speeds reaching 20 m/s. The effects of wind curl and convergence seem to directly match the low sea ice thickness peaks in the SMAP-SMOS sea ice thickness retrieval plot of that year (identical to the third plot in Fig. 3.8).

3.5 2016 and 2019 as compared to 2017 and 2018

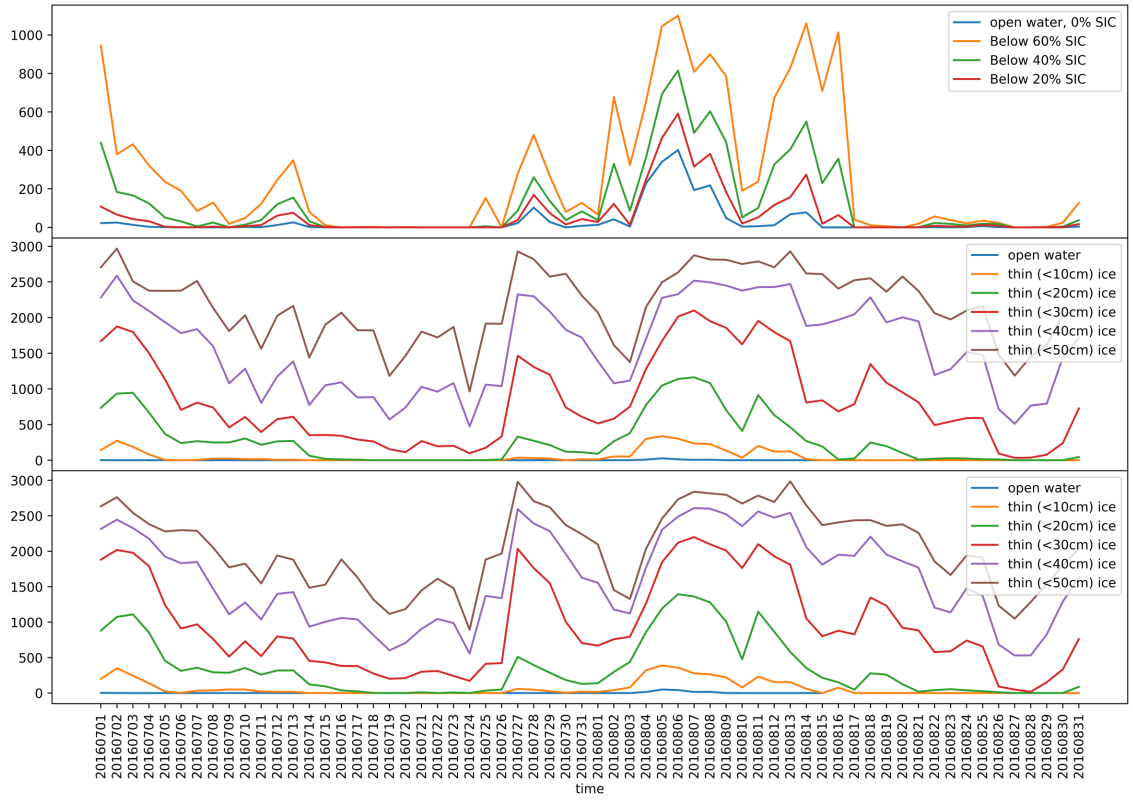

Figure 3.15: From top to bottom: ASI sea ice concentration, SMOS sea ice thickness retrieval and SMAP-SMOS sea ice thickness retrieval, respectively. All data covers the time range 1 July to 31 August 2016.

The 2016 polynya occurred in August; specifically August 3rd. This is captured well in the ASI sea ice concentration plot in Fig. 3.15. In the days leading up to the event, the sea ice concentration data also shows extremely low concentrations as well as areas of open water towards the end of July suggesting preconditioning activity. The sea ice thickness data, the latter plots in Fig. 3.15, show a similar trend as the sea ice concentration plot except for more similar behavior between the early August polynya and the late July opening in terms of ice above 20 cm thick. Months July and August were chosen for 2016 so as to observe the polynya that formed early in August as well as any and all preconditioning events leading up to it. Early July depicts low sea ice concentration for the region which is simply last phase of the freeze-up in the region since, in the month of June, the area still has open water leftover from before the austral winter.

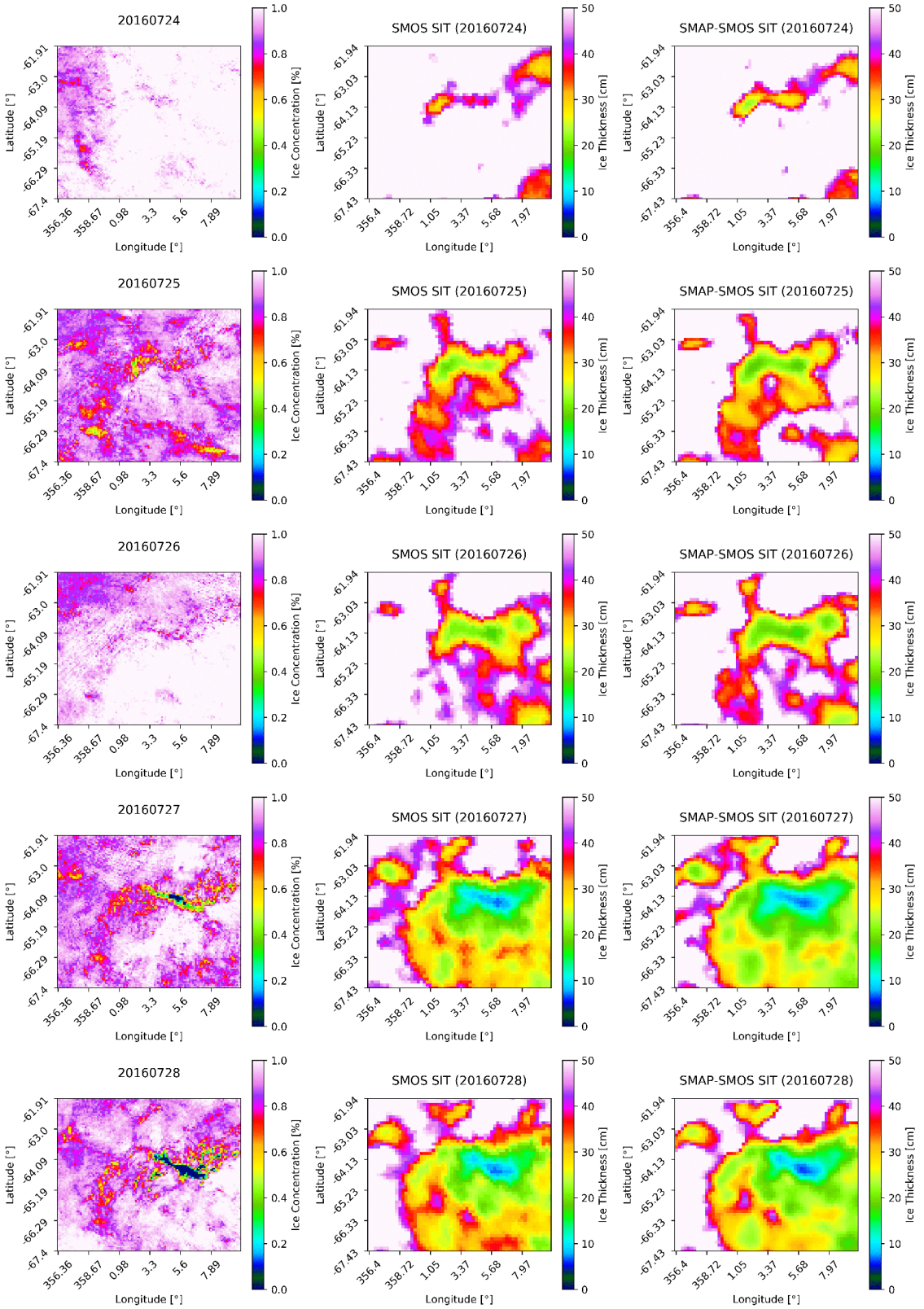

Figure 3.16: 24 July to 28 July 2016 as seen via the AMSR2 data processed by ASI, SMOS sea ice thickness retrieval and the combined SMAP-SMOS sea ice thickness retrieval, respectively.

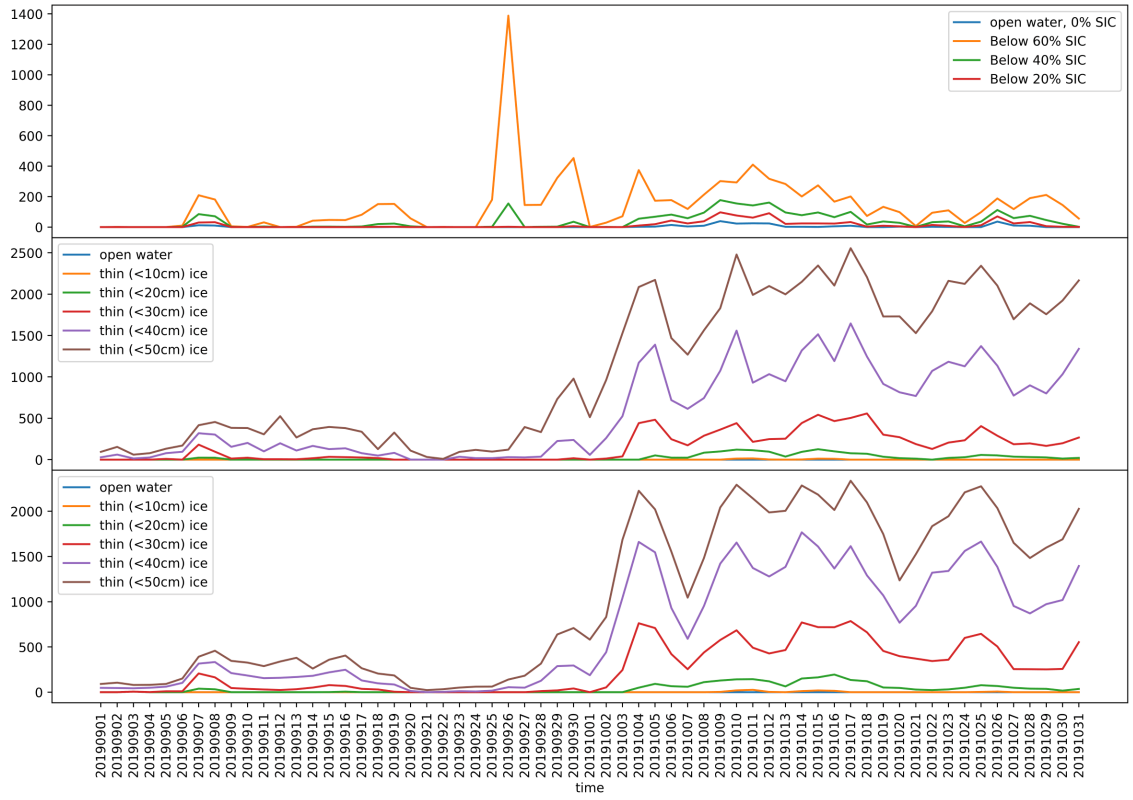

Figure 3.17: From top to bottom: ASI sea ice concentration, SMOS sea ice thickness retrieval and SMAP-SMOS sea ice thickness retrieval, respectively. All data covers the time range 1 September to 31 October 2019.

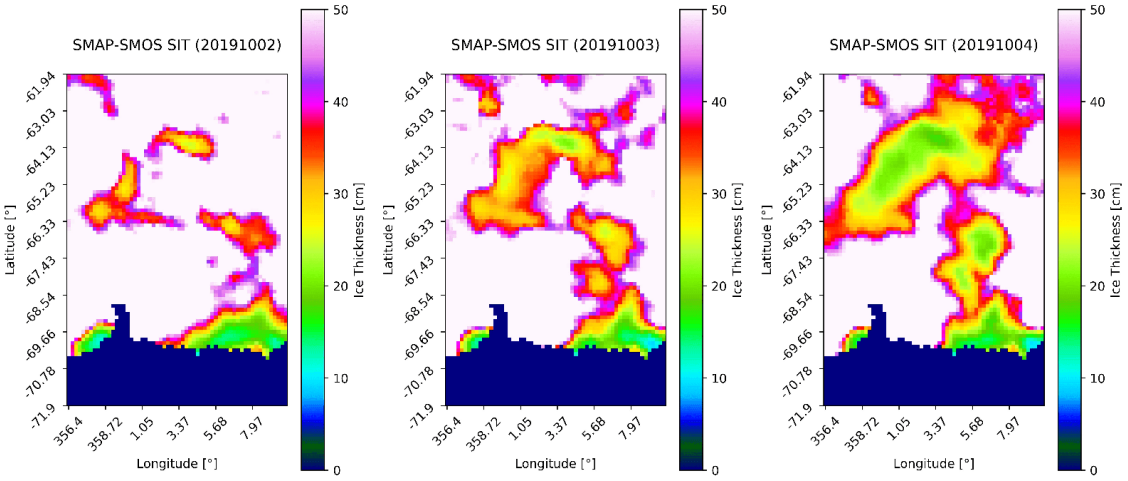

Figure 3.18: 2 October to 4 October 2019 as seen the combined SMAP-SMOS sea ice thickness retrieval

In 2019 the sea ice concentration data shows a pronounced peak of low sea ice concentration late September that seems to trigger a period of low sea ice thickness for the days to come (Fig. 3.17).

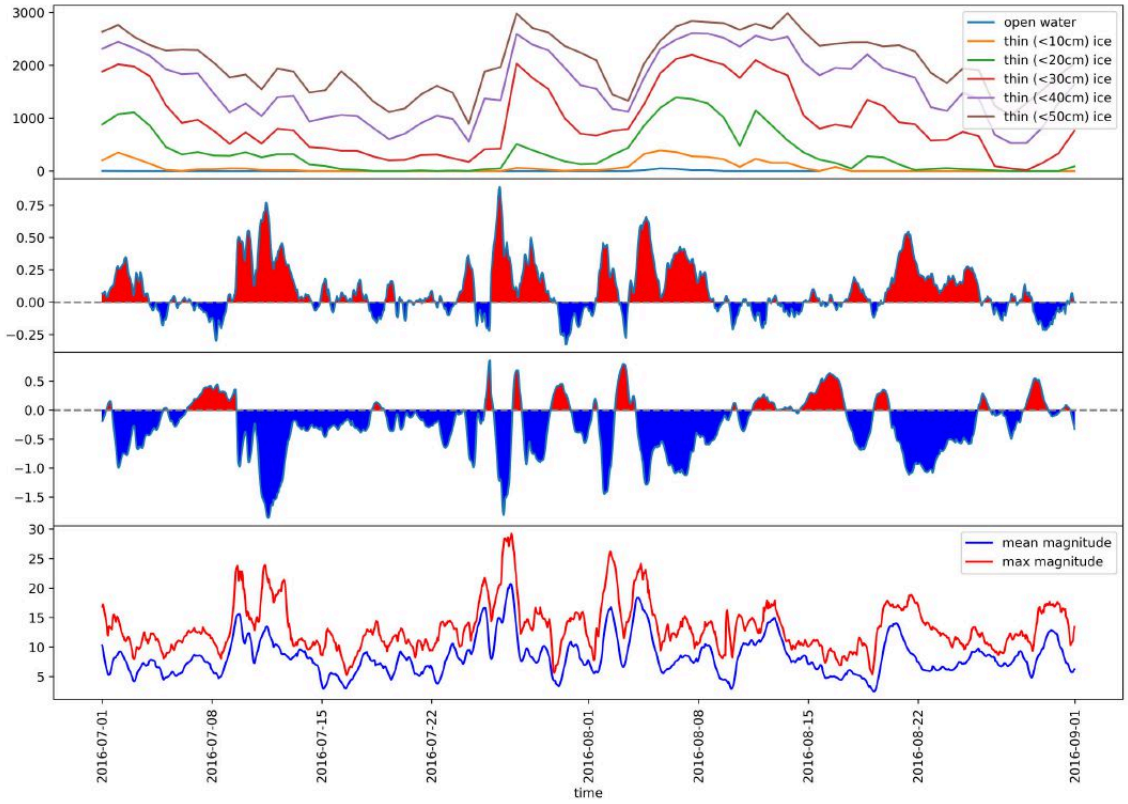

Figure 3.19: From top to bottom: SMAP-SMOS sea ice thickness retrieval as well as wind curl [m/s^2], divergence [m/s^2], mean and maximum magnitude [m/s] during the months July and August 2016 derived from ERA5 data at 1000 hPa. Plots derived from ERA5 data are compared with the SMAP-SMOS SIT retrieval from the same time range.

Interestingly, the main preconditioning event at the end of July 2016 aligns with the most anomalous wind activity where the curl is increasingly positive and the divergence is negative Fig. 3.19. Most intuitive is the correlation between the initial peak and wind speed magnitude: the highest magnitude of the 2 months period just barely precedes the late July anomaly. The 2019 wind data Fig. 3.20 depict interesting effect where positive wind curl in the region coupled with negative divergence and high wind speeds seems to have initiated some type of ice thinning early September. This thinning then continues for several days to come until it goes away only to come back such that it covers a much wider perimeter and remains until the melt season of that year. Both direction plots (Fig. 3.21) show strong Eastward wind as is typical for the region, with 2016 having little to no Southern component and 2019 containing winds Southeast and Northeast as well as East.

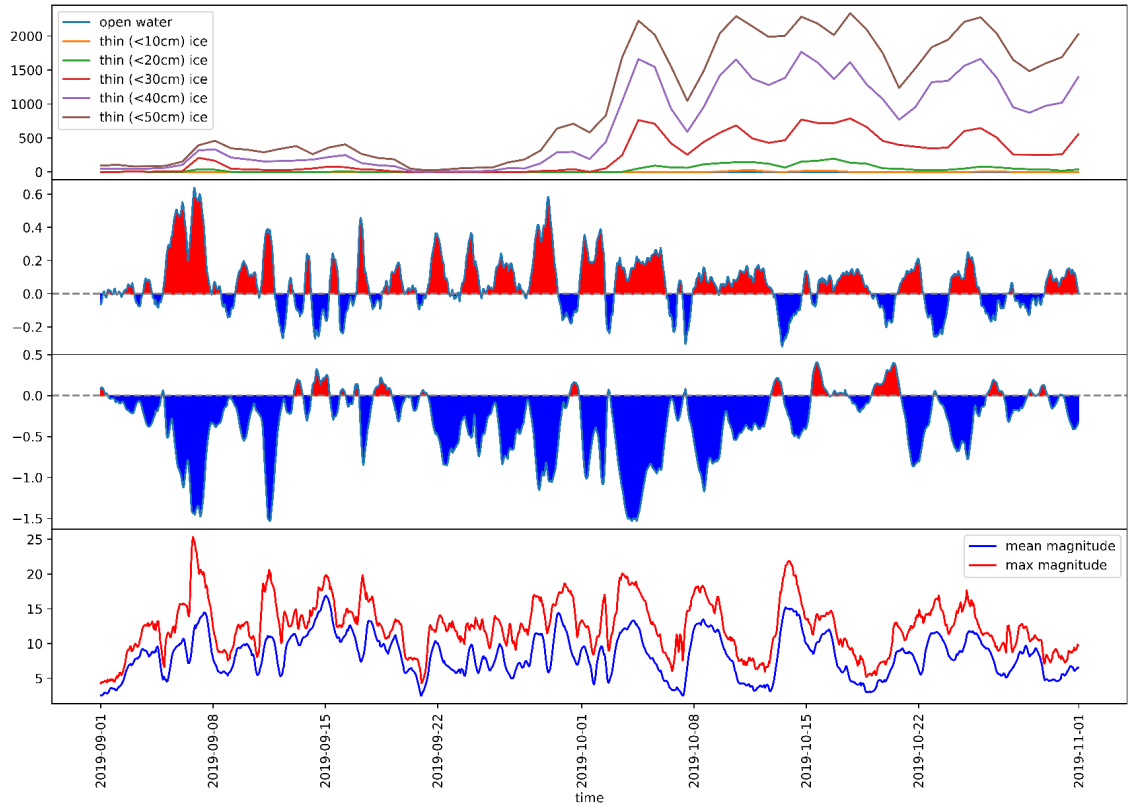

Figure 3.20: From top to bottom: SMAP-SMOS sea ice thickness retrieval as well as wind curl [m/s^2], divergence [m/s^2], mean and maximum magnitude [m/s] during the months September and October 2019 derived from ERA5 data at 1000 hPa. Plots derived from ERA5 data are compared with the SMAP-SMOS SIT retrieval from the same time range.

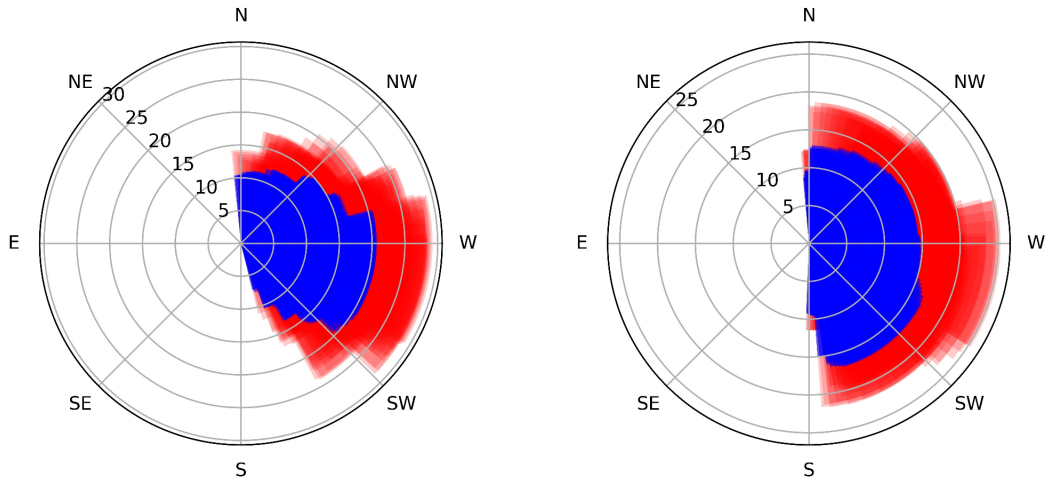

Figure 3.21: From left to right: Wind direction and magnitude 1 July to 31 August 2016 and 1 September to 31 October 2019, respectively, where red indicates the maximum wind speed and blue the mean.

3.6 Ocean Data Comparison

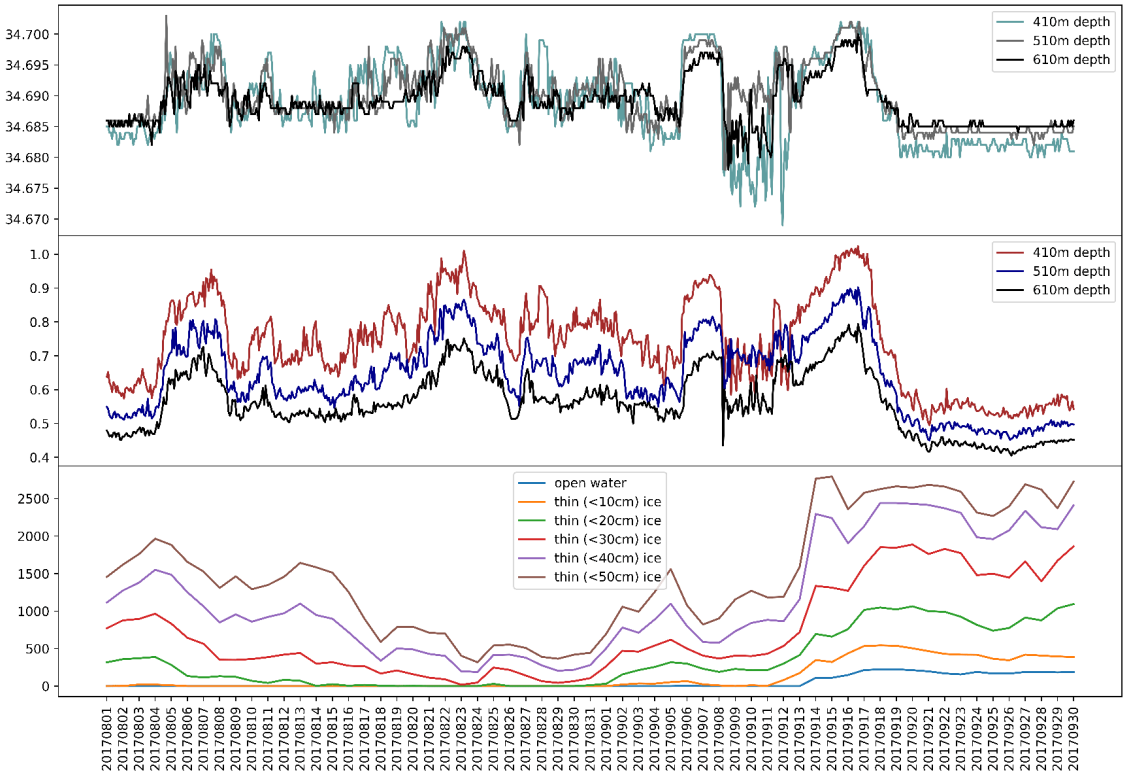

Figure 3.22: Ocean salinity [psu] and temperature [°C] at 64° South along the prime meridian for August and September 2017 collected at mooring AWI229-13. Plots produced from the mooring data are compared with the SMAP-SMOS SIT retrieval from the same time range.

From the plot Fig. 3.22 one can see that the 2017 polynya opening is heavily influenced by the anomalous behaviour of the underlying water during the days leading up to it. Not only can it be seen that both surface salinity and temperature (at 310 and 310 m depth respectively) plummet (on 8 September 2017) before the opening of the polynya on 13 September, 2017, but there is also a an increase that can be seen in the wide temperature and salinity peak (12-21 September 2017) of the time range that accompanies the opening. Lastly, one can see both the temperature and salinity values equilibrating to fixed values after the polynya has opened.

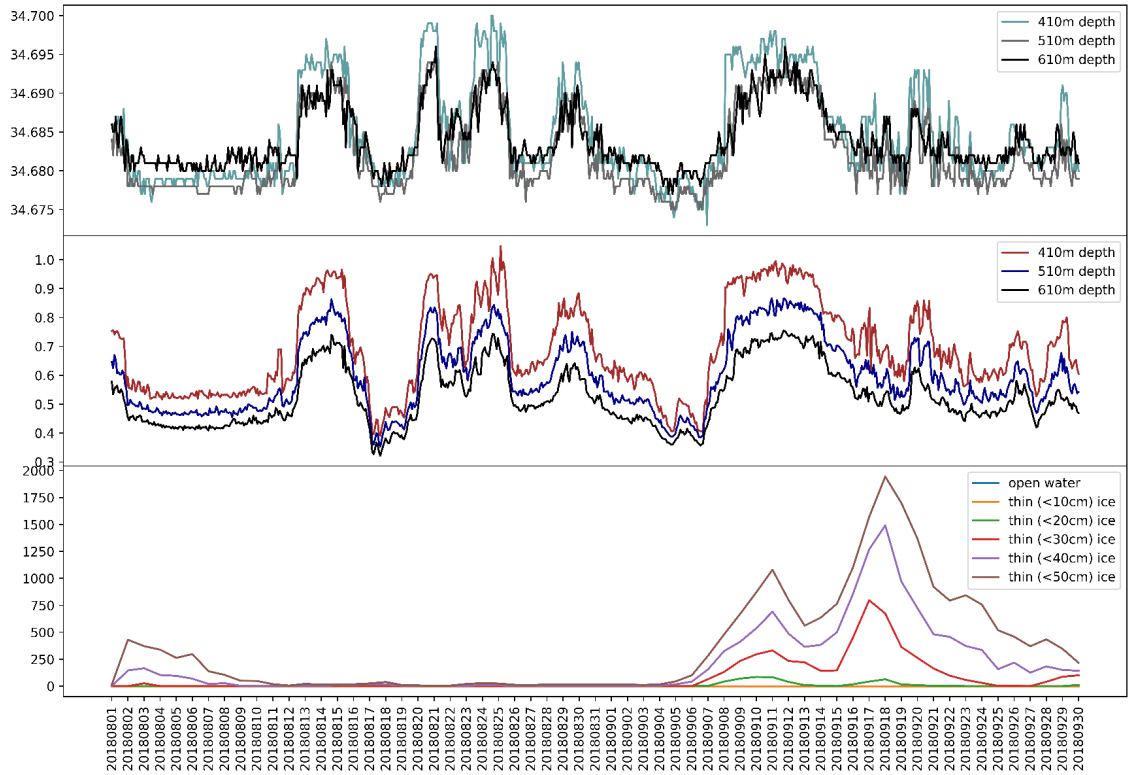

Figure 3.23: Ocean salinity [psu] and temperature [°C] at 64° South along the prime meridian for August and September 2018 collected at mooring AWI229-13. Plots produced from the mooring data are compared with the SMAP-SMOS SIT retrieval from the same time range.

The 2018 plot (Fig. 3.23) shows how the longest high salinity and high temperature peak occurs just a couple of days before the major sea ice anomaly of 2018. Interestingly, the record high temperature of above 1°C at 410 m depth (25 August 2018) seems to have no effect on sea ice most likely due to how brief it is. Comparing the data to 2017, a strong similarity between the 2017 post-polynya decrease in temperature and salinity can be seen at all depths without any sporadic behaviour as in the brief period following the small sea ice anomaly at the start of August 2018.

Chapter 4

Discussion and Outlook

First and foremost, without discussing particular cases, this research has shown that Sea Ice Thickness (SIT) retrieval is an able candidate for Weddell Sea Polynya research. The ability to isolate thinner ice from thick pack ice has proven itself to be able to measure preconditioning events prior and post polynya occurrences, measure sea ice anomalies not evident in sea ice concentration retrievals and access the true scale of polynya event sea ice anomalies by including the wide thin ice rim surrounding each event. In addition to these individual milestones, the findings presented in the result (Chapter 3) show compelling evidence of anomalous behaviour in sea ice above Maud Rise made possible through SIT retrievals of the region. The finding of such anomalies help demystify the apparent dormancy between 1976 and 2016 by showing that the region is prone to anomalous events even in years without any notable polynya occurrences. The data responsible for these findings as well as accompanying data from sea ice concentration retrieval, ERA5 reanalysis data and mooring data, will be thoroughly discussed in this Chapter.

4.1 2017 Weddell Sea Polynya Revisited

Perhaps the best starting point for the discussion of sea ice thickness analysis of the 2017 polynya event is the figure comparing ASI sea ice concentration to SMOS SIT retrieval and SMAP-SMOS SIT retrieval respectively (Fig. 3.4). First point of discussion, in view of the SIT retrieval 100% ice concentration assumption discussed in the Materials and Methods chapter, is the ASI sea ice concentration is predominantly below 100% and thus the SIT values are more commonly less than what is shown. From ratios taken from Paţilea et al. 2019, it is known that at 90% sea ice concentration the SMAP-SMOS SIT retrieval should, in principle, retrieves only 28 cm due to how much sea ice concentration influences SIT retrievals. Even so, from the individual maps in Fig. 3.4 thin sea ice can be seen concentrated around the polynya whereas below 90% sea ice concentration is not. In other words, while this dependency on sea ice concentration may be prevalent, sea ice

thicknesses far from the polynya are sufficiently large (presumably 1-2 m thickness as expected for regular pack ice in the region) such that low sea ice concentration has no effect on the SIT. This effect can be best observed in the Northwest portion of the maps presented in Fig. 3.4.

An interesting observation that is perhaps not so obvious in view of the chosen segment (Fig. 3.1) is the shape of the low sea ice thickness rim around the polynya. For the purposes of analysing the thin sea ice anomalies a bigger segment was not needed for this research and yet even individual maps and the sea ice thickness retrieval from 18 September 2017 of the entire Antarctic continent (Fig 3.1) show the polynya with a tail of thin ice pointing westward. Notably, the Antarctic Circumpolar Current (ACC) that more or less drags the ice layer along with it each austral winter, flows clockwise and yet this thin sea ice extension of the Weddell Sea Polynya seems to extend westward upon the formation of the polynya. The extension can best be seen in the maps from 13 September to 18 September in 2017 that marks when the Weddell Sea Polynya first appeared that year (Fig. 3.2). Effectively, the polynya itself forms a Southwestward branch and the low sea ice thickness tail continues as far as 15°W on the 18th of September 2017 as can be seen in Fig. 3.1. Presumably, this effect is simply the result of the lesser known Antarctic Subpolar Current (ASC) that flows counterclockwise much closer to the Antarctic continent than the ACC.

August and September of 2017 were chosen as the prime months for data analysis. The reason is that September marks the month when the polynya opened and August, along with the first half of September, should be the best time of observing any preconditioning effects that were present. Fig. 3.11 depicts the time series of sea ice concentration and sea ice thickness. The method by which these plots were produced is simple in that the region highlighted in Fig. 3.1 is simply scanned for all pixels below a given threshold and said pixels make up the total value of each day presented in the plot

Looking at the plot Fig. 3.11, which is further subdivided into ASI sea ice concentration, SMOS SIT and SMAP-SMOS SIT (see figure caption), not much is happening on the sea ice concentration plot leading up to the opening of the polynya on 13 September 2017. Meanwhile the SIT record shows an ice thinning comparable to the polynya in magnitude already at the start of August followed by a brief peak in early September that is corroborated by the sea ice concentration record. Interestingly, even during the polynya period there is a difference in behaviour between sea ice concentration and SIT. The SIT retrieval has the highest below-50-cm SIT peak upon the formation of the polynya whereas low sea ice concentrations only reach their first peak on 18 September similar to the <10 and <20 SIT peaks which are most likely heavily influenced by the low sea ice concentration rim of the polynya. Furthermore, low sea ice concentrations disappear to give way to open water (0% sea ice concentration line) on 26 September whereas sea ice thickness maintains a relative stability further solidifying the notion the SIT retrieval is a stand-alone variable and not a low sea ice concentration proxy.

Without cross-referencing with ocean and wind data, some preliminary conclusions that one

could come to are that the preconditioning effect of the early September peak seems to play an important role in the creation of the polynya some days after and that the polynya seems to equilibrate to a fixed size after its sporadic opening. The early September peak has a shift in maxima between the sea ice concentration and SIT plots of about 1 day, with the peaks at 4 and 5 September respectively. This could suggest some type of lead opening, the low sea ice concentrations from this event further increasing the low SIT pixel count. A lead opening would be enough to facilitate the cooling of the surface water layer and as this cooled water then sinks in the non-stratified Antarctic water, a convection cell would form that brings relatively warmer Circumpolar Deep Water to the surface. This hypothesis borrows from the conclusion by Heuzé and Lemos 2020. This warmer water would facilitate the melting of the overlaying thin sea ice (as thin as 20 cm according SIT retrieval) which would effectively open the polynya. Once the polynya is open there are several reasons as to why the its size would equilibrate as opposed to entering a positive feedback loop. Since Maud Rise is in part the reason why the Polynya occurs it is logical to assume that its vicinity more or less predetermines what is known as the Maud Rise Polynya (the subcategory of the Weddell Sea Polynya localized over Maud Rise e.g. 2016 and 2017 Weddell Sea Polynyas). The Taylor cap atop Maud Rise should facilitate a stable convection cell by mitigating orthogonal flow (water flowing perpendicular to the Taylor column). As a result, the convection cell partially responsible for the opening and more and importantly the maintenance of the polynya is limited to Maud Rise unless external forcing drives it to engulf larger regions of the Weddell Sea like in 1974 to 1976. In the absence of such forcing or more specifically the not fully understood ideal conditions for the Weddell Polynya (the subcategory of the Weddell Sea Polynya that spans beyond the Maud Rise e.g. 1974, 1975 and 1976), the Maud Rise polynya is obtained. With a fixed equilibrium size the polynya maintained itself until the melt season of 2017 and did not re-emerge in 2018.

4.2 2018 Sea Ice Anomaly

While the mystery as to why the Weddell Sea Polynya did not occur in 2018 has been long debated (Cheon and Gordon 2019), it is nevertheless of interest to study what actually did occur in 2018. Roughly on the same day of the year as the Weddell Sea Polynya first opened in the previous year, a major sea ice anomaly is forming and taking the shape of the Maud Rise Polynya (Fig. 3.3). While to attribute this event to some annual regularity would be untrue it is apparent that the effects of the polynya from the previous year did not fully dissipate in 2018. Fig. 3.8 captures the time span over which anomalous activity occurred. From the sea ice concentration plot a low sea ice concentration, as low as 40%, can be seen localised to the sea ice anomaly region which is clearly defined by the SIT retrieval. The SIT retrieval depicts how long the said anomaly prevailed, starting small on 5 September and diminishing in late September, reaching a peak on 18 or 19 September 2018 (the exact date is unclear as SMOS and SMAP-SMOS retrievals don't seem to

agree on when exactly the <50 cm and <40 cm SIT peaks were). Looking at Fig. 3.9 the low sea ice concentration values can be seen to be localized predominantly in the Northwestern corner of the segment of interest as defined by Fig. 3.1. Conversely both SMAP-SMOS and SMOS SIT retrievals depict low SIT values at the center of the map, where the year before the 2017 Weddell Sea Polynya opened. Acknowledging the effect of low sea ice concentration on SIT retrieval, it is apparent that although low sea ice concentrations are recorded in the Northwestern sections of the map, the average SIT there is sufficiently above the 50 cm thickness such that erroneous SIT values are avoided for the most part. Notably SMAP-SMOS SIT retrieval in this particular example seems to be more susceptible to this effect especially on 18 September 2018. Looking back at Fig. 3.3 not only retains its relative shape at peak low SIT as depicted in Fig. 3.9 but also begins as a localized wide area region of sea ice as thin as 20 cm (as can be seen on days 8, 9 10 and 11 September 2018).

Conclusively, there was an anomaly in 2018 and it was to a degree an after effect of the 2017 Weddell Sea Polynya much like how the Maud Rise Polynya of 1973 influenced the Weddell Polynya of 1974. From the sea ice record alone, it is inconclusive as to how or why this effect is observed. Save for the anomaly itself, Fig. 3.8 shows an apparent low sea ice concentration peak that occurs on 24 August 2018 and low SIT values throughout early August 2018. Importantly, SIT analysis offers a much clearer view of this anomaly with a fixed beginning and an end. While a higher density low sea ice concentrations is observed in the general region, this effect does not seem to be continuous nor localized. The so-called low sea ice concentration halo can be observed in late September as shown in Fig. 3.10 and it seems to be product of the several days of preconditioning as can be seen in the SIT record. The formation of the anomaly (Fig. 3.3) mirrors the expansion of the polynya (Fig. 3.2) of the previous year and it can be assumed that some essential force was not present this time around to effectively open the polynya and thereby cool the upper layer for the convection cell to form atop Maud Rise.

4.3 2016 Weddell Sea Polynya Revisited

In 2016, the sea ice record (Fig. 3.15) shows low sea ice concentration in early July as that is more or less when the area froze over, and a month later the formation and disappearance of the 2016 Weddell Sea Polynya. Most interesting perhaps is late July and Early August (24 July 2016 to 3 August 2016). After undulation in the SIT record, the highest peak since the early July freeze-up can be seen forming alongside a small peak in low sea ice concentrations. At that point, it is reasonable to assume that this small opening regardless of how it occurred was subject to the frigid atmospheric conditions of the Antarctic and was therefore short-lived. 3 August marks a local minimum in both SIT and sea ice concentration (of the extent of thin sea ice and low sea ice concentrations respectively) and is when this minor polynya is effectively gone only to come back

the next day bigger than it has been for the last 40 years.

As with 2017 and even the 2018 sea ice anomaly covered in previous sections, this is a clear example of low SIT areas facilitating the opening of leads and smaller polynyas which in turn seem to have a direct impact on wider scale sea ice anomalies and the Weddell Sea Polynya events that follow. The hypothesis presented in this paper, as with the 2017 and 2018 cases, is that warm deep water is introduced via convection as the top layer is exposed to the cool Antarctic air. This hypothesis will be further discussed as well as partly verified in the section covering oceanic influence on ice thinning. While analyzing the SIT and sea ice concentration data alone offers little that is conclusive in terms of the underlying causes of the event itself, it is perhaps the best medium for observing what actually happens.

Fig. 3.16 depicts the initial smaller polynya and its formation in terms of sea ice concentration and SIT. Covering the range of days 24 to 28 July (Fig. 3.16) is a large portion of the first peak occurring in late July shown in (Fig. 3.15). Notably, as can be seen from the maps, first there is preconditioning in the form of thin ice in the direct region and a soon after low sea ice concentrations follow. This can be best be explained as an external forcing inducing the thinning of the ice layer which becomes more susceptible to breaking apart and exposing open water (the origins and type of forcing shall be discussed in the following sections). As a result, it is likely that this first peak is what facilitated the Weddell Sea Polynya of 2016.

4.4 2019 Sea Ice Anomaly

2019 (Fig. 3.17) is different to the other three examples in this paper as it is the least noteworthy of all when it comes to anomalous activity in the Maud Rise region. Even so, by looking at the months of September and October, an interesting phenomenon can be observed. Instead of episodes of low SIT leading up to low sea ice concentration on the 26 of September 2019, there is what appears to be a low sea ice concentration peak, which in principle could signify a lead, that triggers a much longer episode of low SIT in the region. The low SIT ice dominates the region until the melt season of that year.

20 days earlier, there is a minor event that acts much the same way where there is small low sea ice concentration followed by a 'shadow' of low SIT. More specifically, while the low sea ice concentration episodes are brief (2-3 days long), low SIT episodes are longer and more prevalent. What sets apart the 26 September peak is the fact that it has no immediate low SIT response. Instead, low SIT is picking up few days after the sudden loss of ice occurs. Considering the dependency of SIT retrieval on sea ice concentration data, this is quite a curious phenomenon that supports the distinction between the two data products.

Fig. 3.18 shows yet another important detail that can only be viewed by extending the chosen

area (Fig. 3.1) down to roughly 71 degrees South, beyond the coast of the Antarctic. Coastal polynyas around the Antarctic continent are common and outnumber the open-ocean polynyas in the region (Martin 2001). But what Fig. 3.18 shows is an off-coast small-scale polynya or at the very least a thin-ice anomaly that connects the Maud Rise sea ice thinning with coastal polynya activity. Large scale dynamics governing how if at all the coastal polynya affects the Weddell Sea sea ice thinning events are neither understood nor convincing. Even so, there is the possibility in view of the lack of a sharp decline in bathymetry that some effects may carry over. It is important to note that the time of the year presented in (Fig. 3.18) is early October which, although it may precede the general melting of the regional sea ice, is well after the sea ice extent peak of the year. Importantly the 'epicenter' of the sea ice thinning can be seen developing from the first map and is consolidated in the last in (Fig. 3.18) at roughly 64° South and 4° East where the sea ice anomaly peaked in 2018 and the Weddell Sea Polynya occurred in 2017.

4.5 Atmospheric Influence on Ice Thinning

Using ERA5 atmospheric reanalysis data, estimates on weather above the area of interest can be made. Using U- and V-components of wind data at 1000 hPa, which is roughly the sea ice surface, the interaction between the overlaying wind and sea ice can be studied. The importance of this comparison lies with the fact that while sea ice data is an able tool for observing anomalous behavior in sea ice above Maud Rise, no conclusive results can be reached with regards to the cause of the anomaly. As discussed in chapter 1, the Weddell Sea Polynya, although more commonly classified as an open-ocean polynya, is actually hybrid (Heuzé and Lemos 2020); in that it is influenced by both atmospheric and ocean effects. Thus, atmospheric data should shed further light on the anomalous activity captured by SIT retrieval.

Contrary to the preconditioning effects discussed in Chapter 1, from the data presented in Chapter 3 a strong positive curl can be seen to dominate over the region of interest. This does not undermine the original theory for the negative wind stress curl that intensifies the Weddell Gyre spans the entirety of the Weddell Sea (Cheon and Gordon 2019). Secondly, the value presented is not the wind stress curl as one would need the drag coefficient in its calculation which is variable when studying a sea ice region that is prone to exposing water (Heuzé and Lemos 2020). Instead, it is simply the curl of the wind vector field computed as

$$\nabla \times F = \left(\frac{\partial v}{\partial x} - \frac{\partial u}{\partial y} \right)_p \tag{4.1}$$

where F is the field and u and v are x and y components respectively. Due to the lack of a vertical component, both other terms of the curl disappear. Lastly the subscripted p indicates that pressure is kept constant, in that case at 1000 hPa.

Dynamics of coastal (latent heat) polynyas are governed by winds pushing away the ice and

maintaining ice-free regions. A positive wind curl moving counterclockwise in the Southern Hemisphere suggests a local high pressure system that, in theory, should induce divergence (Heuzé and Lemos 2020). However as the data seems to show (covered in following sections), the prevailing effect is that of the Coriolis force in that counterclockwise moving air parcels are deflected to the left resulting in local convergence. In addition to curl, the divergence from the wind components was computed as

$$\nabla \cdot F = \left(\frac{\partial u}{\partial x} + \frac{\partial v}{\partial y} \right)_p \tag{4.2}$$

As the vertical component is not considered and assumed to be 0, the two other terms amount to 0 as well. What divergence of wind at 1000 hPa offers as a product is quantification of wind to ice interactions. If the surface winds diverge with sufficient force, then the ice layer beneath, if thin enough, should be dragged via friction to diverge as well. Important to note is that curl and divergence are not opposites of one another and can both assist and negate polynya favorable conditions individually. While there is no feasible way to monitor these quantities solely in relation with the anomalous activity atop Maud Rise, one can come close by selecting specific regions localized to the event at hand. That is what is done by selecting the region of interest (Fig. 3.1) and limiting calculations to that location.

For the purposes of comparing SIT data with ERA5 atmospheric reanalysis data this section is subdivided into 4 subsections covering the time periods of interest in 2016, 2017, 2018 and 2019 chronologically. In addition to the interpretation of the data presented in the Results Chapter offered below, the second section of the appendix offers additional ERA5-based analysis of all the extraordinary dates covered. Several of the days of interest are analyzed via hourly contour and quiver plots to monitor storm movement and the events are viewed in isolation using directional polar plots.

4.5.1 2016

Fig. 3.19 depicts SMAP-SMOS sea ice thickness retrieval, wind curl, divergence, mean and maximum magnitude during the months July and August 2016 as per figure label. Analyzing the parameters in order; wind curl exhibits periods of high positivity around the time the polynya is open as well as just prior to its occurrence.

The calculated divergence of wind is predominantly negative implying 'convergence' that seems to be common for the region based on the reanalysis data. Interestingly, both the initial peak and the Weddell Sea Polynya peak shown in the SIT plot as well as the sea ice concentration plot (Fig. 3.15) is preceded by a brief peak of positive divergence. These two peaks occurring roughly on the 25th of July and 2nd of August seem to have some effect on the events that follow. This effect is perhaps best described as diverging surface winds pushing the ice apart and encouraging the opening of leads and thereafter polynya. Conversely, since this occurrence is brief and the

divergence is averaged over the segment (Fig. 3.1), the previously mentioned implications are not conclusive.

The most intuitive and perhaps the easiest correlation can be drawn from the wind magnitude. Presented in the bottom plot of Fig. 3.19 is the mean (in blue) and maximum (in red) of the wind magnitude obtained from the root square sum of the U- and V-components obtained from ERA5 (Hennermann 2020). The results show that the highest mean and maximum both coincide with the first major sea ice thinning event followed soon by the opening of smaller polynya initiated quite abruptly on the 26th of July as can be seen best in Fig. 3.15. Unsurprisingly the highest wind speeds occur roughly at the same time as maximum positive wind curl. The maximum wind speed recorded then is 25 m/s which is sufficiently above the norm to be classified as storm activity (Campbell et al. 2019). Similarly an equally high mean value albeit a smaller maximum is recorded days before the Weddell Sea Polynya of 2016 initiated on the 3rd of August. Lastly, the plot showing direction of the wind vectors (Fig. 3.21), computed simply as $\theta = \arctan(U/V)$, shows wind patterns blowing mostly towards the West.

4.5.2 2017

2017 (Fig. 3.12) shows similar behavior when it comes to the Weddell Sea Polynya . Curl stays predominantly positive throughout the two month period with the highest peak preceding the first low SIT peak which is accompanied by varying levels of low sea ice concentration as can be seen in (Fig. 3.11). Unlike 2016, the highest peak of positive curl does not coincide with the highest peak in wind magnitude and seems to have a more gradual effect on wind in that the wind speeds increase with a 1 day delay after the positive wind curl maximum and then impact the ice layer by causing the primary low SIT peak in early September. On that note, divergence patterns are predominantly negative as is common with the region, safe for a wide positive peak during this initial low SIT peak. It is likely that the period of positive divergence would aid the breaking apart of any thin ice present in the region.

Similar to 2016, of the different data product, wind magnitude most directly impacts the opening of the polynya itself. With the same above 25 m/s maximum and above 20 m/s mean recorded between 13 and 14 September, about when the polynya first opens. This high magnitude wind seems to have a direct impact on the ice cover, especially in view of how it was perturbed days earlier. Conclusively, there is a direct correlation between high wind speeds and polynya formation. Year 2018 and 2019 should shed further light whether there is also a correlation between the thinning of ice above Maud Rise and storm activity. Looking at the polar plot for direction (Fig. 3.13), the 2017 directions seem to exhibit a similar funnel of westerly winds as in 2016 albeit a bit more in the Northern direction.

4.5.3 2018

August and September of 2018 are perhaps the best period to study the SIT above Maud Rise as it is predominantly near-100% sea ice concentration with a clear low sea ice thickness event captured in late September. For these reasons, this would also be the prime example of any relation between atmospheric forcing and ice cover thickness. First and foremost, building on previous conclusions, looking at the 4th plot in Fig. 3.14 wind with magnitudes staying below the 25 m/s mark are observed throughout the 2 months period. This is unlike the past two years where 25 m/s wind seems to have triggered both polynyas into opening. Despite that, the highest magnitude recorded on 17 September, precedes the highest low SIT peak much like the high wind magnitude peaks preceded the polynya opening dates in 2016 and 2017. The wind direction plot for 2018 (the right plot in Fig. 3.13) is also quite different when compared to that of 2016 and 2017 in that it is a much wider distribution of directions: winds seem to blow anywhere towards South to North in the left portion of the plot.

Most interesting when it comes to wind curl is the two high positive peaks preceding the two low SIT peaks contained within the low SIT episode of late September 2018. Both peaks match the highest wind speeds of the month and clearly have an impact on sea ice cover even in non-polynya years. It suffices to say, highly positive wind curl seems to be to an extent inversely proportional to sea ice thickness where strong positive curl paired with strong winds are more than likely to impact ice cover above Maud Rise. There is little positive divergence throughout the low SIT period suggesting that its absence could be one of the many reasons as to why the Weddell Sea Polynya did not appear in 2018.

Sometime between 21 and 22 August, a wide but not large positive wind curl peak coincides with relatively high above 20 m/s wind. This has no effect on the sea ice cover and initially strikes as a surprise based on previously made assumptions. By tracking these storm activities via quiver and contour plots (contained in the appendix) it can be seen that this episode can easily be explained by the spatial coverage of the storm. The plots from (Fig. 3.14) are taking the full region (Fig. 3.1) and accounting for all data contained within. By taking a closer look at that time period, it was seen that the strong storm activity was limited to the edges of the chosen segment far from polynya-prone areas above and around Maud Rise hence why the maximum for that time period is high but the mean low.

4.5.4 2019

The year 2019 shows even less sea ice anomalies than 2018, for that reason the months September and October were chosen which bring the time span dangerously close to the November which is the month when the Maud Rise region sea ice melts away. As a result, these data are less conclusive especially in view of the fact that SMOS and SMAP-SMOS SIT retrievals were developed to

monitor sea ice as it forms. Even so, there are some aspects that can be analyzed in Fig. 3.20.

The primary reasons for also featuring data from 2019 is to corroborate 2018 data, as 2019 too lacks a polynya. The hypothesis for this year was to exhibit even less polynya-favorable conditions than 2018 while at the same time help to identify a pattern for years that failed to produce the polynya. Even so, to avoid empty plots, the two month period covers September and October to isolate all and any signs of SIT retrieval of low SIT episodes.

Fig. 3.20 shows an interesting development in terms of wind magnitude. 25 m/s magnitude can be seen right around the first sea ice anomaly around 7th September 2019, which is the maximum from that brief period. Unlike both 2016 and 2017 when this 25 m/s storm wind was accompanied by 20 m/s mean around the time of the respective Weddell Sea Polynya events (Figs. 3.19 and 3.12), in 2019 the mean for that same period is around 15 m/s. Intuitively, the mean characterizes the local winds better than the maximum and upon tracking the storm it appears that during that brief period the storm is once again contained on the edges, namely the Eastern edge, from where it cannot directly impact the ice cover above Maud Rise (see 2019 quiver and contour maps in the Appendix). This initial minor sea ice anomaly, which based on previous discussion is most likely smaller leads that thinned the surrounding ice, is also accompanied by the positive wind curl and convergence. The much bigger low sea ice thickness jump early October is inconclusive mainly since it is too close to the melt-period. Likely it is stable wind speed magnitudes that keep the water from being exposed and positive wind curl periods that initially helped cause the anomaly.

4.6 Oceanic Influence on Ice Thinning

As discussed in several sources cited in this paper (e.g. Martin 2001, Cheon and Gordon 2019, Jena, Ravichandran, and Turner 2019), the Weddell Sea Polynya is an open-ocean polynya. While the previous section effectively proves this to be not fully true in that the polynya is heavily subject to atmospheric forcing, it is nevertheless important to analyze the chosen events in view of ocean parameters. Building upon the theory presented in chapter 1, said ocean properties like salinity and temperature should impact and be impacted by the events that the overlying ice cover undergoes.

It is worth mentioning that mooring data is often unavailable for more recent dates and depends solely on when the instruments are retrieved from the ocean and data made available. As a result, 2019 mooring data was unavailable and the chosen mooring AWI229-13 spans only the years 2017 and 2018, covering both the key sea ice anomaly events studied in this paper. 2016 has not been analyzed in depth in this paper and the respective ocean data as well careful analyses of the event can be found in most publications on the topic ever since the return of the Weddell Sea Polynya in the 21st century (e.g. Campbell et al. 2019, Heuzé and Lemos 2020). AWI229-13 is a mooring at 64° S, 0° W (Rohardt and Boebel 2019) which puts it sufficiently towards the center of the region

of interest (Fig. 3.1).

Starting with Fig. 3.22 the data collected by the mooring go hand in hand with the observed SIT values. The water column prior to polynya formation is more or less stratified and with a positive temperature gradient with decreasing depth. First occurrence disrupting this gradient is with the first low SIT peak (4-5 September 2017), which as suggested prior is a sign of smaller leads in the region. This is corroborated by some 60% sea ice concentration pixels during the same time period as can be seen in Fig. 3.11. At roughly 310 m depth, temperature seems to be lower than 410 m depth which is most likely due to low temperature incursions from the atmosphere via the aforementioned leads. Soon after there is higher temperatures at all levels of depth presented and is a clear sign of how cold water sank and allowed warmer deep water to upwell. This is the likely scenario as there is no feasible explanation as to how warmer water could be present in surrounding regions and then flow into the region above Maud Rise, especially in view of the Taylor cap that characterizes the region leaving the water contained within to be in a relatively closed system (Muench et al. 2001). This effect is further shown upon the formation of the Weddell Sea Polynya of 2017. Similar to before but on a much larger scale, the top layer of water decreases to a temperature that is lower than that of 610 m depth water. As to be expected, this has a profound effect on the water column with waters at all levels reaching their absolute maximum throughout the two months period, up to 1.1 °C at 310 m depth, for at least a 5 day period. With the shear amount of atmosphere to ocean contact, $50 \cdot 10^3$ km^2 (Cheon and Gordon 2019) to be precise, it is not surprising that the water temperature quickly cooled and equilibrated to a lower value than before the ice opened now that the column is exposed from the top.

Salinity behaves much like temperature which could be a direct sign of sea ice melting. In fact, salinity flips its stratification, the salinity with depth profile in this case, even before temperature suggesting some melting occurred after the initial minor peak in low SIT (4-6 September). As discussed prior, this minor peak is marked with a high temperature response soon after its occurrence; it is likely that the high temperature response encouraged melting of sea ice which in turn lowered the salinity of upper waters. Similarly, events surrounding the polynya show the upwelling of more saline warm deep water and the freshening of the entire column with the mass melt of the wide area of formerly thick pack ice.

In 2018 (Fig. 3.23) the 310 m depth temperature data are unavailable as the recording current meter attached at that depth, although it has temperature measuring capability, is no longer active for this period. Interestingly, 2018 ocean data exhibit no reversal in stratification which is to be expected but this is not fully clear as the uppermost temperature sensor is no longer active. Focusing on the 2018 sea ice anomaly a wide high temperature and high salinity peak can be seen to coincide with the first peak of the anomaly (6-13 September). As established prior it is highly plausible that the strong wind activity paired with positive wind curl encouraged ice thinning and opening of minor leads. These leads had an impact on the water column as can be seen in Fig. 3.23

and the higher temperature as well as higher salinity are highly indicative of upwelling. With the convection cell in place, it is no surprise the second low SIT peak is even bigger than the first (13-30 September). It is important to also cross-reference these data with sea ice concentration (Fig. 3.8) where the difference between the initial and later peaks can be clearly seen. Although below 60% sea ice concentration can be seen on a wider scale during the second peak, lower sea ice concentration (below 40 %) is in abundance during the first peak. In addition the period over which the lower sea ice concentrations are present is also longer during the first peak (6-13 September) than the second (13-30 September). As a result, it is not surprising that the upwelling caused by the initial lead opening did not solicit the same response during the second peak, at the same time, it is also understandable why in the SIT record the second peak is much larger than the first as warm water would inevitably melt the water from below on a much wider scale encouraging ice-thinning from below as opposed to from wind activity.

Before the anomaly in 2018 ocean record (Fig. 3.23), one can see several coinciding high temperature and salinity peaks characteristic of movement of water masses as opposed to stationary masses warming or becoming saline. This movement seems to have little to no effect on the ice cover with occasional slight thinning below 50 cm in the SIT record. Some reasons for this are the lack of atmospheric forcing and the brief duration over which these peaks are active as opposed to the one coinciding with SIT anomaly. Looking back at Fig. 3.14, it can be seen that events before the anomaly do not align as well as during the event. Some strong winds are noted on the 22nd of August but is paired with a positive wind curl of lower magnitude and the increasing mean magnitude is what eventually leads to the initiation of the anomaly on 7-8 September. As mentioned above, evidence supporting as to why the strong winds were not able to penetrate the ice layer is given in the appendix.

Ultimately, it seems as though atmospheric forcing is the determining factor in the initiation of a polynya or any SIT anomaly unless a convection cell is already in place to facilitate melting from below. Based on examples presented the pattern for both events, although varying in magnitude, are strong winds paired with positive wind curl followed closely by the a period of warm water upwelling from below. In the event of a polynya the water seems to stabilize at a low temperature (0.4°C−0.6°C) that in the 2017 case (Fig. 3.22) is a bit counter-intuitive considering how the polynya maintained itself over the following month. One explanation for this could be how the mooring itself is positioned in such a way that more often than not it is not within the reach of the polynya such that while the polynya seems to have it is center roughly at 65° S, 3° W, the mooring is at 64° S, 0° W (Rohardt and Boebel 2019). Building on that premise, if a convection cell was to be established and overtime stabilized such that the water column exhibits only vertical movement, then it would localized primarily to the core of the polynya where the cold water would sink and warm water rise (as opposed to the its outer edges where the mooring has been deployed). Thus while the positioning of AWI229-13 is not optimal it is the most recent and most relevant mooring from the region and perhaps the best tool at present to retrieve regional ocean data from

2018.

4.7 Error and Uncertainty

It is important to note that the SMOS and SMAP-SMOS SIT retrieval, used here for analyzing the Weddell Sea Polynya sea ice thickness, has originally been developed and tested for retrieving SIT in the Arctic during the freeze-up season (Huntemann et al. 2014). Naturally, there is a lot of ambiguity in using this method for the analysis of periods nearing the melt-season of the Antarctic. SMAP-SMOS SIT retrieval, while superior to SMOS SIT retrieval, is already subject to several factors contributing to its uncertainty: the radiometric accuracy of the observations, RFI contamination in the TB data, the uncertainty in the auxiliary data used for the training of the retrieval, the influence of the sea ice concentration on the TBs and the sub-daily variability of the TBs themselves (Patilea et al. 2019). The quantification of said error that was carried out by Patilea et al. 2019, came to the median value of 1.2 K uncertainty in the brightness temperature values used for the retrieval, as opposed to SMOS for which the uncertainties were clustered around 4 K. Both sensors increase rapidly in terms of uncertainty beyond 20 cm SIT and are generally most accurate for thin ice in the range 5 cm to 20 cm. As a result, the primary application for this retrieval is the freezing up of thin ice in the Arctic where the water is calmed than the Antarctic due to the Arctic Ocean being predominantly landlocked by surrounding continents creating ideal conditions for briefly monitoring thin sea ice as it forms and thickens. During melt, the sea ice cover is too inhomogeneous for SMOS SIT (and SMOS-SMAP SIT) retrieval to be applied, with the mixture of wet sea ice, melt ponds and open water to be expected within one SMOS footprint (Huntemann et al. 2014). As a consequence, the method is intended for the Arctic from October to April and in the Antarctic from March to October (Huntemann et al. 2014). As a results, all the case studies presented in this paper fall between the time range given for the Antarctic.

Similar to the Arctic environment, the water exposed by the Weddell Sea Polynya is calmer than the current-driven waters surrounding the Antarctic. In addition, as shown in this research, anomalous activity in sea ice above Maud Rise is highly susceptible to winds and to melting from below as opposed to atmosphere-induced melting that would lead to wet sea ice and melt ponds. All values bordering the polynya are admittedly flawed and are not to be taken literally due to the high margin of error the SIT retrievals have with low sea ice concentrations. Despite that, event preceding as well as following the polynya should be quite dependable in the absence of large sections of open water. Similarly, areas of thin sea ice far from the ice-water boundary encircling the polynya should be comparatively accurate and be a good indication as to how far the effects of the polynya propagate through the ice cover.

ERA5 uses a weather forecasting model to produce a spatially and temporally continuous data. Like a weather forecast, the resulting data contain some uncertainty (Hennermann n.d.). In the

case of the produced ERA5 plots, the accompanying ensemble spread was obtained and plotted over the time ranges of interest: August and September of 2017 and 2018 respectively as well as average regional error plotted over the region of interest defined by (Fig. 3.1). All 4 plots can be found in the appendix section dealing with ERA5 data. Further error quantified propagation was not done as the uncertainty as defined for ERA5 by the Ensemble of Data Assimilations (EDA) system is not a classical measure of error with respect to the ERA5 reanalysis product (Hennermann n.d.). The EDA takes into account random uncertainties as not systematic model errors, leaving some portion of the uncertainty in measurement unaccounted for. Additionally, EDA has lower resolution than ERA5, both temporally and spatially, meaning that the EDA system is unable to directly describe all the uncertainties of ERA5 (Hennermann n.d.). As a result, while no proper error analysis can be offered, as stated above the available uncertainty contained in the appendix offers the ensemble spread parameter which is inversely proportional to the accuracy of the ERA5 data.

As for the mooring AWI229-13, no quantification of uncertainty accompanied the data (Rohardt and Boebel 2019) and while there is room for systematic and random error, the principal cause of uncertainty with regards to how well the readings of temperature and salinity represent the water underneath the anomalous sea ice region of Maud Rise is the location of the mooring. As previously discussed in the section covering oceanic influence on the sea ice layer, the point where the mooring gathers data is further West than where the polynya opens and so its reliability is not ideal. Even so, it is perhaps one of the few deployed instruments that gives a clearer picture as to what occurred in the waters during the anomalous activity that affected the region for two consecutive winters; as such, it is still presented in this paper and used to study regional water-to-ice interactions with respect to ice thinning and polynya formation.

4.8 SMAP-SMOS and SMOS Retrievals

Direct comparison of the two SIT retrieval techniques has shown little difference within the scope of this research. The three different side-by-side comparisons along with the respective difference maps (Figs. 3.5, 3.6 and 3.7) show little difference in the center of the polynya, and even in the center of the anomaly in 2018, suggesting the two methods agree on thin ice as well as lack thereof. The highest points of contrast occur at the edges where the gradient is high as can be seen towards the Northeastern edge of the polynya on the 14th and 25th September 2017 (Figs. 3.5 and 3.6). This is most likely due to the higher sensitivity of SMAP-SMOS SIT which allows it to display higher variability over thin sea ice as compared to SMOS (Paţilea et al. 2019). Looking at Fig. 3.7 more dissimilarities can be seen at the edges of the anomaly where sections of thin sea ice are simply not contained within the SMOS SIT map further demonstrating the sensitivity of SMAP-SMOS. All in all, the highest differences occur at relatively thicker sea ice between 40 and 50 cm which, as discussed above, is where both retrieval methods have high uncertainty. Out of the two,

SMAP-SMOS SIT retrieval is deemed more accurate since it is the new and improved successor of SMOS SIT retrieval. Even so, in view of the uncertainty in both methods, special attention is given to thinner sea ice where the SIT retrieval methods are known to be more accurate. In this range, there seems to be much less dissimilarity, further verifying the data retrieved.

Viewing the time series plots (Figs. 3.15, 3.11, 3.8 and 3.17) a higher level of smoothness can be observed in SMAP-SMOS data as if the individual sums from each day influence the following day more so than in SMOS data. That would give further credibility to the improvements offered by SMAP-SMOS as it exhibit more natural behavior as opposed to sudden jumps in the time series data seen in SMOS SITs. In addition, SMAP-SMOS SIT retrieval seems to suggest thinner sea ice than what SMOS SIT retrieval shows. The time series plots offer total sums of pixels contained within the chosen thresholds; and the SMAP-SMOS sums, specifically during the days where there is anomalous behavior but no polynya (Figs. 3.8 and 3.17), seem to be slightly larger. While this effect is minimal, it is either from the higher sensitivity of SMAP-SMOS or its higher accuracy which would suggest thinner sea ice where SMOS SIT deems to be slightly thicker. In conclusion, all differences are minimal but some are more note-worthy than others. Without in-situ validation one cannot be definitively proven to be better than the other, but using past validations from the Arctic as well as uncertainty analysis (Paţilea et al. 2019), it is known that SMAP-SMOS is an overall better SIT retrieval giving higher priority to SMAP-SMOS SIT data in this research.

4.9 The Advantages of Sea Ice Thickness Retrieval

SMOS and SMAP-SMOS SIT have proven to be useful candidates of capturing previously unknown information in the the sea ice layer above Maud Rise. While often coupled with sea ice concentration data, the research presented in this paper demonstrated that SIT is an entirely separate data product. What is more, SIT retrieval over polynya-prone regions identifies localized thinning events and anomalous behavior better than a sporadic distribution of small regions of low sea ice concentrations. In 2018 in particular, a clear shape of thin 20 cm ice much like the polynya of the previous year has been made observable via the SIT retrieval.

When comparing to other techniques used in the study of the Weddell Sea Polynya, SIT retrieval offers the following: data requiring no in-situ measurements unlike both moorings and floats, actual data unlike the interpolated and estimated ERA5 reanalysis data and an overall better tool to catch all anomalous sea ice effects above Maud Rise which sea ice concentration retrieval does not show. Naturally, it is not meant for this data to be used in isolation; rather, it is yet another tool with which the anomaly that has baffled scientists for years can be studied and thereby explained. Most importantly, this a data product that must be used in conjunction with other sources of data like sea ice concentration retrieval but also atmospheric and oceanographic sources.

In conclusion, while SIT retrieval has its flaws, it has the potential to be a capable method for studying the Weddell Sea Polynya. From this research it is clear that SIT retrieval offers more in the years where there is no polynya as opposed to years like 2017 where sea ice concentrations capture the situation quite well as is. As it stands, it is much more common for the ice to remain solids throughout the winter hence the surprise when the Weddell Sea Polynya returned in 2016. Using SIT retrieval will help demystify the region that surprised all in 2016 by revealing itself to be a more commonly anomalous than previously thought.

4.10 Summary

In summary, specific cases were studied from 2017 and 2018 and also to a lesser degree 2016 and 2019. 2017 was given special attention to as it was the year that saw the biggest Weddell Sea Polynya since 1976. Though SIT retrieval did not offer much that is new in this particular case study, it identified preconditioning effects as well the full span of the anomaly that affected the region in 2017. ERA5 data is perhaps most intriguing for 2017 as there is clear correlation between wind strength and the resulting low sea ice concentrations. Data from mooring AWI229-13 identifies the movement of warm water masses presumably from below and the cooling that followed from atmosphere to ocean interactions.

The 2018 case study was the best example of ice thinning localized to the same area that exposed ocean waters the previous year. In addition, the low sea ice concentration halo (Lindsay, Holland, and Woodgate 2004) was observed on several days in the sea ice concentration maps. ERA5 data confirmed the effect of wind is present even in years lacking a polynya, and mooring data showed anomalous activity in the waters during episodes of ice thinning and low sea ice concentration. The mooring data also showed episodes of anomalous activity that did not coincide with sea ice events suggesting warming and cooling from the movement of water masses irrespective of sea ice and presumably the uppermost layer of water.

2016 and 2019 were examples of polynya and the lack thereof respectively which offered proxy data for the main two case studies. Much like 2017, 2016 shows how thin sea ice behaves around the ice-water boundary and also how the thin ice persists after the polynya disappears (unlike 2017 where the polynya remains until melt). 2019, like 2018 shows signs of sea ice thinning and potential lead openings but to a much lesser degree and later in the year than in 2018. ERA5 wind speed data once again correlated with both the occurrence of the 2016 Weddell Sea Polynya as well all anomalous activity in 2019 further consolidating the theory that the Weddell Sea Polynya is influenced by wind as well as ocean. AWI229-13 does not contain 2016 nor 2019 in its data.

4.11 Outlook

For the study of Antarctic sea ice phenomena, the SIT retrieval techniques used in this research must be further validated in of the Southern Ocean. The Arctic and the Antarctic are two different environments each with their own types of sea ice. The sea ice present in both locations varies not only in terms of life cycle but also fundamental properties like thickness, salinity, age and mobility. In conclusion, the validation of SIT retrieval in the Antarctic with in-situ measurements could pave way towards improving or tuning the SIT retrieval algorithm as well as verifying the current data that is obtained from the Antarctic.

Once the SIT retrieval is optimized at retrieving the thickness of Antarctic sea ice, areas of thin sea ice can be analyzed with higher detail. Ideally, under these circumstances, uncertainty will be better known and possibly quantifiable. Thin sea ice, as shown in this research, is common in sea ice regions susceptible to polynya. As a result, in addition to monitoring overall sea ice thickness across the Antarctic sea ice rim during freeze-up, areas of anomalous sea ice behavior can be monitored throughout the austral winters.

It is the aim of this research to direct attention to SIT retrieval as an able candidate at researching the Weddell Sea Polynya. Similar to this case, SIT retrieval can also be used to monitor circumstances with other polynya or ice-thinning activities of which there are plenty in both the Arctic and the Antarctic. As such, there is room for improving the SIT retrieval method so that it may be used to study more sea ice phenomena which are related to sea ice thickness. Improvements in this regard would be quantification of uncertainty from low sea ice concentrations, ability to accurately access SIT at polynya-ice boundaries and eliminate any erroneous values from lead openings.

Chapter 5

Acknowledgments

I would like to acknowledge my overarching supervisor Dr. Gunnar Spreen, head of the Sea Ice Remote Sensing Group of the Institut für Umweltphysik (IUP), for allowing me to join his research group and giving me the opportunity to write my master thesis under his guidance. In addition, I would like to thank Dr. Christian Melsheimer of the same group who acted as second supervisor throughout the whole process. Last but not least, I would like to express my gratitude to Prof. Dr. Justus Notholt, director of the entire Remote Sensing department of IUP, for setting time aside from his busy schedule to act as substitute supervisor for when Dr. Gunnar Spreen was away on MOSAiC expedition to the Arctic.

Data retrieved and analyzed in this paper is made possible through the work of Dr. Marcus Huntemann and Catalin Paţilea. Data used for comparisons have been provided by the Alfred-Wegener-Institut, published in PANGAEA (ocean mooring data) and the European Centre for Medium-Range Weather Forecasts (ERA5 reanalysis data).

Bibliography

Bilello, M. (1960). "Formation, Growth, and Decay of Sea-Ice in the Canadian Arctic Archipelago". In: *Arctic*. DOI: 10.14430/arctic3658.

Campbell, E. et al. (2019). "Antarctic offshore polynyas linked to Southern Hemisphere climate anomalies". In: *Nature* 570, pp. 319–325. DOI: 10.1038/s41586-019-1294-0.

Cheon, W. G. and A. Gordon (2019). "Open-ocean polynyas and deep convection in the Southern Ocean". In: *Sci* 9, p. 6935. DOI: 10.1038/s41598-019-43466-2.

Comiso, J. (1986). "Characteristics of arctic winter sea ice from satellite multispectral microwave observa-tions". In: *Journal of Geophysical Research*, pp. 975–994. DOI: 10.1029/JC091iC01p00975.

Hennermann, K. (2020). *ERA5: data documentation*. data documentation. European Centre for Medium-Range Weather Forecasts. URL: https://https://confluence.ecmwf.int/display/CKB/ERA5%3A+data+documentation.

— (n.d.). *ERA5: uncertainty estimation*. data documentation. European Centre for Medium-Range Weather Forecasts. URL: https://confluence.ecmwf.int/display/CKB/ERA5%3A+uncertainty+estimation.

Heuzé, Céline and Adriano Lemos (2020). "Spaceborne infrared imagery for early detection and cause of Weddell Polynya openings". In: *The The Cryosphere Discuss.* DOI: 10.5194/tc-2020-123.

Huntemann, M. et al. (2014). "Empirical sea ice thickness retrieval during the freeze-up period form SMOS high incident angle observation". In: *The Cryosphere* 8, pp. 439–451. DOI: 10.5194/tc-8-439-2014.

Jena, B., M. Ravichandran, and J. Turner (2019). "Recent Reoccurrence of Large Open-Ocean Polynya on the Maud Rise Seamount". In: *Geophysical Research Letters* 46, pp. 4320–4329. DOI: 10.1029/2018GL081482.

Jiang, L. et al. (2020). "Trends in the Stability of Antarctic Coastal Polynyas and the Role of Topographic Forcing Factors". In: *Remote Sensing* 1043. DOI: 10.3390/rs12061043.

Kaleschke, L. et al. (2010). "A sea-ice thickness retrieval model for 1.4 GHz radiometry and application to airborne measurements over low salinity sea-ice". In: *The Cryosphere* 4, pp. 583–692. DOI: 10.5194/tc-4-583-2010.

Lindsay, R., D. Holland, and R. Woodgate (2004). "Halo of low ice concentration observed over the Maud Rise seamount". In: *Geophysical Research Letters* 31. DOI: 10.1029/2004GL019831.

Marshall, G. (2003). "Trends in the Southern Annular Mode from observations and reanalyses". In: *J. Clim.* 16, pp. 4134–4143. DOI: 10.1175/1520-0442.

Martin, S. (2001). "Encyclopedia of Ocean Sciences, 1st Edition". In: 4, pp. 2241–2247.

Muench, R. et al. (2001). "Maud Rise revisited". In: *Journal of Geophysical Research* 106. DOI: 10.1029/2000JC000531.

Paţilea, C. et al. (2019). "Combined SMAP-SMOS thins sea ice thickness retrieval". In: *The Cryosphere* 13, pp. 675–691. DOI: 10.5194/tc-13-675-2019.

Rayner, N. et al. (2003). "Global analyses of sea surface temperature, sea ice, and night marine air temperature since the late nineteenth century". In: 108. DOI: 10.1029/2002JD002670.

Rohardt, G. and O. Boebel (2019). *Physical oceanography and current meter data from mooring AWI229-13*. data set. Alfred Wegener Institute, Helmholtz Centre for Polar and Marine Research, Bremerhaven. DOI: 10.1594/PANGAEA.898781. URL: https://doi.org/10.1594/PANGAEA.898781.

Spreen, G., L. Kaleschke, and G. Heygster (2008). "Sea ice remote sensing using AMSR-E 89-GHz channels". In: *Journal of Geophysical Research* 113. DOI: 10.1029/2005JC003384.

Stirling, I. (1997). "The importance of polynyas, ice edges, and leads to marine mammals and birds". In: *Journal of Marine Systems* 10, pp. 9–21. DOI: 10.1016/S0924-7963(96)00054-1.

Appendices

The appendix section contains all plots and maps from which conclusions were drawn in Chapter 4 but not presented in Chapter 3. Most maps contained serve as an accompaniment to the primary maps presented in Chapter 3 whereas additional ERA5 data serve to further investigate how atmospheric effects act on sea ice cover above Maud Rise. Contour quiver plots presented in section 2 in particular, offer further clarity as to why wind time series plots from 2016-2019 are often inconsistent in terms of gravity of effects on ice cover

Appendix A

Additional Maps

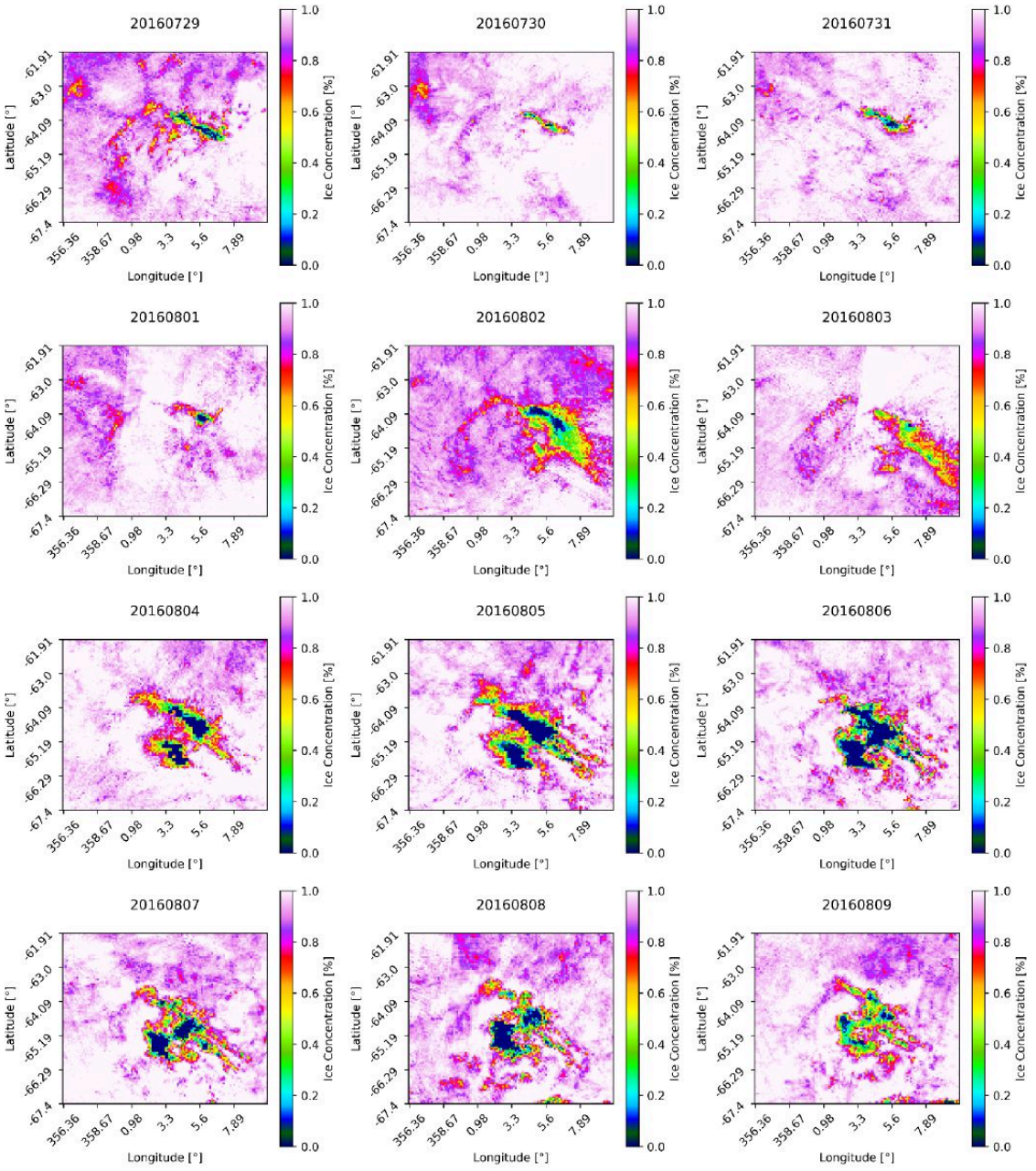

Figure A.1: ASI sea ice concentration maps from 29 July to 9 August 2016.

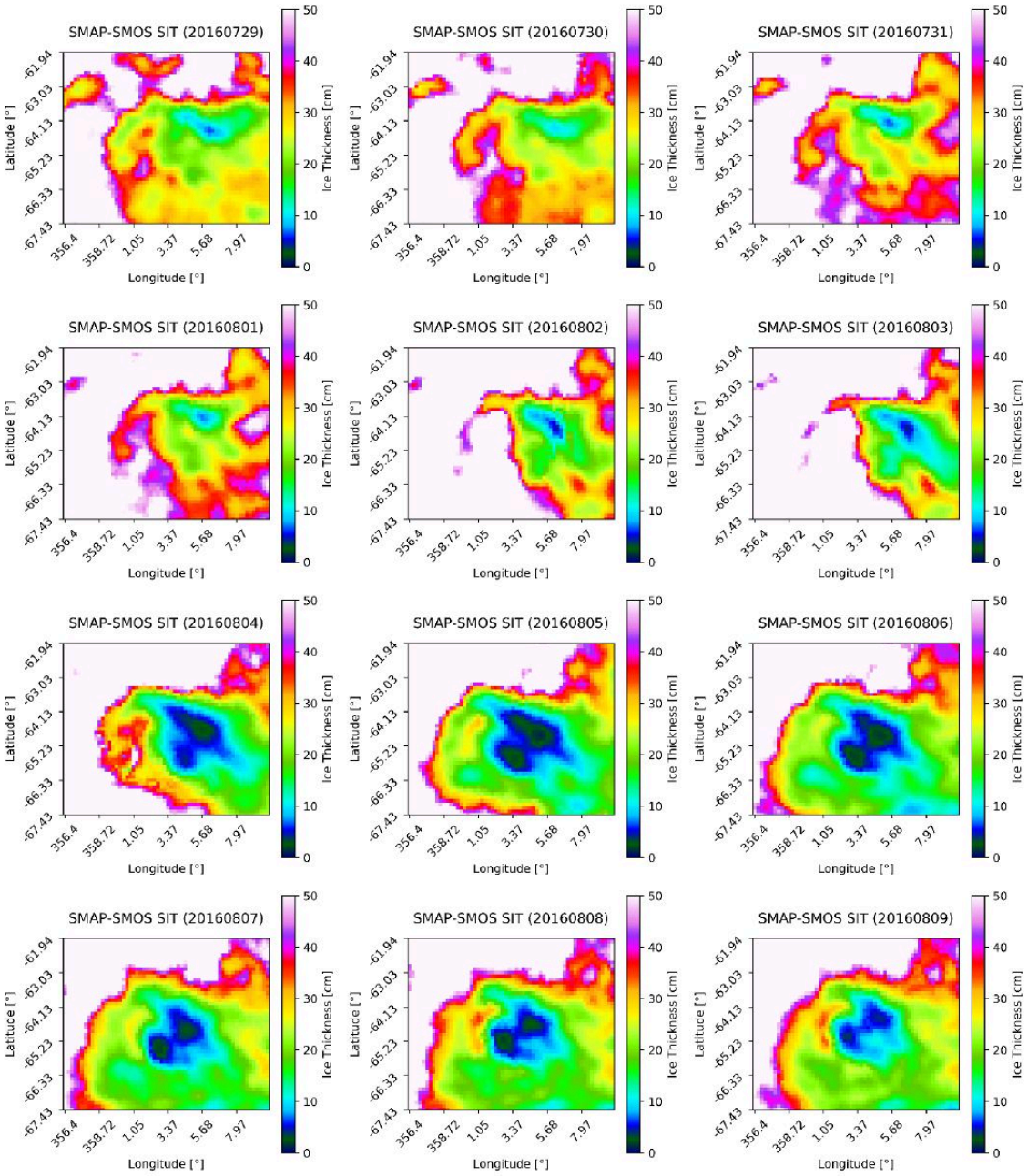

Figure A.2: SMAP-SMOS SIT maps from 29 July to 9 August 2016.

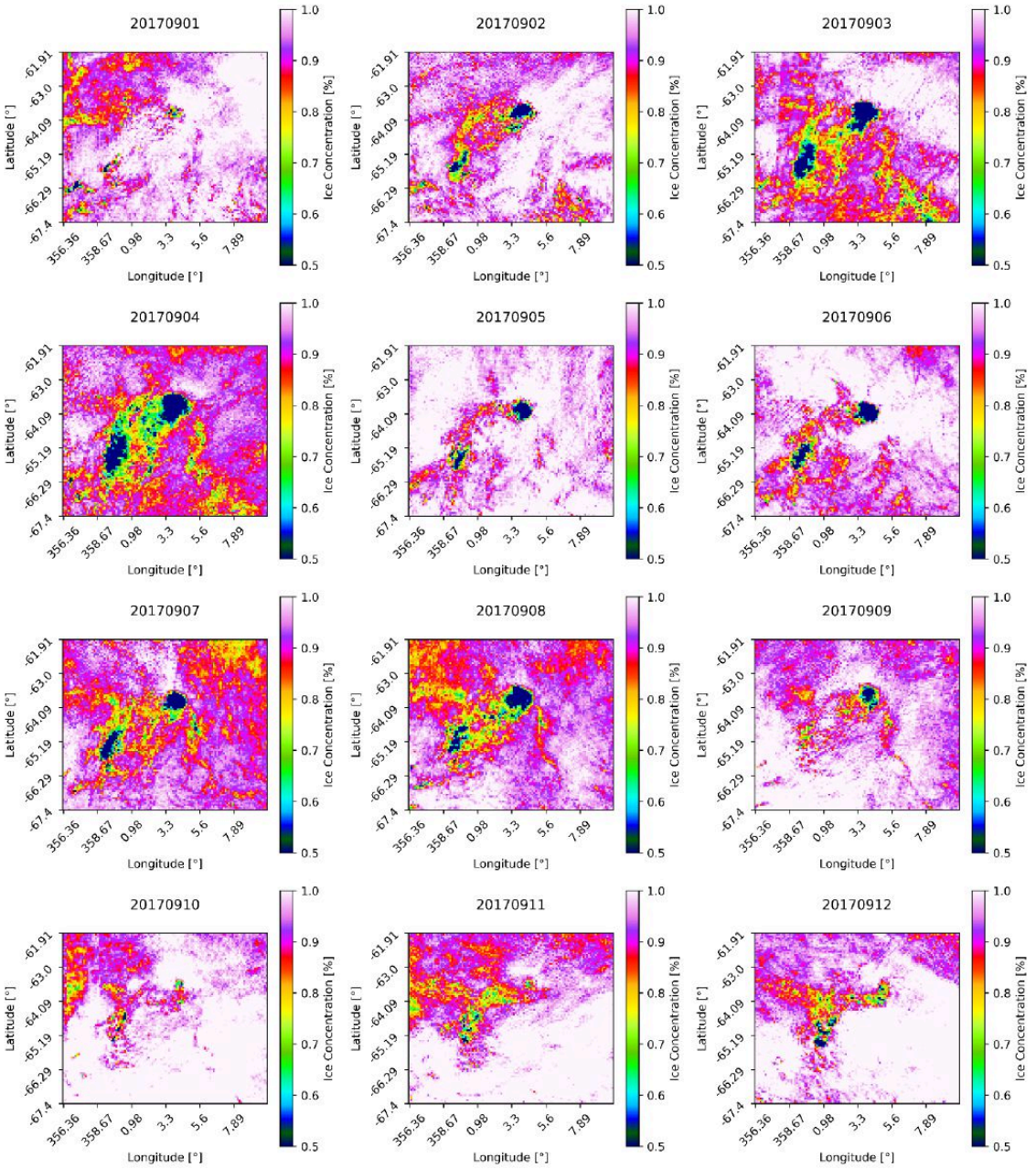

Figure A.3: ASI sea ice concentration maps from 1 to 12 September 2017.

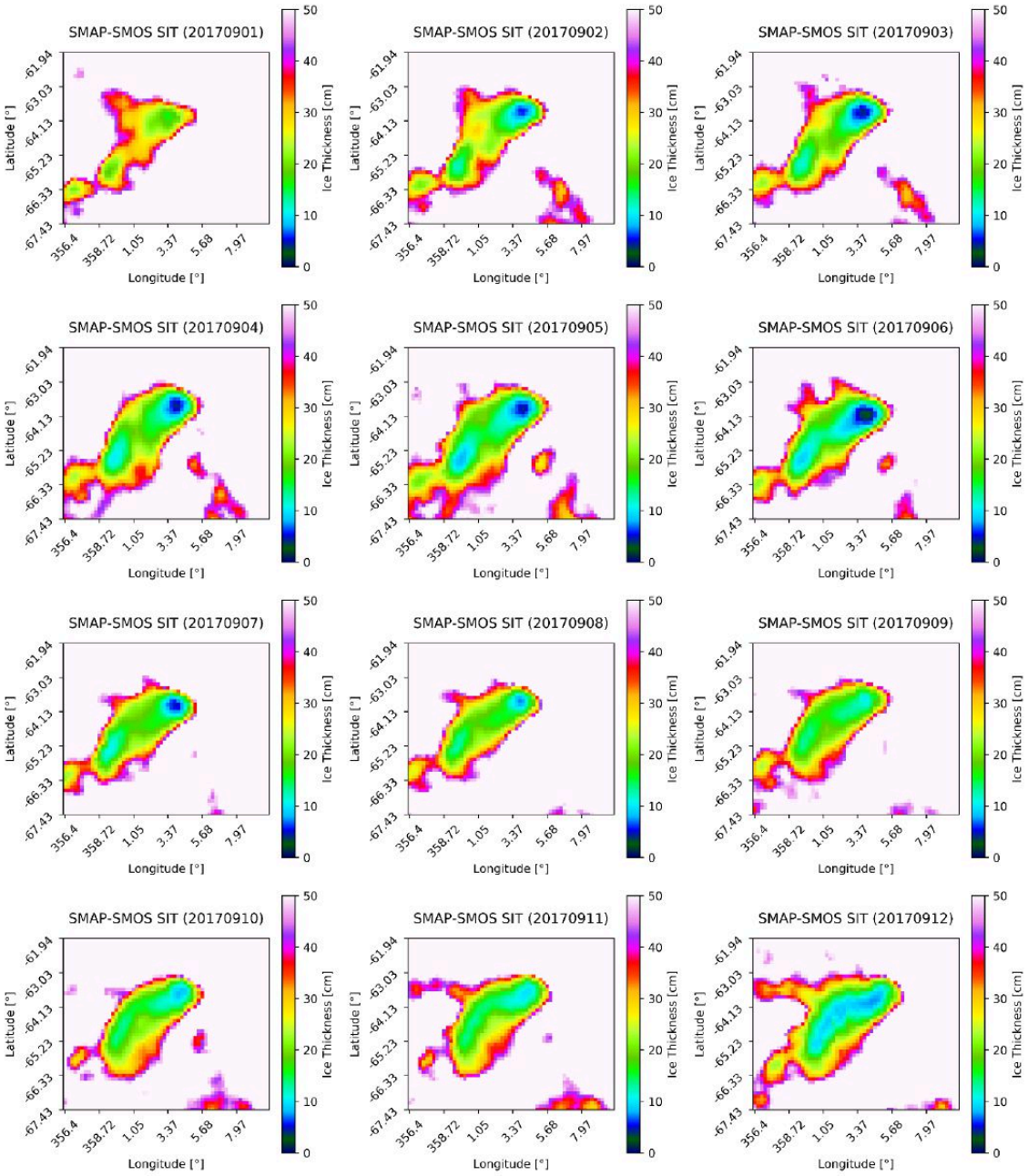

Figure A.4: SMAP-SMOS SIT maps from 1 to 12 September 2017.

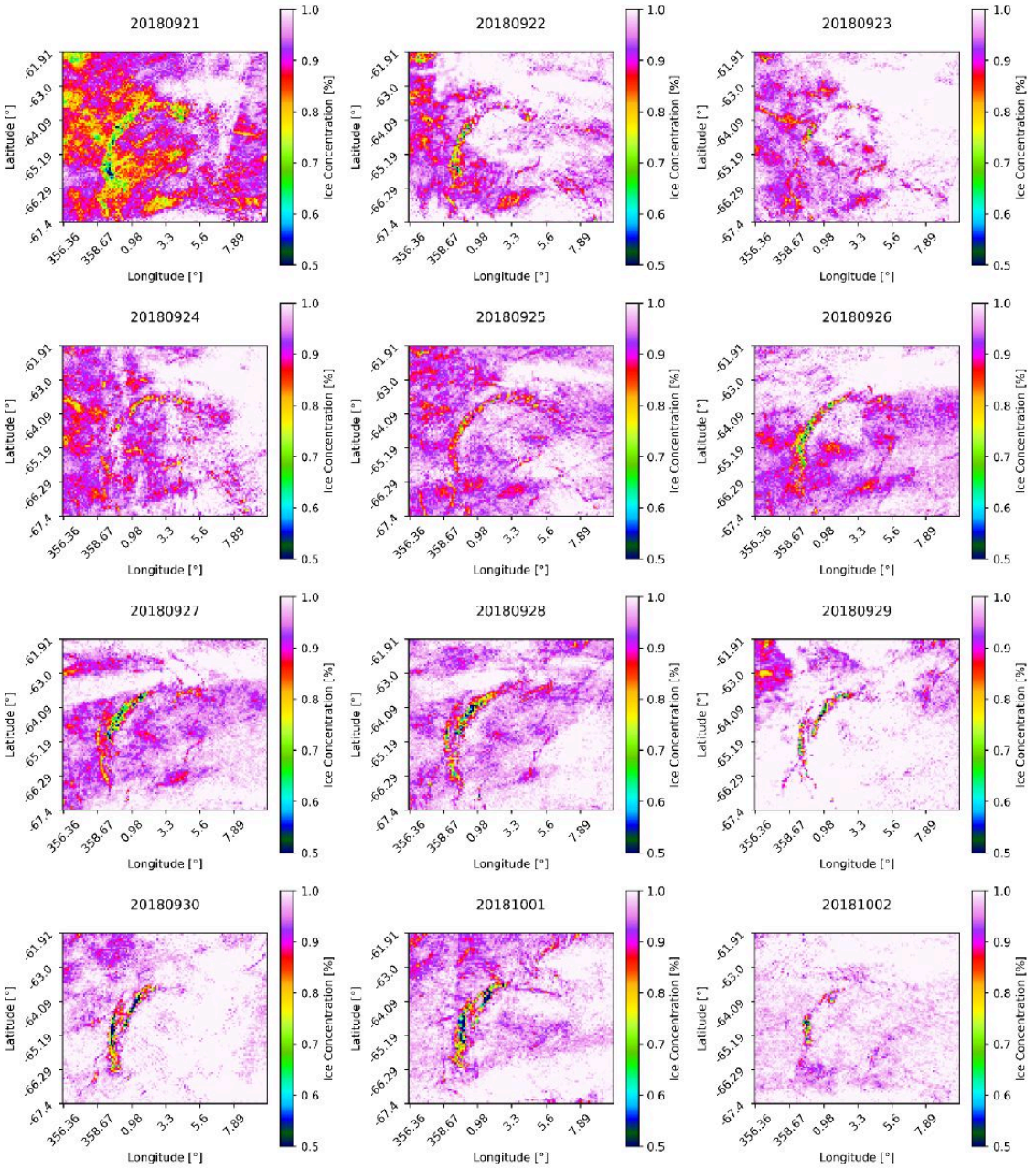

Figure A.5: ASI sea ice concentration maps from 21 September to 2 October 2018.

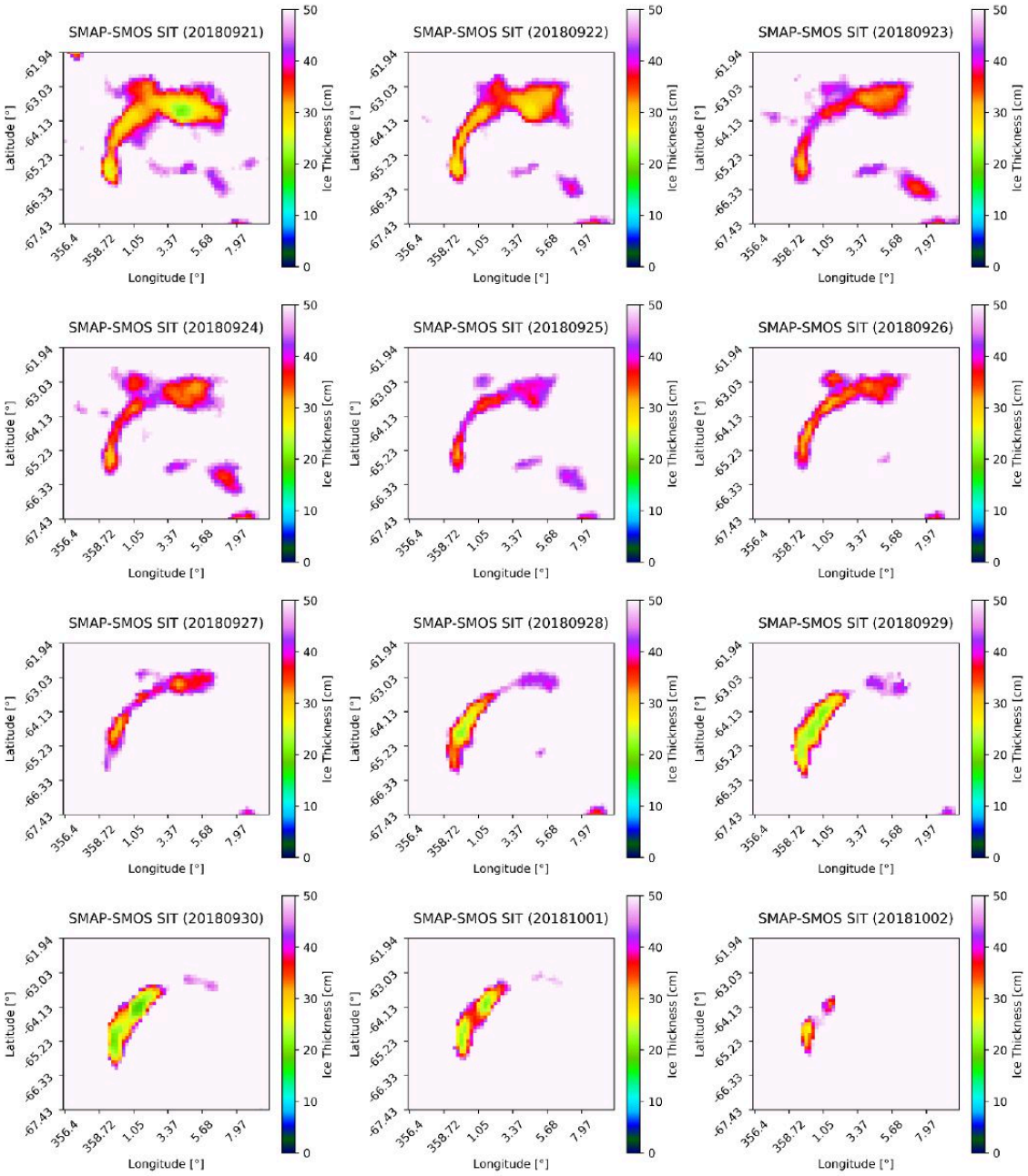

Figure A.6: SMAP-SMOS SIT maps from 21 September to 2 October 2018.

Appendix B

In-depth ERA5 Analysis

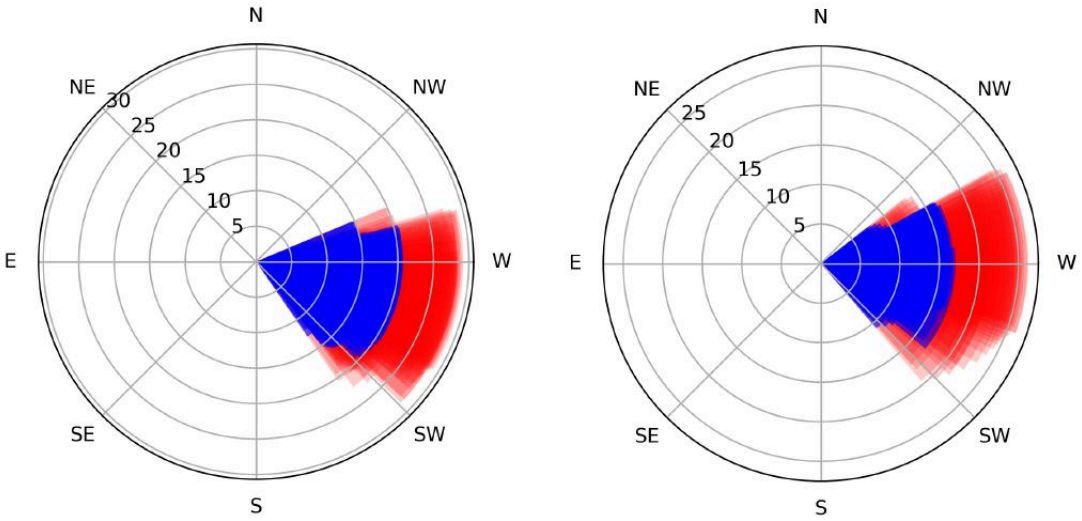

Figure B.1: From left to right: wind directions and magnitudes from 25 to 27 July 2016 as well as from 2 to 4 August 2016.

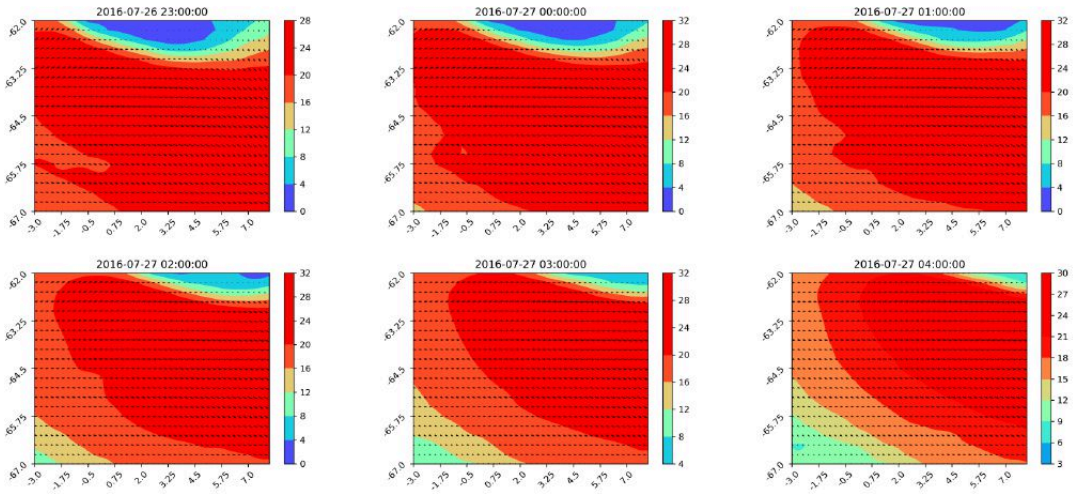

Figure B.2: Wind quiver and contour maps from 11 pm 26 July to 4 am 27 July 2016.

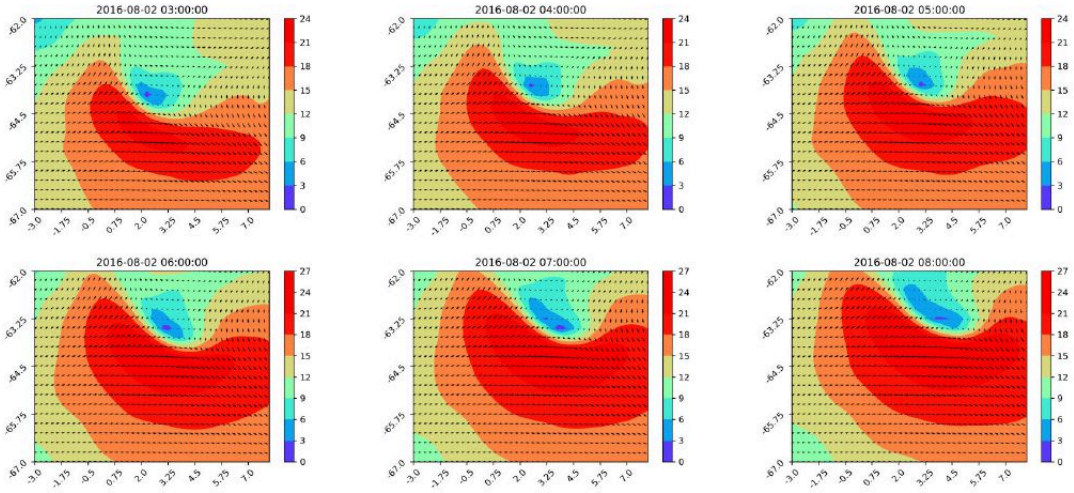

Figure B.3: Wind quiver and contour maps from 3 to 8 am 2 August 2016.

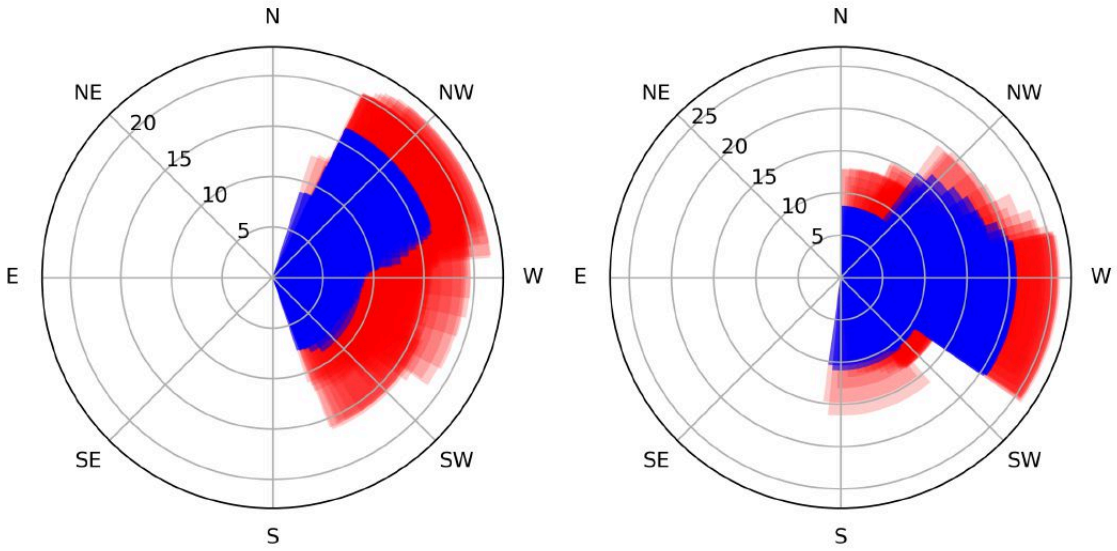

Figure B.4: From left to right: wind directions and magnitudes from 31 August to 5 September 2017 as well from 8 to 14 September 2017.

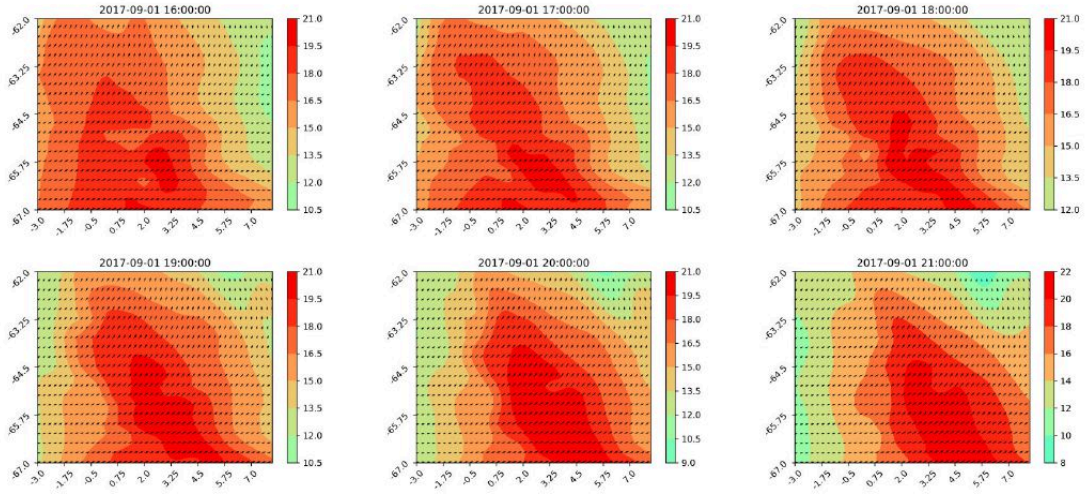

Figure B.5: Wind quiver and contour maps from 4 to 9 pm 1 September 2017.

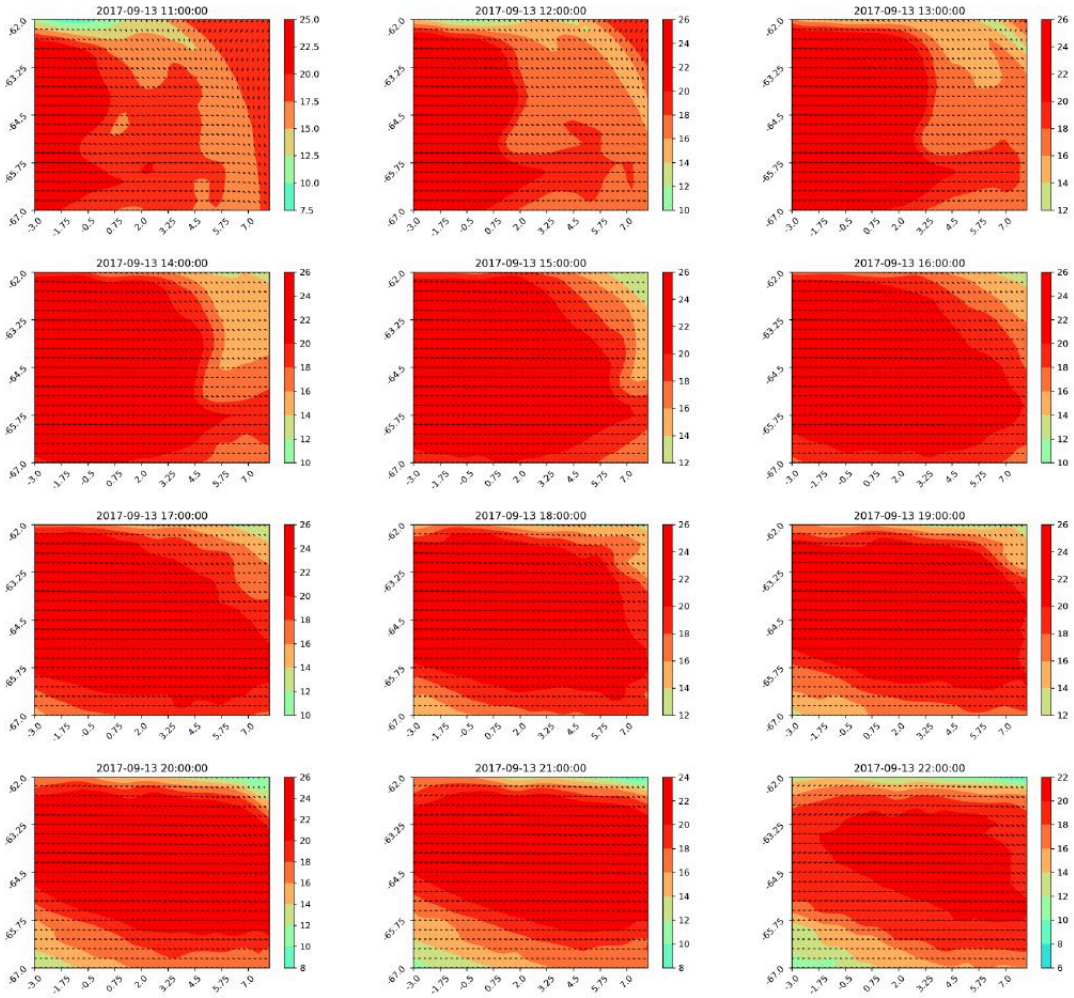

Figure B.6: Wind quiver and contour maps from 11 am to 10 pm 13 September 2017.

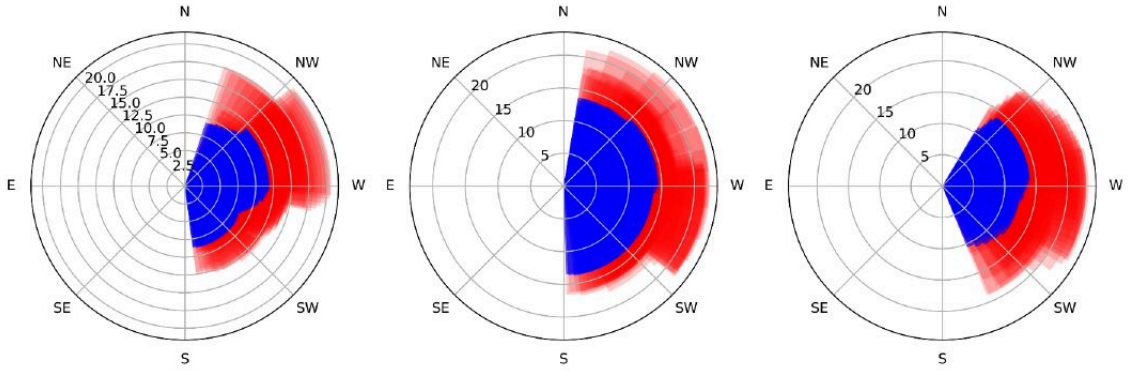

Figure B.7: From left to right: wind directions and magnitudes from 21 to 26 August 2018, 5 to 10 September 2018 and 15 to 20 September

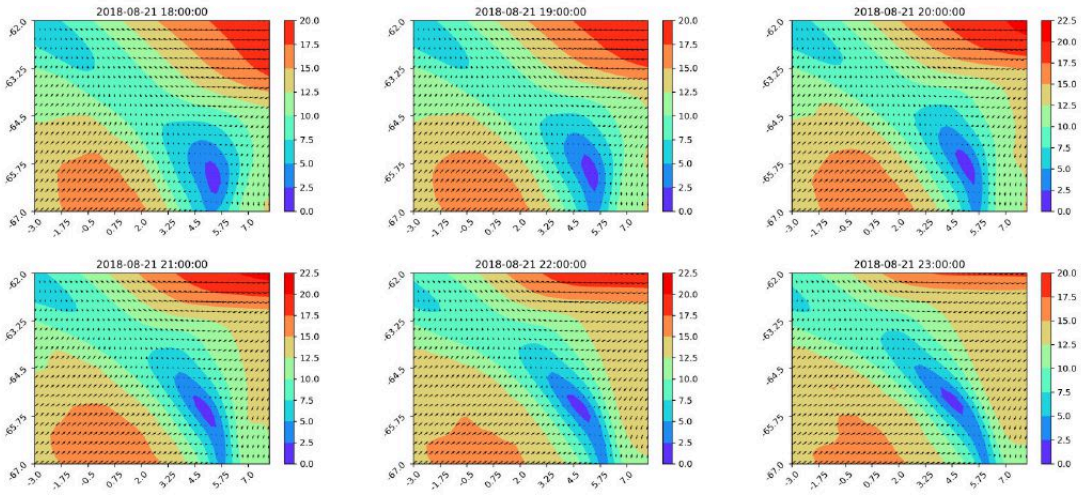

Figure B.8: Wind quiver and contour maps from 6 to 11 pm 21 August 2018.

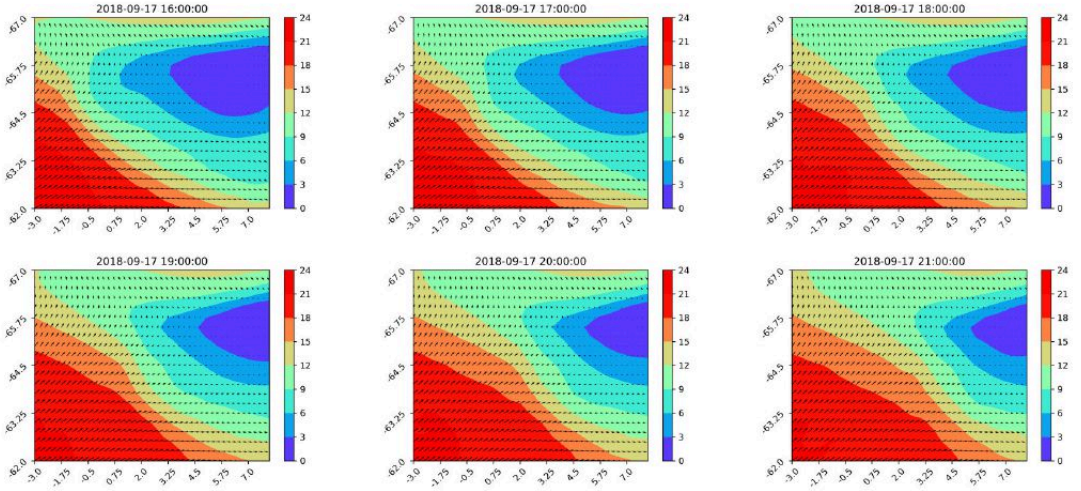

Figure B.9: Wind quiver and contour maps from 1 to 9 am 7 September 2018.

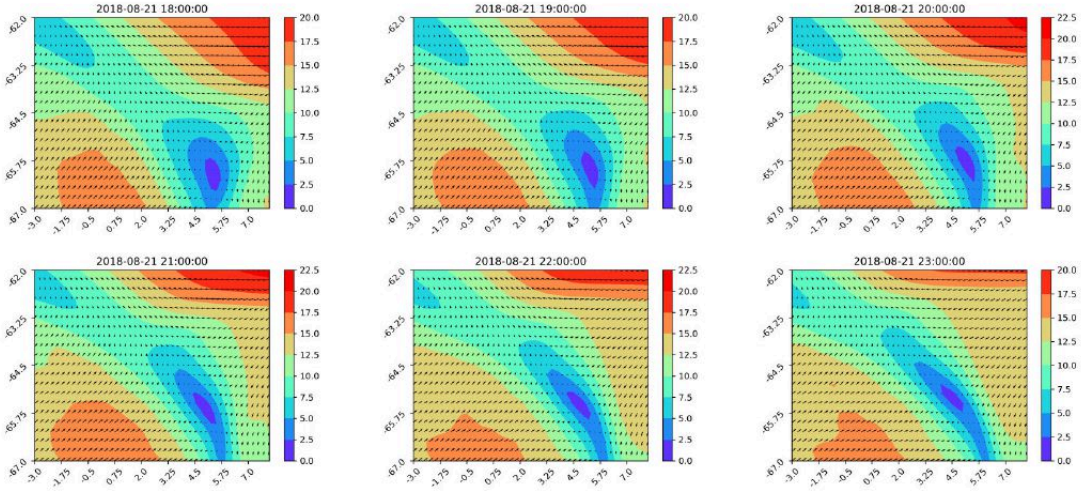

Figure B.10: Wind quiver and contour maps from 4 to 9 pm 17 September 2018.

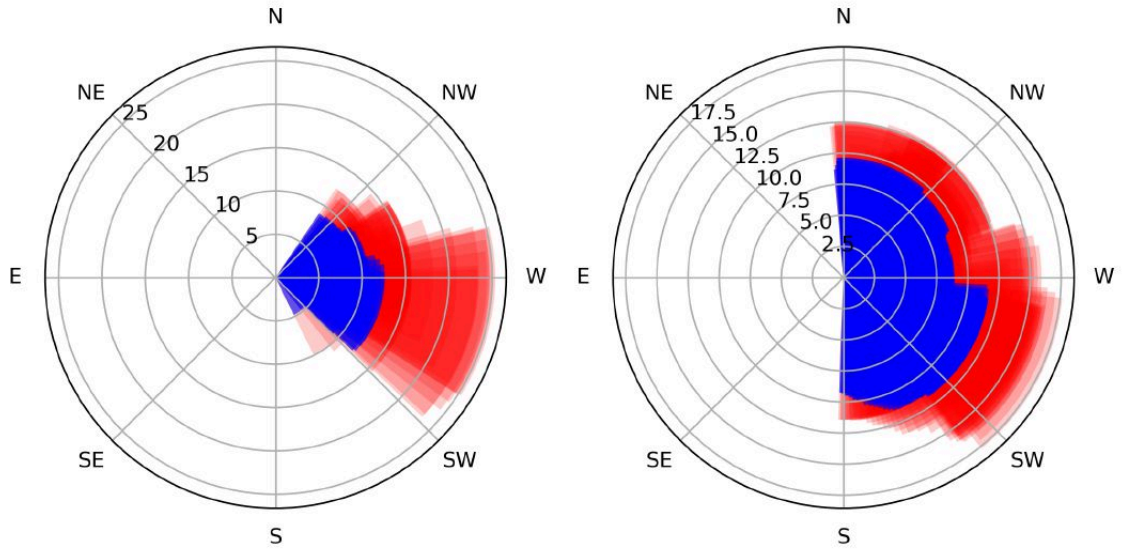

Figure B.11: From left to right: wind directions from 5 to 7 September 2019 as well from 24 to 30 October.

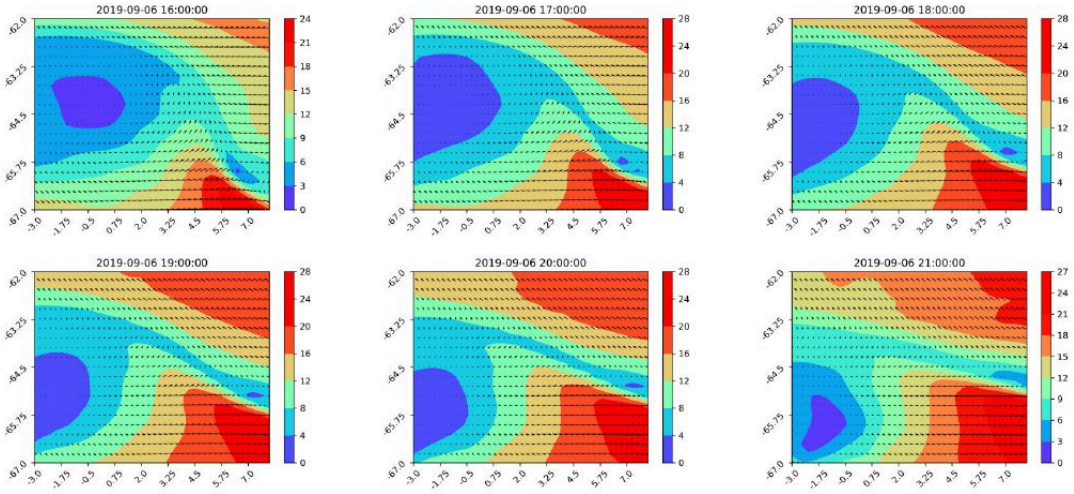

Figure B.12: Wind quiver and contour maps from 4 to 9 pm 6 September 2019.

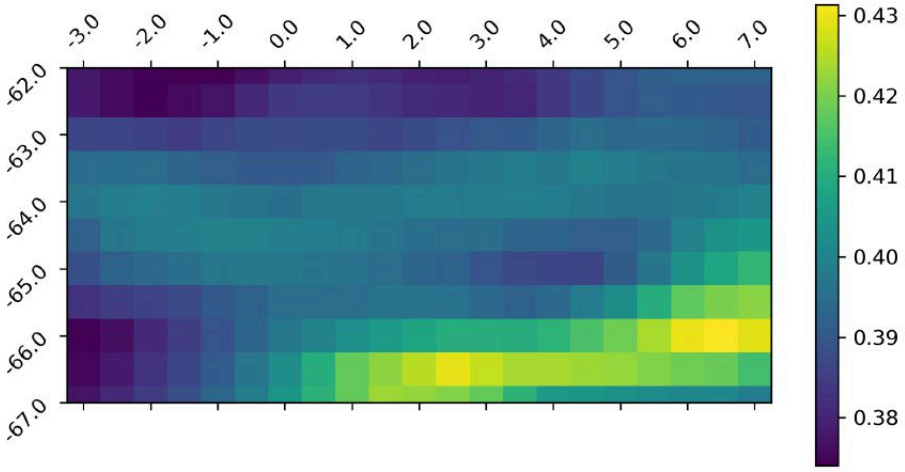

Figure B.13: Ensemble Spread of u-component of wind speeds localized over the region of interest.

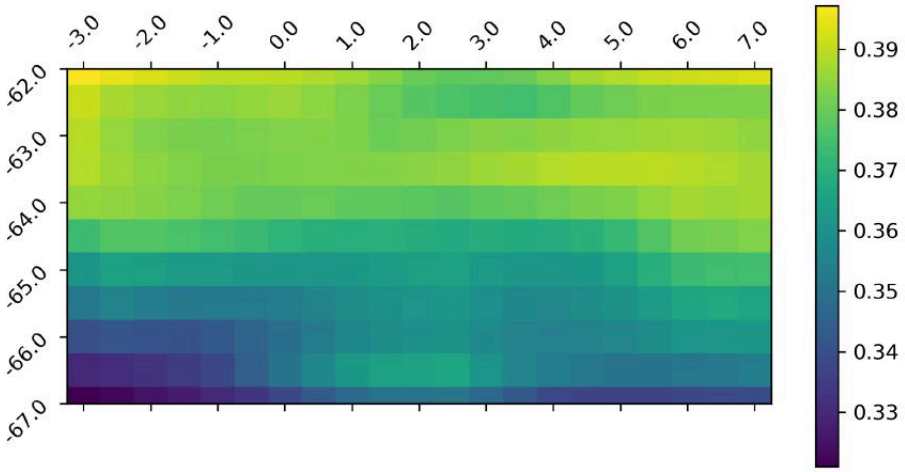

Figure B.14: Ensemble Spread of v-component of wind speeds localized over the region of interest.

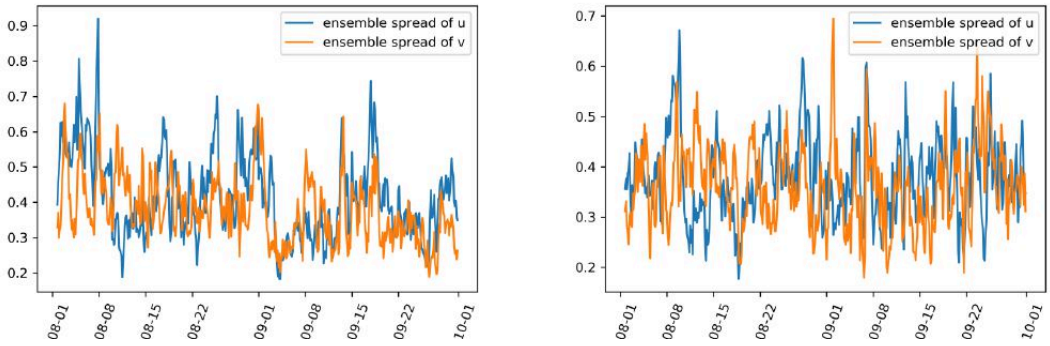

Figure B.15: Ensemble Spread time series of u and v components of wind speeds. On the left is the time series covering 1 August 2017 to 30 September 2017 and on the right the same time range but in 2018.